Master's Thesis

Rasmus Anker Pedersen

Arctic Warming
The effect of a reduced sea ice cover on the vertical structure of warming

Academic advisers: Peter L. Langen, DMI and Eigil Kaas, NBI

March 2013

Title page illustration: Private photo, Arctic Ocean, August 2009

Contents

LIST OF ABBREVIATIONS

ALB-1.5 ...... SOM simulation with sea ice albedo reduction and $1.5 \times CO_2$

ALB-2 .... SOM simulation with sea ice albedo reduction and $2 \times CO_2$

ALB-CTRL ... SOM reference climate with sea ice albedo reduction

ALB-PD ...... Present-day equivalent climate with sea ice albedo reduction

CAM3 .... Community Atmosphere Model, version 3

CMIP .... DOM simulation with SST and sea ice data from the CMIP3 multi-model mean 1995-99

CMIP3 .... Coupled Model Intercomparison Project, Phase 3

DJF .... December, January and February (winter)

DOM .... Data Ocean Model

DSE .... Dry Static Energy

EBM .... Energy Balance Model

ERA-All ...... DOM simulation with SST and sea ice data from the ERA Interim 2006-10 mean

ERA-Ice ...... DOM simulation with SST from the CMIP3 1995-99 mean and sea ice from the ERA Interim 2006-10 mean

GCM .... General Circulation Model

GHG .... Greenhouse Gas

IPCC .... The Intergovernmental Panel on Climate Change

IPCC AR4 .... The IPCC fourth assessment report (2007)

JJA .... June, July and August (summer)

LW .... Longwave radiation

MAM . . . . March, April and May (spring)

MHT . . . . Meridional Heat Transport

MSE . . . . Moist Static Energy

NOALB-1.5 . . . SOM simulation with $1.5 \times CO_2$

NOALB-2 . . . . SOM simulation with $2 \times CO_2$

NOALB-CTRL SOM unperturbed reference climate

NOALB-PD . . SOM simulation with present-day equivalent climate

OLR . . . . Outgoing Longwave Radiation

PS . . . . Surface Pressure

RH . . . . Relative Humidity

SAF . . . . Surface Albedo Feedback

SFC . . . . The Surface

SOM . . . . Slab Ocean Model

SON . . . . September, October and November (autumn)

SST . . . . Sea Surface Temperature

SW . . . . Shortwave radiation

TOA . . . . The Top Of the Atmosphere

Abstract

The Arctic sea ice cover has declined rapidly in recent years. The sea ice loss is primarily ascribed to anthropogenic global warming, which has been observed to be stronger in the Arctic than anywhere else. This increased warming is termed *Arctic amplification*, and is arising from the combined effect of several climatic feedback processes. Investigation of the mechanisms behind the amplification has resulted in a scientific debate on the relative importance of remote and local sources of warming – in practice often meaning the relative warming contributions from changed atmospheric heat transport and surface-based, sea ice related processes. The vertical profile of warming has been widely used as an indicator of the relative contributions, as the warming signals from local and remote sources are expected to be seen near the surface and aloft respectively. Such an analysis of the vertical structure of Arctic warming, performed by *Chung and Räisänen* [2011], has been used to argue that climate models tend to over-estimate the warming from atmospheric heat transport, as the warming aloft in the models exceeds what is seen in reanalysis data. This finding has been contested in this thesis, which contributes to the Arctic amplification debate with an assessment of the effect of a reduced Arctic sea ice cover on the vertical profile of warming.

This analysis is based on simulations with the atmospheric general circulation model CAM3, which was used to simulate the atmospheric response to a reduced Arctic sea ice cover. Two different approaches has been used to induce the diminished sea ice cover: The first experiment uses prescribed, fixed sea ice conditions from the ERA Interim reanalysis, while the second incorporates an active upper ocean and sea ice cover, and induce the sea ice reduction through an albedo change.

The results show that, the sea ice reduction causes substantial surface-based warming, which exceeds the warming aloft. This indicates that, the basis for the conclusion by *Chung and Räisänen* [2011] is invalid, while the results presented here still indicate the need for further investigation of the simulated atmospheric heat transport in general circulation models. The incorporation of an active upper ocean and sea ice cover includes additional feedbacks in the simulation, which improves the estimated vertical warming profile in the model compared to the reanalysis data. The improvement is found to be linked to changes in the atmospheric circulation, and in line with results from similar studies it seems that the sea ice cover somehow is linked to the large-scale atmospheric circulation. Consequently, changes in the sea ice cover has impacts for the climate both within and beyond the Arctic. The details of the coupling remains unclear, while the results here suggest that the crucial factors lie in the feedback processes involving the sea ice and the upper ocean.

1 INTRODUCTION

The recent dramatic decline of the Arctic sea ice cover is seen as one of the clearest signs of climate change. The sea ice cover has, as a very palpable symbol of global warming, received increasing attention both in the public and in the scientific community. *Notz and Marotzke* [2012] conclude that the downward trend in the sea ice extent is beyond what can be explained through natural variability – meaning that the sea ice loss must be owing to anthropogenic global warming, primarily caused by increased amounts of greenhouse gases in the atmosphere. This conclusion was even drawn before the record-breaking low Arctic sea ice extent in September 2012.

The expected continuation of the global warming could cause substantial climate changes, especially in the Arctic, where the large deposits of snow and ice obviously are very sensitive to warming. The Arctic area is furthermore expected to experience accelerated warming rates compared to the rest of the world, and it seems that substantial Arctic climate change is inevitable.

This project is a contribution to the scientific debate, which aims to assess the reasons for the accelerated warming, which has been termed *Arctic amplification*. The idea of Arctic amplification has traditionally been ascribed to the surface-based ice albedo feedback, but from a range of recent studies it is evident that the amplification arises from several, intertwined contributing factors. The debate has been focused on the relative importance of local (meaning within-Arctic) and remote factors, with a special focus on the magnitude of surface-based warming relative to the warming from atmospheric heat convergence. The sea ice cover plays a central role in the surface-based Arctic warming, but – as this project goes on to show – it is also coupled to climatic changes way beyond the Arctic area.

The September Arctic sea ice cover is projected to disappear before the end of this century (*Boé et al.* [2009]), and this expected reduction will change the properties of the Arctic climate substantially. Rather than focussing on the reasons for the sea ice reduction, the aim of this project is to assess the effect of a reduced sea ice cover on the pattern of warming, and the contribution to Arctic amplification. The assessment is based on general circulation model (GCM) simulations of the atmospheric response to a reduced sea ice cover. Two different experiments are done with different approaches to induce a changed sea ice cover: The first experiment

prescribes fixed sea ice and sea surface conditions, while the second employs an active upper ocean and sea ice model, and introduces a sea ice reduction through a change of the sea ice albedo.

The sea ice reduction is shown to have substantial impact on the Arctic warming, by changing both the radiative, heat and moisture budgets. Seasonal differences are large, but the reduced sea ice cover impacts the Arctic climate throughout the year. The analysis further reveals that the sea ice reduction is affecting the atmospheric large-scale circulation, and by extension the climate of the entire Northern Hemisphere.

2   Scientific introduction

The Arctic area has no strict definition, but is often defined as the area north of 66.5°N. This boundary (the Arctic Circle) defines the Arctic as the region, which experiences 24-hour daylight during summer and 24-hour darkness during winter. In this thesis however *the Arctic* is defined as the area north of 70°N, in line with similar studies, to focus on the climatic changes around the Arctic Ocean. The region north of 70°N consists of about 3/4 ocean and 1/4 land, and average values will thus be dominated – but not entirely decided – by the changes over the Arctic Ocean.

2.1   The Arctic energy budget

The energy budget for the Arctic as a whole is settled by a combination of three main net energy fluxes. If the Arctic is defined as a box bounded by the 70°N latitude band, the Earth's surface and the top of the atmosphere, the sum of the energy fluxes across the borders decides the state of the Arctic climate – whether it gains or losses energy. In this view the Arctic box only contains the atmosphere, and any changes in the underlying ocean, ice and land covered parts of the system will influence the flux balance at the surface. Schematic setup and flux definitions are chosen in line with *Nakamura and Oort* [1988]. The fluxes across the borders can be divided into three terms as:

$$\frac{\Delta E}{\Delta t} = F_{\text{TOA}} + F_{\text{SFC}} + F_{\text{MHT}} \tag{2.1}$$

where the left hand side describes the change in energy within the Arctic (ΔE) over the time (Δt), which is equal to the sum of the net energy flux at the top of the atmosphere (TOA), the net surface energy flux (SFC) and the horizontal energy flux (or *meridional heat transport*, MHT) across 70°N. A climate change in the Arctic thus originates from a change in the sum of the three flux components. The three terms can be further elaborated to give a better overview of the physical processes determining the energy fluxes. The TOA flux can be detailed as:

$$\begin{aligned} F_{\text{TOA}} &= (1 - \alpha) \, F_{\text{SW}} - F_{\text{LW}} \\ &= (1 - \alpha) \, F_{\text{SW}} - \sigma \epsilon T_{\text{ems}}^4 \end{aligned} \tag{2.2}$$

where α is the albedo, F_{SW} denotes the incoming shortwave (solar) radiation, and F_{LW} the outgoing longwave radiation (OLR). The sign convention used here is that positive (negative) fluxes correspond to an energy gain (loss) for the Arctic atmosphere. In (2.2) the OLR is re-written using *Stefan-Boltzmann's Law* for the longwave emission from a so-called grey-body (counterpart to black-body with emissivity $\epsilon < 1$), where σ is the Stefan-Boltzmann constant, ϵ the emissivity and T_{ems} the effective emission temperature.

Likewise, the surface flux balance F_{SFC} of (2.1) can be rewritten to illustrate some of the underlying physics. Assuming that the change in heat stored in the ocean-ice-land system is balanced by the vertical flux across the surface, the surface flux balance can be written as:

$$F_{\mathrm{SFC}} \quad = \quad -\left(S_{\mathrm{LHI}} + S_{\mathrm{Ocean}} + S_{\mathrm{Ice}} + S_{\mathrm{Land}}\right) \tag{2.3}$$

$$\Rightarrow F_{\mathrm{SFC}} \quad \approx \quad -\left(S_{\mathrm{LHI}} + S_{\mathrm{Ocean}}\right) \tag{2.4}$$

where the S-terms denote heat storage in ocean, ice, and land respectively and latent heat storage in the form of snow and ice (LHI). The assumption behind (2.3) means that direct horizontal heat transfers from ocean heat convergence and sea ice export from the Arctic are neglected, as these fluxes are comparatively small throughout the year. A more recent study by *Serreze et al.* [2007] indicates that this original assumption from *Nakamura and Oort* [1988] is valid: "*Because horizontal oceanic heat flux convergence and sea ice transport out of the Arctic via Fram Strait are fairly small, the net surface flux is in turn the primary driver of seasonal changes in ocean heat storage*". Equation (2.4) follows from (2.3) as storage in land (soil) and ice is small compared to the relatively large values of latent and ocean heat storage.

The MHT is a moist static energy (MSE) flux, and consists of three types of energy transports: latent heat, sensible heat, and potential energy flux (the latter two combined are also referred to as the *dry static energy* (DSE)). The three components of the moist static energy are defined as (*Wallace and Hobbs* [2006]):

$$\begin{aligned} E_{\mathrm{MSE}} \quad &= \quad E_{\mathrm{LH}} + E_{\mathrm{SH}} + E_{\mathrm{POT}} \\ &= \quad E_{\mathrm{LH}} + E_{\mathrm{DSE}} \\ &= \quad L_{\mathrm{v}}q + c_{\mathrm{p}}T + gz \end{aligned} \tag{2.5}$$

where L_{v} is the latent heat of evaporation, q the specific humidity, c_{p} the specific heat of the atmosphere, T the temperature, g the gravitational acceleration, and z the height above sea level. The last term gz is also known as the geopotential (Φ, the work required to raise a unit mass to height z).

The three detailed energy flux equations (2.2), (2.3) and (2.5) only hints to the complexity of the Arctic climate system. All of the variables are affected by numerous physical and chemical processes, and many are interconnected directly or indirectly. A change in one parameter can initiate a chain of events that might

amplify or dampen the original change through a so-called *feedback process*. Climatic changes such as a reduced sea ice cover, thus not only affects a single term in the equations above, but might change the Arctic energy budget altogether.

2.2   THE SEA ICE COVER

All components of the Arctic cryosphere are for obvious reasons sensitive to warming, and the growth or decline of ice in different forms can be seen as an indicator of the general trend of the climate change. The time scales of change and sensitivity to warming, however, varies greatly among the different elements, and the response of one of the cryospheric elements may be delayed more or less compared to the changing climate. One of the more sensitive and quickly responding parts of the cryosphere is the sea ice cover, which is seen as a key indicator of climate change (ACIA, by *Hassol* [2004]).

The extent of the Arctic sea ice has a strong seasonal cycle, driven by the vast difference in downwelling solar radiation between winter and summer – often illustratively termed *the polar night* and *the polar day*. The sea ice cover reaches annual maximum extent shortly after the spring equinox (by the end of March), and minimum extent shortly after fall equinox (by the end of September). A warmer climate will affect the sea ice throughout the year, as an increase in the summer temperatures will cause a bigger ice loss in the melting season, and a warming in winter will limit the build-up of new ice in the freezing season.

The formation of sea ice in the Arctic Ocean is made possible by the combination of extremely low temperatures, and the existence of a relatively fresh surface ocean layer. This fresh layer is primarily caused by extensive freshwater input from river run-off from North American and Eurasian rivers, combined with inflow of low-salinity water through the Bering Strait and a general positive net precipitation – i.e. total precipitation exceeds total evaporation (*Serreze and Barry* [2005]). The freshness of the surface layer makes it buoyant in the more saline ocean water, even if it is cooled towards freezing. This fresh surface layer in combination with the dark, cold Arctic winter means that new sea ice is expected to be form during winter even in future, much warmer climate conditions. In such a scenario, the sea ice cover will thus have a limited build-up of ice each winter, which is completely melted each summer – creating a seasonally ice free Arctic Ocean.

The sea ice cover is a key feature of the Arctic climate system and has great influence on the energy budget. The often thick layer of sea ice limits the interaction between atmosphere and ocean by acting as an insulating layer between the two. Although some heat conduction is possible through the ice, the magnitude of the flux is minimal compared to the heat transfer over open ocean. As the Arctic Ocean for a large part of the year is considerably warmer than the overlying atmosphere, the ice cover limits the heat transfer from the ocean to the atmosphere, which further contributes to already extreme low winter air temperatures.

Additionally the sea ice cover also limits the ocean heat uptake from the incoming solar radiation, as the white sea ice has a relatively high albedo compared to the darker open ocean – and hence increases α in Equation (2.2). The average albedo for sea ice of 0.55 to 0.75, which can be further increased by snow cover on top of the ice, is very high compared to open water's value below 0.1 (values are taken from *Serreze and Barry* [2005, Table 5.3]). The albedo effect, while significant in summer, has limited or no influence during the winter, where sunlight for a large part is absent. As the ice begins to melt the albedo is somewhat reduced by melt ponds on the sea ice surface, but the average albedo still exceeds that of open ocean. The albedo of sea ice also depends upon its thickness and age, with older thicker ice being more reflective.

The seasonal cycle of the sea ice cover also affects the energy budget along with the reflective and insulating properties. In the melting season the ice cover acts to keep near-surface temperatures at a minimum, as the melting of sea ice takes up all excess energy, keeping temperatures near-surface temperatures close to freezing – as long as sea ice is present in the vicinity. This drawing of heat from the lower atmosphere is countered by the opposite process in the freezing season: sea ice growth release latent heat from the phase change, which transfers energy to the upper ocean and lower atmosphere. These latent heat fluxes from the phase changes are described in the energy flux equations above as S_{LHI} in (2.3).

It is obvious from the above descriptions that the sea ice cover is important for the surface energy flux F_{SFC} and the radiation budget in F_{TOA}, which underlines the important role of the sea ice cover. However – as this project goes on to evaluate – a changed sea ice cover might even affect the horizontal heat transports in and out of the Arctic through a chain of intertwined processes. This means that the sea ice cover plays a central role in all three components of the energy budget (Equation (2.1)).

2.3   THE VERTICAL TEMPERATURE PROFILE

The vertical temperature profile is important for the atmospheric circulation, and thus for the climate. The often very cold surface temperatures in the Arctic gives rise to creation of surface-based temperature inversions (temperature increase with height), which affect the circulation and heat distribution. Low-level inversions are in general a result of a negative net radiative balance at the surface, where the OLR exceeds the downwelling solar and infrared radiation, combined with warm air advection (from lower latitudes) above the colder surface layer (*Bradley et al.* [1992]). These mechanisms indicate that inversions are common in the Arctic, as such a radiative imbalance at the surface is likely during the polar night with no incoming sunlight. Furthermore, due to the temperature gradients, there is a general transport of heat from lower latitudes into the Arctic, which could retain a warmer level above a cold surface. In the Arctic the inversions can however also be affected

by several other factors – e.g. radiative changes from clouds and ice crystals (e.g. *Overland and Guest* [1991]). Observations lends support to the above theory, as surface-based inversions are common in the Arctic during winter: *Serreze et al.* [1992] and more recently *Zhang et al.* [2011] show that surface-based temperature inversions are very frequent in the period from October to March. The inversions increase the static stability by inhibiting vertical mixing, and thus prevent heated air near the surface from rising to a higher altitude. In climate analysis Arctic vertical temperature profiles can thus be used as indicators of spatial origins of warming, as warming originating near the surface to a large degree will be confined below the inversion, and not be spread throughout the atmospheric column. Hence, any warming signals above the inversion-layer indicate that the warming originates somewhere other than the surface – e.g. from radiative absorption at that altitude or from atmospheric heat transport from lower latitudes. This way of analysing the vertical structure of the warming, will be utilised in this project in line with a range of other studies (see Section 2.5.2)

2.4 Feedback processes

As touched upon earlier the different components of the climate system are often linked and coupled in ways, in which an initial perturbation in a single parameter can initiate a chain of following changes. Such couplings gives rise to the concept of feedback processes. A feedback describes a process, where an initial perturbation of a component in the climate system is either dampened or amplified through interactions with other components. These feedbacks are of course central, when dealing with climate change, as they are possible causes of accelerated change, and thus can increase the *climate sensitivity*. The climate sensitivity is defined as the ratio of temperature change to the radiative forcing, which yields units of $\left[\frac{\text{K}}{\text{W m}^{-2}}\right]$, and is a measure of how drastic the climate will respond to a given forcing. The importance of feedbacks in relation to the sensitivity is recognised by *Randall et al.* [2007] in the IPCC Fourth Assessment Report (AR4), which states that "*Climate sensitivity is largely determined by internal feedback processes*". *Wallace and Hobbs* [2006] gives a quantitative example of the effect of the feedbacks through a back-of-the-envelope calculation, which illustrates that the apparent sensitivity of the climate system is more than doubled by inclusion of feedback mechanisms. The following feedbacks are known to be crucial in Arctic climate change:

The surface albedo feedback (SAF)
> In the Arctic (and in the context of this project) the surface albedo feedback (SAF) is primarily an *ice-albedo feedback*. The process behind the feedback is that an initial warming melts off snow and ice, reducing the surface albedo and increasing absorption of incoming solar radiation, which favours further warming and melt of snow and ice. Hence the SAF is a positive feedback that amplifies the original perturbation. Arctic albedo changes also happen in smaller magnitudes than complete melt of snow or sea ice: an initial

warming can also reduce the albedo through creation of melt ponds on sea ice or ice caps and through reduction of sea ice thickness.

The water vapour feedback

Water vapour is an efficient greenhouse gas (GHG), and a general increase of the atmospheric water vapour content is expected to cause a warming. This gives rise to a positive feedback, as the warming will subsequently increase the evaporation from the ocean (and continental water sources), which will further increase the amount of water vapour in the atmosphere. Furthermore the warmer air can hold more moisture. If the relative humidity (RH) is to remain constant in a warmer climate, it follows from the *Clausius-Clapeyron equation* that the amount of atmospheric water vapour will rise with the temperature (*Wallace and Hobbs* [2006]):

$$\frac{\mathrm{d}e_{\mathrm{s}}}{\mathrm{d}T} = \frac{L_{\mathrm{v}}}{T\left(\nu_{\mathrm{g}} - \nu_{\mathrm{l}}\right)} \tag{2.6}$$

The Clausius-Clapeyron equation describes the change in saturation vapour pressure of water e_{s} with temperature T, where L_{v} is the latent heat of evaporation and ν is the specific density (ρ^{-1}) of water as vapour (g) and in liquid (l) form. The amount of water vapour rises with temperature, as $\nu_{\mathrm{g}} \gg \nu_{\mathrm{l}}$ such that the right hand side is positive, which implies that e_s grows exponentially as a function of T. To maintain a constant RH (RH $= \frac{e}{e_{\mathrm{s}}}$) the vapour pressure of water e (measuring the amount of water vapour in the atmosphere) must follow e_{s}. The exponential growth of the solution to Equation (2.6) suggests that the water vapour feedback is stronger at higher temperatures, and thus will be less effective in the Arctic relative to lower latitudes. A recent study of feedbacks by *Langen et al.* [2012] also indicates that the warming effect of water vapour is limited in the Arctic compared to lower latitudes, but that water vapour increases the climate sensitivity, and therefore can amplify Arctic warming tendencies caused by other processes.

It should be noted that the LW warming effect of water vapour depends on the vertical distribution in the atmosphere, as greenhouse gases are more efficient higher in the atmosphere, where the effective emission temperature (T_{ems} in Equation (2.2)) is lower. The greenhouse effect of water vapour in the lowermost atmosphere is small, as it does not change the effective emission temperature significantly compared to the surface (e.g. *Harvey* [2000]). The availability of water vapour however also affects the energy budget indirectly – especially in relation to clouds.

Planck feedback

The Planck feedback, perhaps the most fundamental feedback in the climate system, is clearly seen from Stefan-Boltzmann's Law relating temperature to OLR (OLR $\propto T^4$, as used in Equation (2.2)). When the temperature is increased, an increase in the OLR follows to re-obtain equilibrium. The Planck feedback is thus a negative feedback countering the initial change.

As the OLR changes with the fourth power of the temperature, the Planck feedback will be stronger at higher temperatures – i.e. more pronounced in the tropics than in the Arctic.

Lapse rate feedback

The magnitude of OLR is not only decided from the Planck feedback, but also greatly affected by the temperature profile of the atmosphere. The lapse rate (the temperature change with height, $\Gamma = -\frac{dT}{dz}$) is directly connected to the greenhouse effect, as a relatively cold upper troposphere will reduce the OLR, and a stronger decrease of temperature with height will thus increase the greenhouse effect (*Bony et al.* [2006]). Depending on the vertical distribution of a given warming, the following lapse rate change can result in either a negative or a positive feedback: The feedback is positive, if the lower troposphere warms more than upper, and negative if the opposite is true. A uniform vertical warming constitutes no lapse rate feedback, as the structure of the vertical profile is unaltered.

Cloud feedbacks

The effect of the cloud feedback is hard to define for multiple reasons. Clouds have both warming and cooling properties, through increasing the greenhouse effect and reflecting incoming solar radiation (hereafter *the greenhouse effect* and *the albedo effect*), and the net outcome of the two competing effects depend upon the type of cloud in question. Both the warming and cooling effects depend on factors like cloud type, cloud height, and optical depth, and the effect may be completely different in different regions – the same is true for the response of the cloud cover to warming. In very broad terms, the net effect of clouds can be illustrated by comparing two categories of clouds: low-level dense clouds will have a net cooling effect, while high-level thin clouds will have a warming effect. The dense low-level clouds are highly reflective, and will limit the amount of incoming solar radiation that reaches the surface dramatically. The competing warming greenhouse effect will be limited, as the cloud top temperature is comparable to the surface temperature, leaving the effective emission temperature almost unchanged. Conversely, the high-level thin cloud will be easily penetrated by the incoming solar radiation, while its very low temperature will lower the effective emission temperature considerably, causing the greenhouse effect to dominate the reflective effect.

The sign of the cloud feedback thus depends on the type of cloud and the question of whether the clouds increase or decrease in a warming climate. The IPCC (IPCC AR4, *Meehl et al.* [2007b]) present an multi-model average for the current general circulation models (GCMs), which show that the models tend to increase both low and high cloud fractions in the Arctic following a temperature increase. *Vavrus et al.* [2009] and *Liu et al.* [2012] analyse cloud changes in a warming Arctic, and both studies also conclude that Arctic clouds increase with increasing temperature and diminishing sea ice cover. It should be noted that the response of clouds to global climate

change is mentioned (e.g. by the IPCC) as one of the key uncertainties in future climate projections, and that the response varies significantly between GCMs.

Assuming that there is a general cloud increase in a warming Arctic, the sign of the feedback is still unclear due to the clouds' opposing radiative effects. Results from climate models provides an estimate of the net effect, and (on a global scale) feedback analyses by *Colman* [2003] and *Soden and Held* [2006] find that the cloud feedback is positive in current GCMs.

In the Arctic the assessment of the cloud feedback is further complicated, as noted by *Curry et al.* [1996], "*due to the presence of the highly reflecting snow and ice, the absence of solar radiation for a large portion of the year, low temperatures and water vapour amounts...*". The first arguments point towards a diminished albedo effect: If the underlying ground is already very reflective, adding a reflective cloud above will not change the amount of absorbed solar radiation, as this is already limited. Likewise, when it is dark, the albedo effect is irrelevant. In line with this thought, recent studies reveal that both observations (*Intrieri et al.* [2002]) and reanalysis data (*Screen and Simmonds* [2010b]) indicate that the greenhouse effect of Arctic clouds is dominating except for a short period during summer. This suggests that the cloud feedback is positive in the Arctic, except for a brief period during summer (as suggested by *Vavrus et al.* [2009]). Observations indicate that the feedback may be strongest in the fall, when newly ice free areas create favourable conditions for cloud formation (*Kay and Gettelman* [2009]).

In addition to the feedbacks mentioned above there are several other feedbacks with importance for Arctic climate change. Especially carbon cycle feedbacks, which have been left out here since they are irrelevant in the context of this project, are central in the Arctic climate system in connection to release of methane and carbon dioxide from thawing permafrost (e.g. review by *McGuire et al.* [2006]).

The listing of feedback processes above may indicate – undesirably – that the feedbacks are individual, isolated processes. This is certainly not the case in the Arctic, where the processes to a large degree are coupled and intertwined. The high degree of coupling makes it difficult to assess, which processes that are most critical for the Arctic climate change in a warming climate, and recent Arctic climate research has had increasing focus on the relative importance of the different processes.

2.5 ARCTIC AMPLIFICATION

The knowledge of the feedback processes leads to the expectation that climate change in the Arctic may be different from that at lower latitudes. Especially the surface ice-albedo feedback (SAF), which is almost unique to the Arctic, due to

the high abundance of snow and ice at temperatures relatively close to the melting point, has led to the thought of accelerated warming in the Arctic – often termed *Arctic amplification*. The concept of Arctic amplification describes that the Arctic temperature changes are amplified compared to the global (or Northern Hemisphere) average, even though the forcing is globally uniform – as an increased atmospheric GHG concentration is. The idea was presented as early as 1896 by *Arrhenius* [1896, p. 265], who in assessing the effect of CO_2 in the atmosphere argued that the snow- and ice-albedo effect would move the maximum temperature change "*from lower parallels to the neighbourhood of the poles*". While SAF traditionally have been acknowledged as the key factor in Arctic amplification recent studies reveal that there may be other factors in play. This thesis is contributing to the on-going debate of the underlying causes of the Arctic amplification, which is at present day evident in observations (*Bekryaev et al.* [2010]) and a near universal feature in climate models (*Holland and Bitz* [2003]).

2.5.1   THE ARCTIC AMPLIFICATION DEBATE

Holland and Bitz [2003] show that Arctic amplification of near-surface warming following an atmospheric CO_2 doubling is evident in all state-of-the-art climate models, with Arctic warming 1.5 to 4.5 times greater than the global mean (shown in Figure 2.1). The increased warming is primarily ascribed to SAF, while other factors are found to contribute to a smaller degree. The warming is not found to increase all the way to the pole, but the maximum warming is found over the Arctic Ocean or near the edge of the sea ice cover – indicating that the biggest warming is spatially correlated with areas of sea ice loss (evident from Figure 2.1, where a few models have maximum warming around 80°N). Areas of increased wintertime cloud cover (meaning that the greenhouse effect is dominating, as the albedo effect is nullified by the absence of sunlight) also correlate with areas of maximum warming, but the authors speculate that it might be the cloud cover responding to warming and newly ice free regions – underlining the intertwined relationships in the climate system, and especially in connection to clouds. The study also finds a correlation between poleward oceanic heat transport and the strength of amplification.

The changing sea ice cover is also appointed as the primary cause of amplification in the overview presented by *Serreze and Francis* [2006]. At the time of publication (2006) the warming amplification signal was yet to emerge clearly in observations (as noted by *Polyakov et al.* [2002]), which was explained with the Arctic being in an initial warming state, where the sea ice cover was thinning and retreating, while still not reduced enough to accelerate warming through SAF. While the validity of this conclusion is somewhat uncertain, it is clear that a warmer Arctic with a thinner sea ice cover would give rise to stronger SAF processes.

The general decrease in the area of the sea ice cover (which is the important
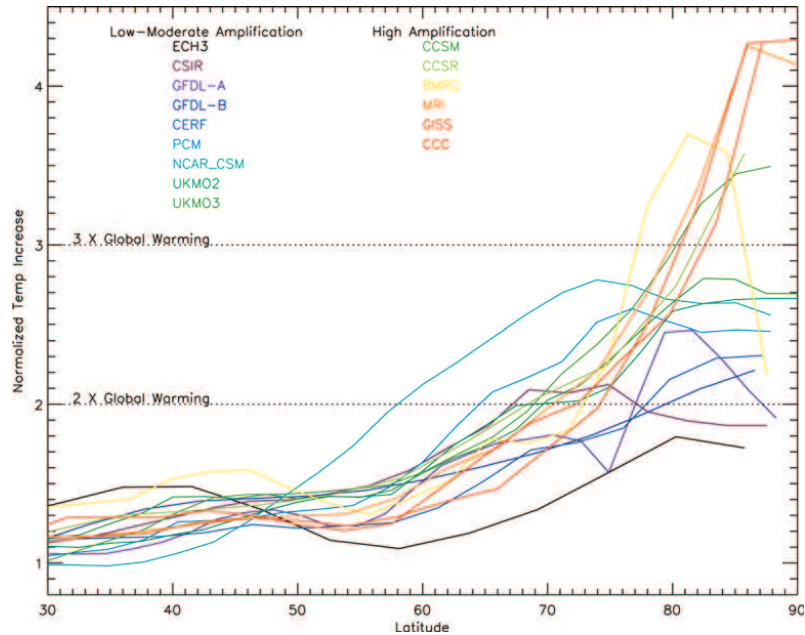
Figure 2.1: Arctic amplification in GCMs resulting from a $2\times CO_2$ forcing. The warming is normalized with global mean values. From: *Holland and Bitz* [2003].

measure in relation to SAF) has been accompanied by a thinning of the ice cover, which is evident in both observations (*Kwok and Rothrock* [2009]) and models (*Schweiger et al.* [2011]). Dynamic effects may have increased export of older, thicker ice from the Arctic Ocean (*Nghiem et al.* [2007]), but *Bitz and Roe* [2004] suggests that the thinning can be explained through thermodynamics alone, and is related to the fact that thin ice grows faster than thicker ice. This thermodynamic process is stabilising and constitutes a negative feedback, which limits the reduction of sea ice extent, as thin ice regrows faster than thicker ice. This process will thus limit the effect of the SAF, which would work to reduce the thin ice more than the thicker. Regardless of the background, the thinning of the sea ice cover has big consequences for its properties, and the response to future climate change. Following the 2007 record low sea ice extent minimum (at that time) *Maslanik et al.* [2007] concludes that general thinning of the ice cover gives increased potential for rapid extensive sea ice loss through warming or changed (wind-driven) transport patterns. The latter effect is another dynamical side to the SAF: increased export of sea ice from the Arctic Ocean and compacting of ice due to ocean currents and wind stress, also affects the albedo by changing the sea ice covered surface area. And as concluded by *Maslanik et al.* [2007] thinner and younger sea ice is more easily compacted than thicker ice that possibly have survived several melting seasons. *Holland and Bitz* [2003] also find that models with a thinner sea ice cover tend to have stronger Arctic amplification. This is however most likely connected to SAF caused by increased melting rather than changed circulation and compacting, as not all models include sea ice drift.

As recent years (beginning from the record low sea ice extent in 2007) have seen substantial reduction in the annual minimum sea ice extent, a clear warming signal should be expected following the arguments of *Serreze and Francis* [2006]. The paper has been followed up by a more recent review by *Serreze and Barry* [2011], in which it is concluded that "*the awaited signal is now here*" (referring to a clear Arctic warming amplification signal). The effect of SAF is still described as a dominant cause for the amplification, but several other contributing effects are recognized. These contributing effects have been investigated in a range of studies in the intermediate period, where Arctic amplification has become one of the main foci of climate research.

Climate models and specifically general circulation models (GCMs) are strong tools in investigating the mechanisms of the climate system, and have also been used widely in investigating Arctic amplification. Besides from providing estimates of future climate scenarios from induced changes and forcings, the models can also be used to isolate or eliminate certain mechanisms through "alterations" of the climate system in the model. *Alexeev* [2003] uses GCM simulations in such an altered climate system to assess the temperature response to a doubling of atmospheric CO_2. The climate system is altered into an *aquaplanet* without continents or sea ice (freezing ocean remain as water), where the surface albedo and solar radiation are fixed, and clouds have been omitted. These changes of course brings the model "world" further from the actual climate system of the Earth, but with all other processes intact the changes from the simplified model can be interpreted and extended to actual changes in the real climate system, and might reveal processes that are hidden in the more obscured, entangled system of mechanisms in the complete climate system. Simulations by *Alexeev* [2003] reveal that even with albedo effects excluded a clear pattern of Arctic amplification is seen in a climate forcing simulation – contesting the *traditional* interpretation of the amplification with sea ice related SAF as the main cause.

The finding that SAF effects may not be crucial to the existence of Arctic amplification is supported by *Winton* [2006], who analyses global warming simulations from 12 GCMs. The models exhibit clear Arctic amplification of 1.9 times global warming on average, which is within the lowest part of the range found by *Holland and Bitz* [2003] in the previous generation of models. An analysis of the underlying factors reveals that SAF, longwave (LW) feedbacks (here meaning the combined LW effects of changes in clouds, water vapour and temperature), and net TOA forcing (here meaning the sum of net surface flux and atmospheric heat convergence) all are favouring the amplification in the models, while "*SAF is shown to be a contributing, but not a dominating, factor*", as SAF produces the minor of three mentioned contributions. The analysis further reveals that direct CO_2 forcing and non-SAF shortwave (SW) feedbacks (meaning SW effects from clouds and water vapour) is inhibiting factors for the Arctic amplification. The former is a result of the relatively low vertical temperature gradient in the Arctic limiting the efficiency of greenhouse gases.

The approach used by *Winton* [2006] does unfortunately not allow for separation of the different contributions within the used groupings of longwave feedbacks and the TOA net forcing. In general, the pin-pointing from general changes to individual feedbacks or other mechanisms is difficult, which again gives rise to the use of modified GCM climate simulations. *Alexeev et al.* [2005] follows up on the earlier study, again using similar aquaplanet setups to assess the warming patterns in simulations with uniform global forcing, to simulations where the forcing is confined to the tropics and the extra-tropics respectively. The global uniform forcing yields the characteristic polar amplified warming response, which turns out to correspond quite accurately to the sum of the warming from the separate tropical and extra-tropical forcing simulations. Whereas the warming from the extra-tropical forcing is primarily confined to the extra-tropics, the tropics-only forcing results in a relatively uniform warming at all latitudes. This pattern is seen in simulations from two different GCMs that – otherwise – show quite different responses to the forcings (compare Figure 2.2 (a) and (b)). The authors find that this globally uniform warming from confined tropics-only forcing is a result of increased meridional heat transport (MHT) leading to a heating and moistening of the higher latitudes – i.e. the tropics-only forcing leads to higher latitude warming through heat transport and by initiating a local LW feedback in the polar region. This finding is supported by calculations with an energy balance model (EBM), which also indicates that the poleward latent heat transport increases in a warmer atmosphere (in line with similar findings by *Flannery* [1983]). The warmer air holds more moisture (following Equation (2.6)) and with constant north-south temperature gradient and eddy activity, this will result in increased latent heat transport towards high latitudes. This finding is supported by *Solomon* [2006], who based on GCM studies concludes that coherence between cyclone-development and latent heat release in a warmer, moister atmosphere results in significant increase in poleward dynamical heat transport, which causes additional warming of polar regions. The conclusions from these studies thus indicate that the Arctic amplification following a globally uniform forcing – such as an increased CO_2 concentration – is a combination of a local response to the high-latitude forcing and a remote response to the low-latitude forcing through increased atmospheric transports.

The role of this possible increase in MHT has been a key subject in the so-called *Arctic amplification debate*, and the relative importance of the local response (mainly SAF) and remote contributions (especially through atmospheric transport) has been the focus of many studies. Another GCM study by *Graversen and Wang* [2009] investigates the importance of SAF in Arctic amplification by locking the surface albedo to average climatological values. This setup is comparable to the aquaplanet studies mentioned above, but disables the albedo feedback without simplifying the system further. This makes parallels to the real world climate system more straightforward, but may cause problems with energy budget inconsistencies (cf. the authors' own discussion in the paper). A comparison of the
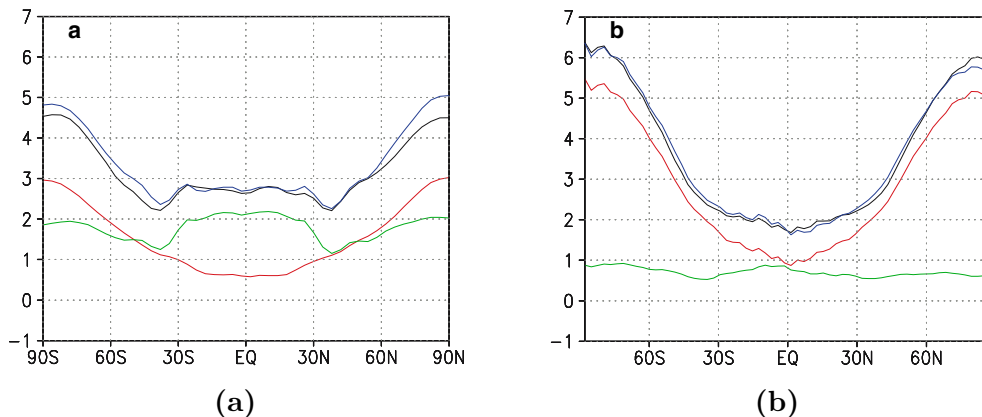
Figure 2.2: Warming [K] from 4 Wm^{-2} forcing in two different GCMs (**(a)** and **(b)**): Globally uniform forcing (*black*), tropics-only forcing (*green*), extra-tropics-only forcing (*red*) and the sum of tropics- and extra-tropics-only forcing (*blue*). From *Alexeev et al.* [2005].

locked albedo experiments to a "normal" variable albedo experiment reveals that both simulations have characteristic Arctic amplification, and that the warming only is 15% higher with an active SAF. The increased warming from inclusion of SAF is not only caused by SW forcing, but has a large contribution from LW forcing owing to increased amounts of atmospheric water vapour. The moistening is due to increased temperatures and sea ice reduction with SAF included – indicating that the model also simulate a coupling of the different feedbacks. Both simulations show increased heat and moisture transport into the Arctic, supporting the findings of the earlier mentioned studies. The authors conclude that the main factors behind the amplification are LW effects of increased water vapour and clouds, and that this increased moisture is caused partly by local, Arctic sources and partly by remote, low-latitude sources (through increased poleward latent heat transport).

In summary, these different model studies indicate that SAF may not be the main cause of Arctic amplification, as traditionally assumed. Ideally these results should be compared to observations in order to test the model-based hypotheses, but unfortunately there are only very sparse observational data for the Arctic, due to the area's remoteness and inaccessibility.

2.5.2 Re-analyses and the vertical structure of warming

Due to the limited amount of observational data from the Arctic, the so-called climate re-analyses have become central tools in analysing the Arctic climate. Re-analyses provide "complete" global datasets of meteorological parameters from simulations with a numerical weather prediction model, which assimilates a wide range of observed data. If the atmospheric parameters (e.g. temperature, wind, pressure, etc.) are known in two separate locations the model simulates a realistic pattern between the two observations, which creates global fields of all values. The

fields can of course not be considered as actual observations, but provide a plausible estimate, where no actual data is available. Caution is advised especially when observations are sparse. When observations are far apart, the area in between will be almost solely based on the model simulation, and remain unrestrained to the actual observed climate. Unfortunately the problem of sparse observations is very much relevant in the Arctic, where meteorological stations and observation are quite rare (cf. distribution of meteorological stations in *Bekryaev et al.* [2010] and *Polyakov et al.* [2002]). The "satellite era" has however increased availability of some types of observations, which has given increased accuracy of Arctic data in the re-analyses – for example by providing a continuous dataset of the sea ice extent. Among the most widely used re-analyses are the European Centre for Medium-range Weather Forecasts' (ECMWF) 40 year re-analysis spanning the period from 1957 to 2002 (*ERA-40, Uppala et al.* [2005]), the National Center for Atmospheric Research (NCAR) and National Centers for Environmental Prediction's (NCEP) re-analysis providing data from 1948 until the present (being continuously updated) (*NCEP/NCAR, Kalnay et al.* [1996]), and the more recent ECMWF Interim reanalysis, which is used in this project, covering the satellite era from 1979 to the present (*ERA Interim, Dee et al.* [2011]).

These reanalyses have also been widely utilised to assess the Arctic amplification – especially in the recent years of more dramatic Arctic climate change. As described above, the vertical distribution of warming can be used as an indicator of the origin of warming. Reanalyses contain extensive datasets of temperature fields throughout the vertical extent of the atmosphere, which – with the potential problems described above – provide a solid basis for assessment of the temperature changes throughout the vertical profile of the atmosphere. *Graversen et al.* [2008a] analyse data from ERA-40 to assess the underlying factors of the Arctic amplification. The data shows that the maximum warming is located "well above the surface" in all seasons except spring, which indicate that near-surface processes – such as SAF and increased ocean heat release – cannot be the main factors behind the accelerated warming. The warming signals correspond well to the idea that increased atmospheric heat transport into the Arctic is an important contributor to the amplification, and thus the authors regress the temperature field with the atmospheric heat transport across 60°N. The regression show a clear link between the atmospheric transport and the warming signal aloft in the summer half-year (April to October). The authors speculate that other possibly contributing factors to the warming aloft are changes in cloud cover and increased water vapour content (partly linked to the atmospheric transport of warmer, moister air). Although the static stability of the Arctic atmosphere is limited in much of the period from April to October, the warming peak aloft and the correlation with the increased transport, seems to clearly indicate that the upper level warming is caused by remote factors.

The study by *Graversen et al.* [2008a] has been contested afterwards, as the validity of the ERA-40 data within the Arctic has been questioned. Other data

sources like radiosonde data and passive microwave soundings (arising debate by *Thorne* [2008], *Grant et al.* [2008], and *Bitz and Fu* [2008]) compare poorly to the ERA-40 data. The debate of quality of the ERA-40 Arctic data is on-going, and several studies have been dedicated to investigate the differences between ERA-40 and other reanalyses with conflicting conclusions: *Mauritsen and Graversen* [2012] finds a high level of consistency in the overlapping period of ERA-40 and ERA-Interim, while *Screen and Simmonds* [2010a] conclude that ERA-40 is "*poorly suited to studying Arctic temperature trends*". *Graversen et al.* [2008b] argue that even though the magnitude of warming may be faulty in ERA-40 the vertical structure is similar to data from another reanalysis (JRA-25, *Onogi et al.* [2007]), and hence the conclusions from *Graversen et al.* [2008a] are valid. The findings are supported by the analysis of atmospheric circulation patterns by *Zhang et al.* [2008b], which using observations and NCEP/NCAR reanalysis data find a shift in the Northern Hemisphere circulation (from 2001 and onwards) that strengthens poleward heat transport.

Other reanalyses have been examined in the same way in a range of studies. Using the NCEP/NCAR and JRA-25 reanalyses *Serreze et al.* [2009] conclude that while there is evidence of warming aloft, the maximum warming is indisputably confined near the surface and highly correlated with regions of sea ice loss. The correlation is clearly seen in the graphic presentation of warming and sea ice loss in the autumn (September – November, SON) in Figure 2.3. This finding contrasts the signals in the ERA-40 data, and indicate that SAF and sea ice related changes are dominating. The near-surface warming signal is most pronounced in recent years – after the end of the ERA-40 data series – which combined with differences in data-assimilation, may cause some of the difference between the drawn conclusions. The somewhat varying conclusions from the different data sets stresses that reanalyses should not be viewed as actual observations, and that caution should be exerted when drawing conclusions based solely on reanalysis data.

As mentioned above, one of the newer reanalyses ERA-Interim covers the era of satellite observations from 1979 to present, which ensures consistency in the incorporated data, which cannot be achieved in reanalysis extending further back. The ERA-Interim data have been examined by *Screen and Simmonds* [2010b], who analyse the vertical structure of warming from 1989 to 2008. Again, the maximum warming is clearly situated at the surface, which the authors conclude is connected to the diminishing sea ice cover through a strong SAF and low level specific humidity increase (especially in newly ice free areas). Significant warming aloft is confined to winter, which hints that atmospheric heat transport does contribute to the warming, but the warming is still weaker than near the surface. A recent more comprehensive study by the same authors compare model simulations with data from ERA-Interim and three other reanalyses to investigate the contributions to the amplification further – with focus on the relative importance of local (mainly related to changing sea ice cover) and remote factors (mainly atmospheric heat
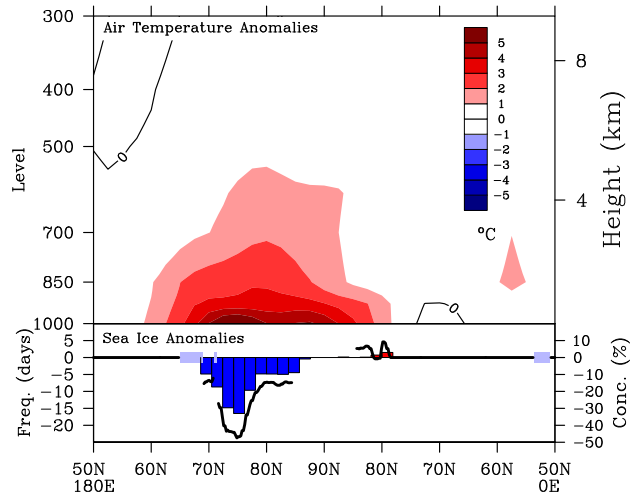
Figure 2.3: Near-surface warming – correlation between sea ice loss from satellite observations (lower panel, **black** graph) and warming (upper panel, **red** shading) in NCEP/NCAR. Values are means from 2003-07 compared to 1979-2007 means. From *Serreze et al.* [2009].

transport). *Screen et al.* [2012] uses three different model setups, with different combinations of sea surface temperatures (SSTs) and sea ice changes simulated with two different GCMs. The simulations reveal that changes in lower latitude SSTs cause an increased atmospheric heat transport, which is seen as a warming aloft in the Arctic, which is strongest in the fall (September-October). The authors conclude that this effect of remote SST changes account for 1/4 of the simulated Arctic warming (while only 1/6 of the "observed" – meaning in reanalysis data – Arctic warming). The remaining 3/4 are caused by local sea ice and SST changes. Figure 2.4 show the "observed" and modelled warming divided into two-month seasons together with the simulated contributions from local (ARC) and remote (REM) changes, and panel (d) clearly shows that the remote contribution to the Arctic warming can be seen as an elevated warming signal.
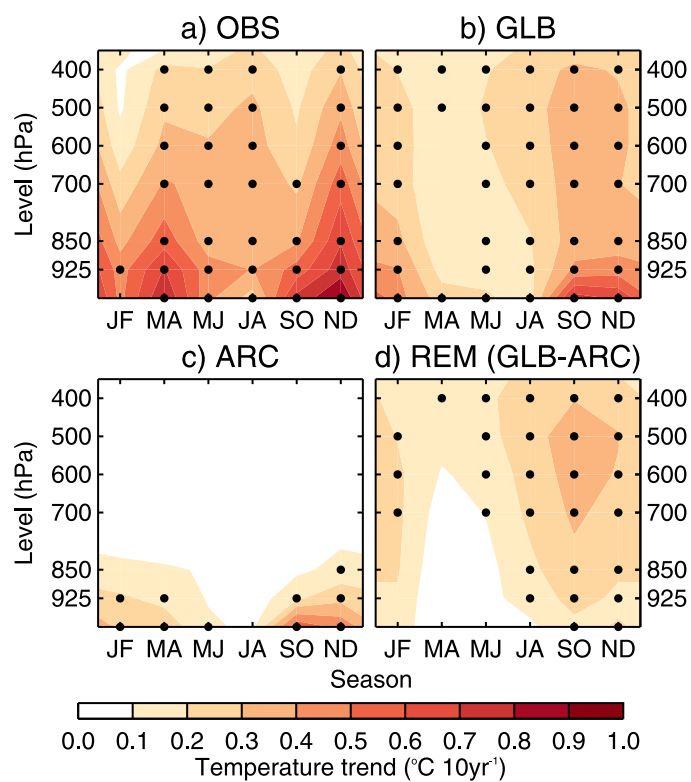
Figure 2.4: Vertical and seasonal structure of **(a)** re-analysis mean (OBS, upper left) and **(b)** simulated warming (GLB, upper right), which is divided into **(c)** local (ARC, lower left) and **(d)** remote (REM, lower right) contributions. From *Screen et al.* [2012].

2.5.3 Contributing factors to Arctic amplification

In summary of the studies mentioned above, Arctic amplification is resulting from the combined warming contributions from the following factors (compare with the review by *Serreze and Barry* [2011]):

– Surface albedo feedback (SAF)

– Heat flux from the ocean to the atmosphere (the insulation effect)

– Cloud cover

– Water vapour (increased humidity)

– Atmospheric heat convergence (poleward meridional heat transport)

– Heat storage in upper ocean (delayed warming effect)

Additionally changed ocean heat transports (*Holland and Bitz* [2003]), increased amounts of soot particles and black carbon on ice (*Hansen and Nazarenko* [2004]), and changes in the abundance of airborne aerosols (*Shindell and Faluvegi* [2009]) can be mentioned as possible contributing factors, but they are irrelevant in the context of this study.

It is noteworthy that a changing sea ice cover influences all of the listed factors (as the analyses here goes on to show), which underlines the importance for studying the impact of the recent and expected future reductions of the Arctic sea ice cover. The sea ice cover acts as the coupling between several feedbacks, and is one of the main reasons for the complexity of the climate system. This is clearly indicated by the linear patterns of change found in many idealized sea ice free, aquaplanet simulations (e.g. *Langen et al.* [2012]): the inclusion of the sea ice cover likely plays a central role in the introduction of more complex, non-linear patterns of change, through coupling of the different feedbacks.

3   Motivation and Method

The Arctic amplification debate is on-going, and contributions in several fields are needed in order to settle some of the disagreements presented above. The work presented in this thesis, is adding another piece to the puzzle, and seeks to clarify one of the cornerstones in the mechanism behind Arctic amplification.

3.1   Motivation

The inspiration for this thesis comes from the work by *Chung and Räisänen* [2011], in which the authors compare the characteristics of Arctic warming in climate model data to reanalysis data. As evident from the research described earlier, results from GCM modelling studies and reanalyses are not always in agreement, and thus a comparison and an assessment of the background for the differences is an obvious and needed contribution to the Arctic amplification debate. Some of the conclusions by *Chung and Räisänen* [2011] have unfortunately been drawn on a questionable basis, and hence the analyses in this thesis aim to investigate the validity of these conclusions.

Chung and Räisänen [2011] present results on the relative importance of the underlying reasons for Arctic amplification, specifically the role of SAF (and other surface based changes) compared to the changes in poleward atmospheric heat transport. One part of this investigation is a comparison of GCM and reanalysis data, which aims to assess the performance of the models in describing "the actual climate" (here represented by reanalysis data). The reanalysis data is taken from the ERA-Interim reanalysis (*Dee et al.* [2011]), and the GCM data is taken from the *World Climate Research Programme's Coupled Model Intercomparison Project (Phase 3)* (CMIP3), which is a collection of model output from the leading climate models (*Meehl et al.* [2007a]). The different models simulate identical scenarios, and the average of the results from the respective models (the multi-model mean) have been widely used as a "best estimate" of a given climate scenario, as individual model biases seem to cancel out (as concluded in the IPCC AR4, *Randall et al.* [2007]). The CMIP3 collection of data was intended as a basis for the analyses in the IPCC AR4 (published in 2007), and thus represents data from state-of-the-art models at that time.

The authors compare seasonal means of the vertical structure of warming in the model and reanalysis datasets averaged over the entire Arctic domain (70 - 90°N), and focus on the changes in winter (DJF, December-February) and summer (JJA, June-August).
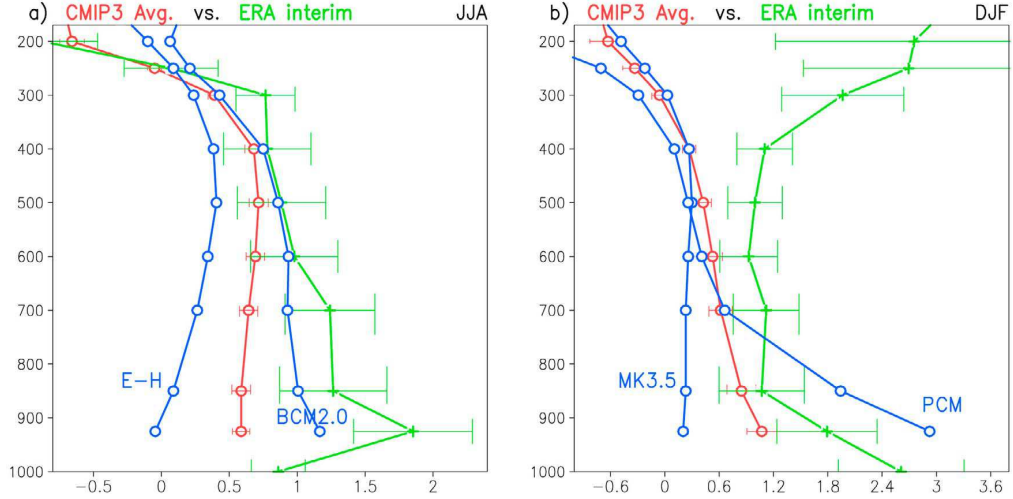

Figure 3.1: Arctic temperature change from ERA-Interim 1979-2010 (green) and CMIP3 multi-model mean 1970-99 (red) with selected individual models that deviate the most from the mean (blue). Vertical levels [hPa] on the y-axis, temperature change [K] on the x-axis. **Left**: summer/JJA average, **Right**: winter/DJF average. From *Chung and Räisänen* [2011].

The vertical structure presented in Figure 3.1 is used to argue that climate models "*over-simulate the role of poleward energy transport in Arctic warming*", since the models generally show warming at higher levels than the reanalysis. The authors especially focus on the JJA mean, as they argue that this is the best season to assess the influence of remote forcing (i.e. poleward heat transport), as their modelling studies suggest that remote forcing "*creates warming maxima at much higher altitudes than the local forcing in summer*". From the first glance at Figure 3.1 the conclusion seems valid; the vertical structure of CMIP3 mean does have maximum warming around 500 hPa in JJA, and seemingly fails to capture the near-surface warming in both JJA and DJF.

Closer examination of the compared data however reveals that the different structures may have an entirely different explanation. The first issue is that the compared data does not represent the same period, as the CMIP3 data spans 1970-99, while the reanalysis data cover 1979-2010. A very central question is thus if the same structure should be expected from the two only partially overlapping periods? My expectation is that the vertical structure of warming should be different in the two periods, as the reduction of the Arctic sea ice cover has rapidly increased in recent years, which would cause a pronounced change in the warming – especially near the surface. The authors do briefly note that the comparison between

mismatching periods is "undesirable".

Additionally the widely cited work by *Stroeve et al.* [2007] shows that climate models as a group (specifically the CMIP3 models) tend to underestimate the sea ice loss in a warming climate. The biggest sea ice loss is seen around the yearly minimum in ice extent[1] in September, but both the sea ice loss and the "overly conservative" ice melt in the models are evident throughout the year. Figure 3.2 clearly shows that the CMIP3 models dramatically underestimate the sea ice loss – a fact that is emphasized further by extending the observational time series with the latest all-time minimum ice extent observation from September 2012.
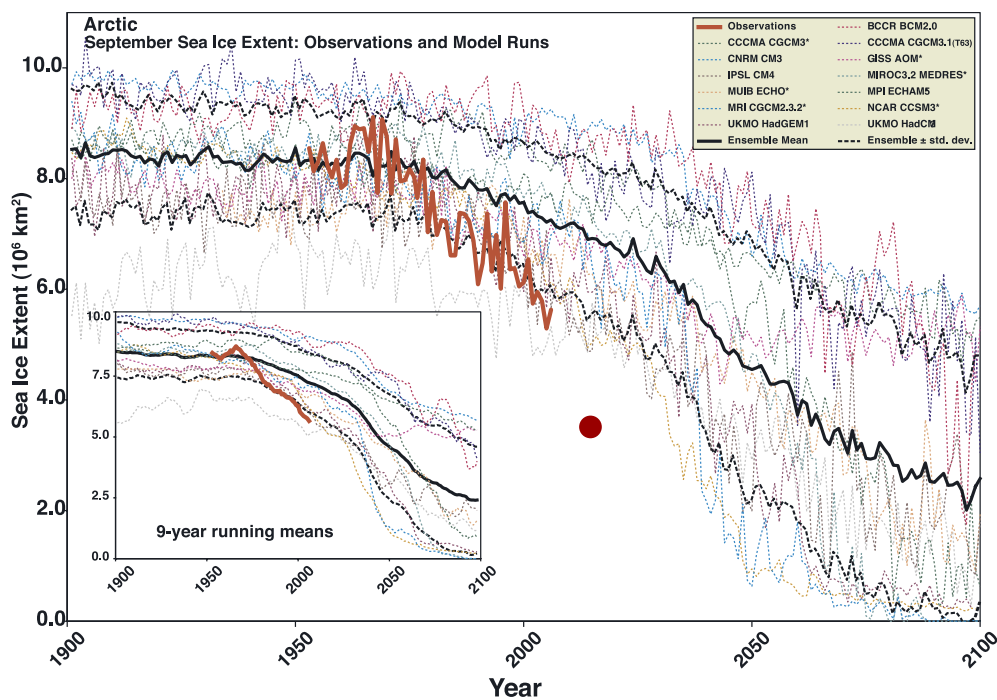
Figure 3.2: Mean September sea ice extent in 10^6 km^2. Individual CMIP3 models in various colours, CMIP3 mean in **thick black** and observed value in dark-red. Dark-red dot denotes approximate 2012 September extent ($3.41 \cdot 10^6$ km^2, source: NSIDC web [2012]). From *Stroeve et al.* [2007] (modified).

The reduction of the sea ice cover is expected to affect the vertical structure of warming, and by extension the comparison in Figure 3.2 could indicate that the models perhaps under-simulate the low-level warming, rather than over-simulate upper-level warming – a conclusion that could also be drawn from Figure 3.1.

I suspect that the difference between the compared vertical profiles is entirely

---

[1]Sea ice *extent* is here defined as the area with at least 15% sea ice concentration.

caused by the reduction of the sea ice cover in recent years, and that the conclusion of the over-simulation of the high-level warming by the models thus may be invalid. As a consequence of the two described issues, the CMIP3 mean represents a warming signal from a much smaller reduction of the sea ice cover, and should be expected to show a more limited near-surface warming than the ERA-Interim data. The aim of this thesis is therefore to assess the effect of a reduced sea ice cover on the vertical structure of warming, and in that light re-evaluate the conclusions of *Chung and Räisänen* [2011].

3.2 Experiments

To investigate the effect of a reduced sea ice cover on the vertical structure of warming, two GCM experiments are proposed. The experiments take two different approaches to enforce a reduced ice cover in the model climate system, and let different parts of the climate system respond to the changes. One lets only the atmosphere respond, while the other allows for a "more complete" response incorporating an active upper ocean and sea ice cover. The experiments are designed to examine the direct effect of a changed ice cover with all other factors being constant. Although relatively different in technical setup, the two approaches are essentially used to assess exactly the same thing – the response of the chosen atmospheric circulation model to a reduced sea ice cover.

Experiment 1: Fixed SST setup

The first approach is using an atmosphere-only GCM coupled to a sea surface with fixed temperature and sea ice conditions. Sea surface temperatures (SSTs) and sea ice conditions are prescribed in monthly mean values, which are then temporally interpolated in the model to vary daily. The objective is to compare the atmospheric response to the two different sea ice conditions behind the CMIP3 and ERA-Interim warming signals from *Chung and Räisänen* [2011]. Two model simulations will be made with the same SST field, but with sea ice cover from the CMIP3 multi-model mean and ERA-Interim respectively – the ERA-Interim sea ice cover being more reduced than the CMIP3. The results from the two simulations, combined with a common reference climate from a control simulation, will then be analysed in terms of the vertical structure of warming, and compared to the results from *Chung and Räisänen* [2011] – i.e. the model output will be used to create a new version of Figure 3.1 with the model's reproduction of the warming structure. The result will indicate, how the atmospheric climate model responds to a reduced sea ice cover, and reveal whether a reduction could explain the difference between the vertical structures in Figure 3.1.

Experiment 2: Slab ocean setup

The approach above keeps SST and sea ice conditions fixed at all times, and thus prevents interaction and feedbacks from ocean and sea ice cover. These feedbacks

could be included in the response with an inclusion of an active ocean and sea ice cover in the model. Including ocean and sea ice as active elements in the model, however, means that it is not possible to prescribe the conditions, and thereby induce a stronger reduction of the sea ice cover. In light of the analysis by *Stroeve et al.* [2007] the model is expected to respond with too little sea ice reduction in response to warming. A touch of creativity is thus needed, in order to obtain an increased sea ice reduction, while still keeping the physics of the model unchanged. The approach used here, is to reduce the albedo of the sea ice. An albedo reduction will cause an increased absorption of incoming shortwave (solar) radiation, which will work towards an increased melt of sea ice during the sunlit period in the Arctic. The albedo change should not be seen as an attempt to *fix* the model, but simply a way of letting the model climate system respond to a more reduced sea ice cover. How the more reduced state arises is not central – the effect of the reduction is the focus of this work. These simulations will be done by coupling a so-called *slab ocean* (representing the upper, mixed layer of the ocean) with a thermodynamic sea ice scheme to the atmospheric model. Within the relative small climatic changes investigated here, this study most likely would not benefit from incorporation a full ocean model – this would only result in longer, more costly simulations.

3.3 Model technicalities

The climate model employed here is the Community Atmosphere Model version 3 (CAM3) developed by the National Center for Atmospheric Research (NCAR) (*Collins et al.* [2004]). CAM3 is an atmospheric GCM, which is integrated together with a land model (CLM, Community Land Model, *Bonan et al.* [2002]), and either a data ocean or slab ocean model, which includes a thermodynamic sea ice model. All experiments in this project are done in a T-42 spectral resolution, corresponding to a grid of 64 latitudes by 128 longitudes producing a resolution of approximately $2.8° \times 2.8°$. The atmosphere is divided into 26 levels in the vertical, which are described in hybrid-sigma pressure coordinates (purely sigma coordinates near the surface gradually changed towards pure pressure coordinates at the TOA – illustrated in *Collins et al.* [2004, Fig. 3.1]).

Ocean and sea ice models

CAM3 can be run with either a data ocean model (meaning fixed SST and sea ice conditions, *DOM*) or a slab ocean model (*SOM*) with a thermodynamic sea ice model and an active upper ocean. The DOM requires input of monthly mean SST and sea ice concentration values in all grid points, which will be set as conditions in the middle of each month. Both SST and sea ice values will vary daily, and each day will be assigned values based on linear interpolation between the two neighbouring monthly means – i.e. the value on the first day of a given month will be the average of the previous and the current monthly means. The flux balance at the surface is decided by the specified SSTs over open ocean, while some variation happens over land and sea ice surfaces, where the temperature, snow cover and

other factors are allowed to vary. The read-in sea ice cover is given by the fractional ice cover (i.e. sea ice concentration) in a given grid cell, and will be set to a thickness of 2 meters in all points (in the Arctic, only 0.5 meters in the Antarctic). In the DOM case the sea ice model thus only decides the fluxes between the sea ice and the atmosphere, which depends on surface temperature, snow cover and energy transfer through the ice (*Collins et al.* [2006]), as the annual cycle of the sea ice cover is completely fixed.

The SOM model is designed to mimic the flux exchange in a fully coupled GCM, while avoiding the expense of fully integrated ocean and sea ice models. In the SOM setup the SSTs and sea ice fraction and thickness are calculated actively by the model, as the ocean temperature is decided by the heat content of the slab mixed-layer ocean column, and ocean points below freezing will initiate sea ice formation. The mixed layer depth can vary between 10 meters and 200 meters, and is allowed "smooth" variations between the grid cells. Here, however, the mixed layer depth is chosen to the constant value of 50 meters everywhere. The mixed-layer ocean is motionless, and perfectly mixed vertically, and has an internal energy source, corresponding to ocean heat transport convergence. The energy fluxes corresponding to the transports of the ocean (e.g. seasonal deep water exchange and horizontal ocean heat transport) are incorporated through the so-called Q-flux. The Q-flux is usually obtained through a DOM simulation, with prescribed SSTs and sea ice cover, and all other parameters corresponding to the desired climate for the SOM simulation. The Q-flux should "distribute" energy such that the flux balance at the surface in the SOM simulation is similar to that of the control DOM simulation, and can thus be derived from the net surface flux F_{NET} in the DOM simulation:

$$\rho c_p h \frac{\partial \text{SST}}{\partial t} = F_{\text{NET}} + Q \tag{3.1}$$

where ρ is the density of sea water, c_p is the ocean heat capacity, and h is the depth of the mixed layer. The Q-flux is adjusted to ensure energy conservation (i.e. that the global mean is zero), and further adjustments are made in regions of sea ice, to ensure that the additional heat convergence or divergence does not alter the sea ice cover in a non-physical manner (*Collins et al.* [2006] and *Bitz et al.* [2012]). The active sea ice model calculates sea ice concentration and thickness (i.e. growth and melt), which primarily depend on the temperature. Additionally the model calculates the surface albedo (from the combination of the sea ice surface and snow cover), the energy flux through the ice, the internal energy of the ice (including creation of brine pockets), and the ice growth from snow-to-ice conversion.

3.4   Model modifications

Bitz et al. [2012] describes how the original CAM3 SOM produces some poor results, especially in relation to sea ice and the Arctic area in simulations of a warming climate. The errors are owing to an undesired effect of the Q-flux formulation and an oversight in the energy budget scheme. As the Arctic sea ice is

the focus of this study, these unphysical forcings have been corrected following the improvements suggested by *Bitz et al.* [2012].

The first problem is related to the Q-flux adjustments, which are calculated continuously "on-the-fly" in the original model. The continuous adjustment causes a gradual reduction of the poleward oceanic heat transport, because the surface fluxes are changed, when the Arctic sea ice cover decreases. This un-physical, undesired redistribution of energy changes the spatial pattern of the warming, and thus might affect the climate change – especially through feedback processes. This problem is avoided by fixing the Q-flux, i.e. turning off the on-the-fly adjustment, and instead include a constant, climatological mean value of the Q-flux adjustment in each grid cell. This introduces the need for an additional SOM control simulation, which is used to obtain a climatology of adjustments corresponding to the desired climate state.

The second issue is that the model does not account for the latent heat release from snow falling into the ocean. Snow falling on land and ice is treated correctly, and the atmosphere is gaining heat when ice is formed, however this part of the latent heat budget has been overseen. The magnitude in terms of the global energy budget might not be huge, but this additional latent heat is very relevant within the Arctic. A minor code change has been made to the SOM, which now includes the latent heat from snow falling on the ocean surface in the simulations.

3.5 EXPERIMENT DETAILS

FIXED SST

The DOM simulation is done with input from the ERA-Interim reanalysis and from the CMIP3 multi-model mean, in the form of global fields of SSTs and sea ice fractions. All the CMIP3 models have simulated a range of scenarios, and the output from the individual models[2] contains a wide range of climatic output variables. The scenario used in this context is the "Climate of the 20th century" (*20C3M*) experiment, which is a *historical* simulation with known forcings (e.g. orbital parameters and CO_2 levels). The model outputs are provided on the native grids of the individual models, meaning that interpolation is needed to obtain a multi-model mean in the desired T-42 resolution used in this experiment. A bi-linear interpolation scheme has been chosen, as the – originally preferred – spectral interpolation scheme (interpolation between fixed and Gaussian grids using spherical harmonics) resulted in a noticeable diffusion of the fields. The diffusion probably arises as a result of poor treatment of steep gradients, which are relatively common in connection with sea ice fractions. The bi-linear scheme on the other hand performed the interpolation without any significant modification of the fields. Following the interpolation sea ice values were rounded off to ensure values between

---

[2]collected by PCMDI, available from the ESG data portal archive (see PCMDI web [2013])

0 and 1, and the SST minimum was set at the assumed freezing point at -1.8°C
(following *Hurrell et al.* [2008]).

To ensure a fair basis for comparison the CMIP3 multi-model mean was calcu-
lated from the same group of models used in *Chung and Räisänen* [2011] – the 10
selected models are shown in Table 3.1[3].

3.1 CMIP3 Model Ensemble		
Developer	**Country**	**Model acronym**
Bjerknes Centre for Climate Research	Norway	BCCR-BCM2.0
National Center for Atmospheric Research	USA	CCSM3
Canadian Centre for Climate Modelling&Analysis	Canada	CGCM3.1
Centre National de Recherches Météorologiques	France	CNRM-CM3
CSIRO Atmospheric Research	Australia	CSIRO-Mk3.5
Max Planck Institute for Meteorology	Germany	ECHAM5/MPI-OM
NOAA / Geophysical Fluid Dynamics Lab.	USA	GFDL-CM2.1
NASA / Goddard Institute for Space Studies	USA	GISS-AOM
National Center for Atmospheric Research	USA	PCM
Hadley Centre / Met Office	UK	UKMO-HadGEM1

Table 3.1: List of models used in CMIP3 multi-model mean

The sea ice fraction and SSTs are re-gridded and averaged into multi-model means
over 5-year periods. This is done to ensure that the annual cycle is fairly smooth
(i.e. contains no discontinuous jumps from December to January). The reference
simulation (CTRL-DOM) is based purely on CMIP3 data: the multi-model mean
of sea ice and SST from 1979-83. The two *forced* scenarios to be compared, in the
style of *Chung and Räisänen* [2011], are both based on SST fields from the mean
of the CMIP3 models from 1995-99 (the last five years of the 20C3M simulations).
The ice cover, which is the only parameter that varies, is based on the CMIP3 mean
from 1995-99 and the ERA-Interim mean from 2006-10 respectively (hereafter
CMIP and ERA-Ice). The years from 2006-10 are chosen for the ERA-Interim
mean, as these are the latest five years of the reanalysis and represent the recent
period with a more reduced sea ice cover. A third simulation is made solely with
data from ERA-Interim: both sea ice and SST mean fields from 2006-10 (ERA-
All). A comparison between the three simulations, referenced to the CTRL-DOM,
should then illustrate the influence of (1) a reduced sea ice cover and (2) more
recent (warmer) global SSTs. All four simulations are done with the same physical
parameters (insolation, atmospheric composition, etc.) to isolate the effect of
the induced changes in sea ice cover and SSTs. The differing details of the four

---

[3]Note that 12 models are part of the original multi-model mean, as three versions of the
GISS model is included in the original study by *Chung and Räisänen* [2011]. Only one version
is included here due to lack of available data.

simulations are shown below in Table 3.2.

| 3.2 DOM Simulations: Sea ice and SSTs		
Simulation	**Sea Ice Data**	**SST Data**
CTRL-DOM	CMIP3 1979-83	CMIP3 1979-83
CMIP	CMIP3 1995-99	CMIP3 1995-99
ERA-Ice	ERA Int. 2006-10	CMIP3 1995-99
ERA-All	ERA Int. 2006-10	ERA Int. 2006-10

Table 3.2: List of input fields in DOM simulations. "CMIP3" refers to the multi-model mean annual cycle, and "ERA Int." to the mean annual cycle from the Interim reanalysis data.

Figure 3.3 shows the seasonal means of the different Arctic sea ice covers used in the simulations. The comparison of the sea ice covers reveals two main differences between the CMIP and the two ERA simulations: (1) A reduction near the Siberian coast in summer (JJA) and autumn (SON), and (2) A year-round reduction of sea ice in the Barents Sea area. (1) corresponds well to the observed reduction in the sea ice cover observed in recent years (*Comiso et al.* [2008] and *Kumar et al.* [2010]), while (2) does not correspond to any observed pattern. *Arzel et al.* [2006] notes that the CMIP3 models generally tend to build up too much sea ice in the Barents Sea area. *Chapman and Walsh* [2007] suggest that the build up of ice could be connected to model inability to simulate North Atlantic storm tracks, which causes a cooling bias in the Barents Sea area. A second speculation could also be that the models build up ice in the Barents Sea due to poor representations of dynamic features like the Transpolar Drift Stream (which causes the vast export of sea ice southward through the Fram Strait) – *Kwok* [2011] does find a general displacement of large-scale features in the sea ice circulation pattern. According to *Arzel et al.* [2006] the Barents Sea area is the only major deviation, and otherwise there is *reasonably agreement* between the CMIP3 model mean and the observed sea ice extent. From a spatial large-scale point of view, this agrees well with the sea ice covers used here, as the remaining differences between the CMIP3 1995-99 and the ERA Interim 2006-10 mean corresponds well to the observed changes in the intermediate period.
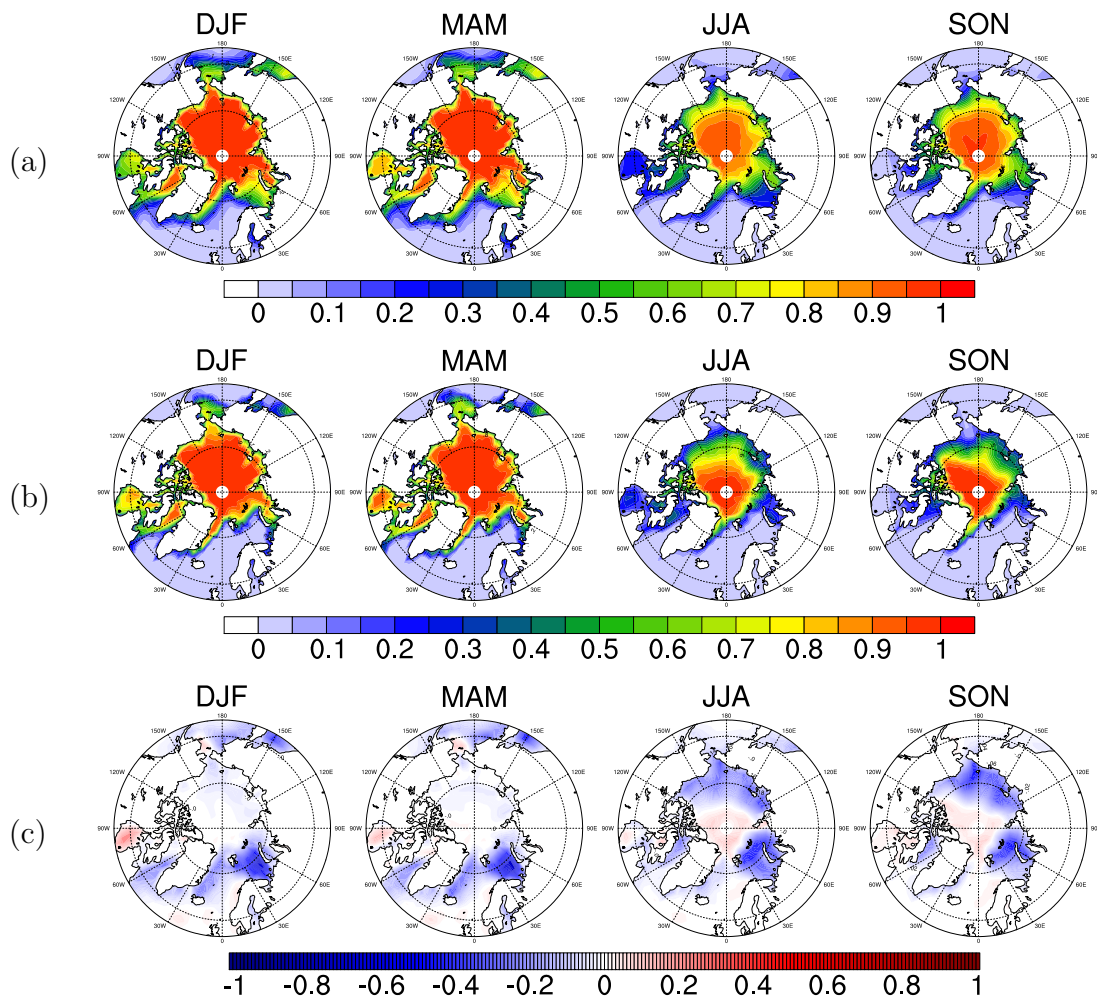
Figure 3.3: Sea ice cover fields used as input for the DOM simulations. (a) CMIP3 multi-model mean 1995-99, (b) ERA Interim 2006-10 mean, (c) Difference: **Blue** (**red**) shading indicates reduction (increase) in the ERA simulations compared to CMIP.

A similar comparison of the global SST fields reveal – as expected – that the ERA Interim 2006-10 mean is significantly warmer than the CMIP3 1995-99 mean – Figure 3.4 displays the difference between the seasonally averaged zonal means of the two Northern Hemisphere SST fields.
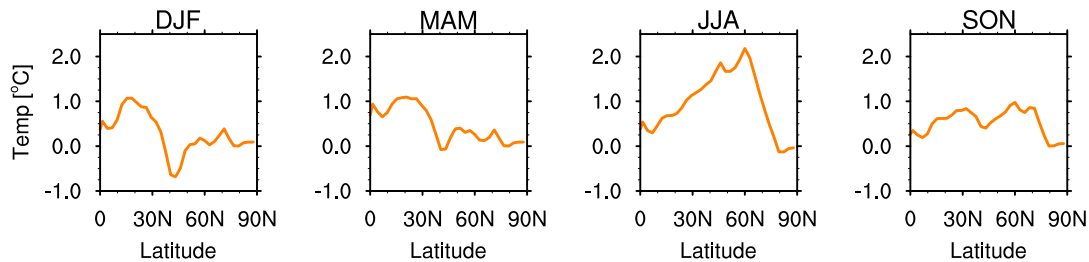
Figure 3.4: Difference in SST between CMIP3 1995-99 multi-model mean and ERA Interim 2006-10 mean – positive values indicates that the latter is warmer.

Generally the ERA SSTs are warmer with a few seasonal, regional exceptions. The polar region has comparable temperature in the two fields, while the lower latitudes show a spatially varying warming pattern throughout the year. Winter (DJF) and spring (March, April and May, *MAM*) show maximum warming in the Tropics, while summer (JJA) warming peaks in the mid-latitudes (45°-60°N) and the autumn (SON) show a more evenly spread warming throughout the hemisphere (excluding the polar area). The warming trends shown in Figure 3.4 should *not* be interpreted as an analogue to the actual warming from 1995-99 to 2006-10, as it is the difference between two different data sources: the CMIP3 model mean, which have no constraints with respect to real climate observations, and the ERA Interim data, which is assimilated towards observed data. The CMIP3 SST field is affected by model biases such as the unnatural cooling in the Barents Sea (described above), which can distort the temperature patterns – meaning that the difference between model mean data and re-analysis data should not be interpreted as actual climate change.

SLAB OCEAN

The slab ocean experiment consists of two series of simulations, which differ only in the value of the albedo of the sea ice cover. Both series consist of four scenarios: a reference climate, a "present day" climate, and two future scenarios with 1.5 and 2 times the reference atmospheric CO_2 concentration. The unchanged series is referred to as "NOALB", while the series with albedo reduction is entitled "ALB".

Using Q-flux tuning (by means of a DOM simulation, as described above) the control climate is tuned towards the ERA Interim SST and sea ice data means from 1979-83 (corresponding, but not exactly similar, to the control climate of the fixed SST experiments, which are based upon the CMIP3 mean of the same

period). Note that since the sea ice cover is generated with the sea ice model, it cannot replicate the reanalysis data. Hence, some significant differences can be expected, as the purely thermodynamic ice model does not include the dynamic effects of wind and ocean currents, which greatly influence the configuration of the ice cover in the real climate system. The tuning does, however, ensure that the SOM model climate state is similar to that of the introduced data fields.

The forced scenarios are obtained from the control climate simply by increasing the CO_2 level. In the present day scenario the CO_2 is changed corresponding to the observed increase in radiative forcing from 1979 to 2010. This induced change in CO_2 level thus corresponds to the combined radiative forcing from all GHGs, aerosols and ozone changes in this period, and the value is found through a back-of-the-envelope calculation based on radiative forcing data from the IPCC AR4 (*Forster et al.* [2007]): The total growth in radiative forcing from 1960 to 2000 is approximately 1.13 W/m^2, and assuming linear growth in this period (fair assumption, cf. Figure 2.23 in IPCC AR4, *Forster et al.* [2007]), an estimate for the increase in forcing per year can be found. Utilizing the fact that a doubling of the atmospheric CO_2 concentration corresponds to a radiative forcing of 3.7 W/m^2 (*Forster et al.* [2007]), this growth rate can be expressed as a change in CO_2 – which can be extended beyond 2000 assuming that the growth pattern is unchanged. The radiative forcing has a logarithmic dependence on the CO_2 concentration, and can be expressed as (e.g. *Harvey* [2000]):

$$\Delta F \propto \log\left(\frac{C}{C_0}\right) \tag{3.2}$$

$$\Rightarrow \quad \Delta F = A + B \log C \tag{3.3}$$

$$\Leftrightarrow \quad C = \exp\left(\frac{\Delta F - A}{B}\right) \tag{3.4}$$

where ΔF is the radiative forcing (equivalent to the change in flux-balance), C the atmospheric CO_2 concentration (expressed as mixing ratio), and A and B are constants. Using the control simulation as starting point, the two points

$$(C, \Delta F) \in \left\{\left(355 \text{ ppm}, 0 \text{ W/m}^2\right); \left(720 \text{ ppm}, 3.7 \text{ W/m}^2\right)\right\}$$

are used to calculate values of A and B, and the CO_2 concentration can thus be estimated from equation (3.4) using radiative forcing estimates based on the IPCC AR4.

The increased loss of sea ice is achieved through an albedo reduction, which will effectively reduce the sea ice cover in the sunlit months, due to increased absorption of solar SW radiation. The same procedure has been used by *Sedláček et al.* [2012], who employ albedo reductions of sea ice and snow cover as a "*physically consistent way to introduce a perturbation*". The tuning of the sea ice albedo is here done in a quite simple manner, by introducing a parameter (`albsic_factor`) expressing the change factor corresponding to the desired increase or decrease in

the albedo – meaning that a factor of 0.9 will result in a 10% decrease of the sea ice albedo in all points. The albedo module of the model is left unchanged, and the surface albedo of the sea ice is calculated as designed taking e.g. ice thickness and possible snow cover into account. At the very end of the routine, when all factors have been accounted for, the albedo-value is multiplied by the factor, changing the following calculations of the radiative balance. This has been implemented in the model using a flag (`albsic`), to indicate whether albedo modifications are desired or not.

```
if (albsic) then
   asdir(i) = asdir(i)*albsic_factor
   aldir(i) = aldir(i)*albsic_factor
end if
```

where `asdir` and `aldir` denotes the albedo-value of directly incident radiation in two different wavelength intervals (both in the shortwave range of the spectrum).

Alteration of the sea ice albedo will of course also alter the reference climate, and comparison between the changes with and without the albedo-change might therefore not be ideal. To circumvent this issue, the control climate of the albedo-tuned simulation is Q-flux tuned towards the same climatic state as the unchanged reference – towards ERA Interim mean values 1979-83. This ensures some resemblance of the two control climates, while they might not be exactly similar. The SST values should be comparable, as they are largely determined by the Q-flux, but nevertheless the albedo change might change the conditions for the sea ice cover. The conceptual idea of the Q-flux tuning towards the same climate is illustrated in Figure 3.5.

The promising look of the conceptual idea is not exactly obtained, as it seems the sea ice cover is not completely constrained by the Q-flux field, which results in a difference between sea ice covers of the two control climates – as shown in Figure 3.6. The ice covers are completely identical in winter, as the darkness means that the albedo-change has absolutely no effect on the energy budget. In summer (JJA) and autumn (SON), where the albedo change has a significant effect on the system, there is a slight difference in the sea ice cover of the two control simulations. The general difference of the climate states is, however, significantly reduced, compared to what could be expected without the Q-flux tuning procedure.

This SOM experiment is, as mentioned, done for different magnitudes of forcing. The 2006-10 (present day) analogue is designed to approximate the observed sea ice cover from this period (within the limitations of the SOM sea ice model), and should be equivalent to the scenarios in the DOM experiment. The climate change, and hence the induced forcing over the approximately 30 years examined here is
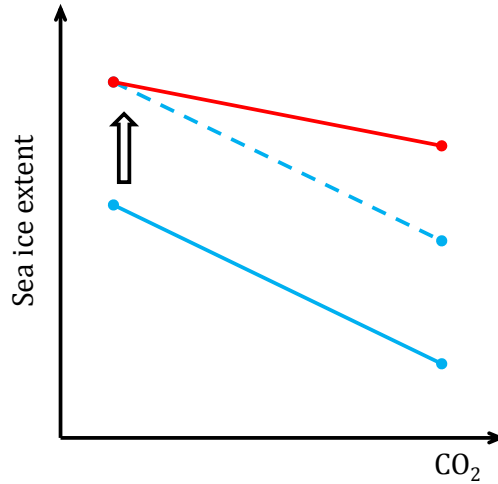
Figure 3.5: Conceptual sketch of the difference between the reference (red) and the albedo-tuned (blue) simulations. The starting point illustrates the level of sea ice in the control simulations, while the end point represents the forced simulations. The Q-flux tuning is illustrated by the thick **black** arrow, which acts to "move" the sea ice cover in the albedo-tuned simulation from the solid to the dashed blue line.
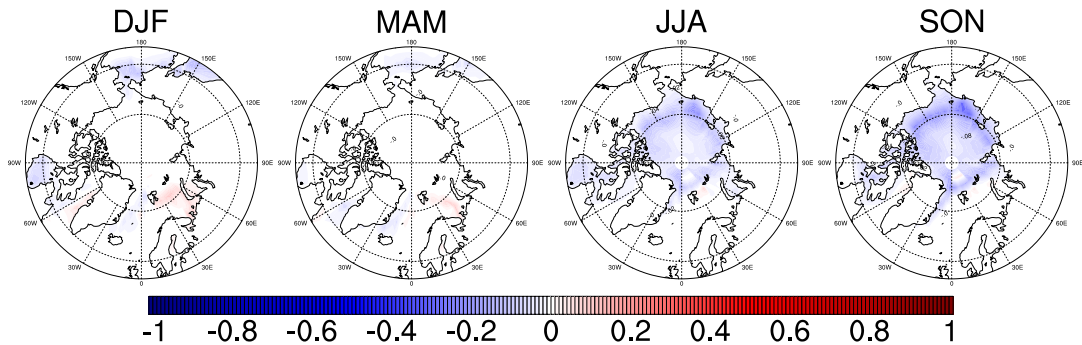
Figure 3.6: Difference in sea ice cover between the reference simulation of the SOM control (NOALB-CTRL) and albedo-tuned simulations (ALB-CTRL). **Blue** shading indicates that the sea ice cover is reduced in the latter.

however limited, and the results of the changing ice cover might "disappear" in the noise of the natural variability of the model climate system. Therefore the two more severe forcing scenarios of 1.5 and 2 times the reference CO_2 level is included, as the pattern of change might be clearer in the scenarios with notably larger forcing. An overview of the two series of simulations is given in Table 3.3.

The albedo-factor of 0.94 (corresponding to a 6% reduction of the albedo) is chosen, based on an estimate calculation and a series of test-simulations. A "ballpark" estimate of the albedo change has been made based on the Arctic mean of the downwelling shortwave radiation at the surface (obtained from a control simulation), and an estimate of the approximate forcing from 1980-2010 (based on the IPCC AR4, *Forster et al.* [2007]). This rough estimate yields an albedo reduction

3.3 SOM simulations: Albedo and CO_2		
Simulation	**Albedo-factor**	**CO_2 level**
NOALB-CTRL	–	355.0 ppm
NOALB-PD	–	409.5 ppm
NOALB-1.5	–	532.5 ppm
NOALB-2	–	710.0 ppm
ALB-CTRL	0.94	355.0 ppm
ALB-PD	0.94	409.5 ppm
ALB-1.5	0.94	532.5 ppm
ALB-2	0.94	710.0 ppm

Table 3.3: List of SOM simulations.

of about 2%, while the following test-simulations indicated that $\sim 6\%$ was a better fit to the expected forcing resulting changes in the sea ice cover.

This set of simulations constitutes a solid basis for multiple comparisons analogue to (but perhaps more extensive than) the DOM experiments. Comparisons within each series gives estimates of the warming resulting from the combination of different magnitudes of CO_2 forcing and the following SST and sea ice changes, while comparison "across" the series (i.e. comparing NOALB and ALB simulations with equal forcing) corresponds to assessing the warming caused by sea ice changes only. The main focus will be on the comparison of the near-present-day climates NOALB-PD and ALB-PD simulations, as they can be seen as an analogue to the changes induced in the DOM simulations. The more severely forced scenarios, however, reveal how the climate changes in the (perhaps not so distant) future, with a more reduced sea ice cover tending towards seasonally ice free conditions. The ice covers of the different simulations are presented under Results (Section 4.2).
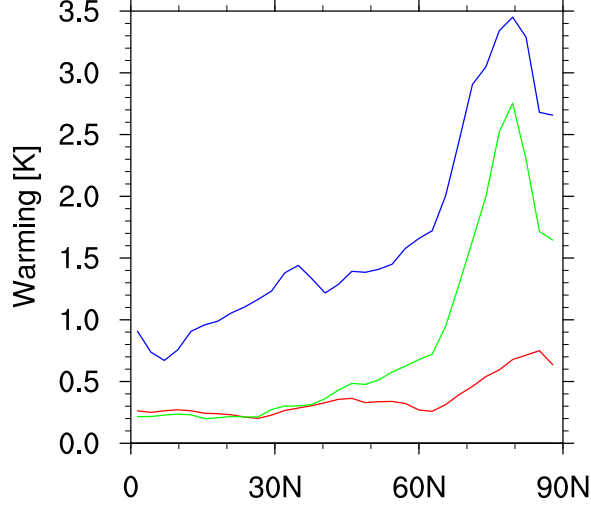
4 RESULTS

All simulations (DOM and SOM) are run for at least 30 model years. The mean of the series of model years is used as a best estimate of the climate response to the introduced changes, which in this contexts is either a sea ice cover reduction, SST increase, or CO_2 increase. The initial years are excluded from the mean, as the model climate is allowed to respond to the changes and reach a new quasi-equilibrium climate state. This period, in which the model climate adjusts to the changes, is often called the spin-up period, and its length depend upon the type of model (here DOM or SOM) and the initial conditions. The spin-up time is longer when the slab-ocean and active sea ice is included, as the atmosphere responds relatively fast to changes. Hence the spin-up time of the DOM simulations is primarily decided by the changes in the land points, which has slightly longer response time than the atmosphere. The response of the land points is in turn quicker than the response of the upper ocean in the SOM setup. A "better safe than sorry"-approach have been employed here, and thus 2-3 years have been excluded in each DOM simulation and approximately 10 years in each SOM simulation (depending on the magnitude of the introduced changes compared to the initial conditions). The length of the spin-up period has been decided in each individual simulation using an assessment of the net TOA radiative balance and the global mean temperature – the climate is assumed to be in a quasi-equilibrium state, when the two variables reach steady values. The analysis in this project will be based on the mean, quasi-equilibrium climate states, but the individual years will be used to assess the variability and the statistical significance of the observed changes.

4.1 DOM EXPERIMENTS

4.1.1 ARCTIC AMPLIFICATION

The results from the simulations of the three DOM scenarios indicate that both the sea ice cover and the SSTs greatly influence the warming pattern in the Arctic. All three simulations show clear Arctic amplification of near-surface warming, and both the SST increase and the more drastic sea ice reduction causes an increased amplification – individually, as well as combined. The Arctic amplification is clearly seen in Figure 4.1, where the Northern Hemisphere zonal mean warming

compared to the reference climate (CTRL-DOM) is shown for all the simulations.

Figure 4.1: Zonal mean warming in all DOM simulations compared to CTRL-DOM: CMIP (**red**), ERA-Ice (**green**) and ERA-All (**blue**).

The reduction of sea ice from CMIP to ERA-Ice results in a noticeable increase in the Arctic amplified temperature response. The latitude of maximum warming is not at the pole, but located around 80°N, coinciding with the area of sea ice retreat. The same pattern is seen in a few models in Figure 2.1, while the maximum warming is further north in the majority of the models. This is most likely explained through the $2\times CO_2$ forcing behind the warming in the analysis by *Holland and Bitz* [2003]. The stronger forcing causes a bigger reduction of sea ice than induced here, meaning that the sea ice edge would retract further north.

The warmer SSTs in ERA-All do not seem to favour Arctic amplification, as the additionally Arctic warming is of the same size (if not smaller) than that of the mid-latitudes compared to ERA-Ice. To further clarify this difference, the so-called *amplification index* is calculated. The amplification index is the ratio of average Arctic warming relative to the entire Northern Hemisphere average. The values for the three simulations are displayed in Table 4.1.

| 4.1 DOM: Arctic Amplification	
Simulation	**AA index**
CMIP	1.98
ERA-Ice	4.55
ERA-All	2.37

Table 4.1: Arctic amplification indices for the DOM simulations: Arctic warming relative to average Northern Hemisphere warming.

The amplification indices show that the ERA-Ice simulation have the strongest Arctic amplification signal. The SSTs in ERA-All have a significant warming in the lower latitudes (Figure 3.4), and the direct effect is not expected to favour an amplified Arctic signal. Arctic warming is however increasing (Figure 4.1) even without any significant warming of Arctic SSTs. This indicates that the lower latitude SST warming in an indirect manner affects the Arctic climate.

4.1.2 SURFACE ENERGY FLUXES

The induced changes in the sea ice cover affect the climate through alterations of the shortwave, longwave, and the turbulent energy fluxes, as explained in the Scientific Introduction (Section 2.2), while changing the SSTs further changes the longwave and turbulent budgets. The shortwave budget is not directly affected by the SSTs, but can be altered indirectly, e.g. through increased evaporation resulting in cloud formation. The surface flux differences between the CMIP and ERA-Ice simulations show the direct effect of the induced sea ice changes – presented in Figure 4.2. Note that due to the nature of the experiment, the shortwave flux is neither shown nor included in the net flux, as shortwave changes due to sea ice reductions do not work to warm the atmosphere. Warming of the ocean would occur in the actual climate system, which would lead to indirect warming of the atmosphere through increased turbulent and longwave heat fluxes, but these effects are disabled in this fixed SST setup. As SSTs are fixed, the additional heat from absorbed SW radiation "disappears" into the ocean surface. From an energy conserving perspective, the DOM setup is therefore somewhat problematic, as warm (cold) SSTs will act as *unlimited* sources (sinks) of heat. Despite the energy concerns the fixed-SST setup is, however, accepted as an easily computed, but yet accurate estimate of climate change (e.g. *Hansen et al.* [2005]). *Deser et al.* [2009] compared flux changes resulting from reduction of the sea ice cover in an atmospheric GCM with prescribed sea surface conditions to the results of a fully coupled GCM simulation, and found very similar responses.

Figure 4.2 indicates that the flux changes follow the changing sea ice cover. The biggest sea ice reduction is in autumn (SON), and results in a significant increase of longwave and turbulent energy from the surface to the atmosphere, which continues into winter (DJF). In the autumn, the incoming sunlight is already limited in the Arctic, and the ocean is generally warmer than the atmosphere. The now ice free ocean can freely transfer energy to the atmosphere, where the sea ice before acted as an insulating layer between ocean and atmosphere. The increased heat transfer is especially seen in the increased sensible heat, but also in the longwave flux. The increase in the turbulent heat fluxes from the ocean to the atmosphere is balanced by an opposite effect in the adjacent areas equatorward of the sea ice reductions. The same pattern is observed in similar studies of sea ice reduction (*Magnusdottir et al.* [2004] and *Deser et al.* [2000, 2009]), and can be explained through the atmosphere-ocean interaction at the edge of the insulating sea ice
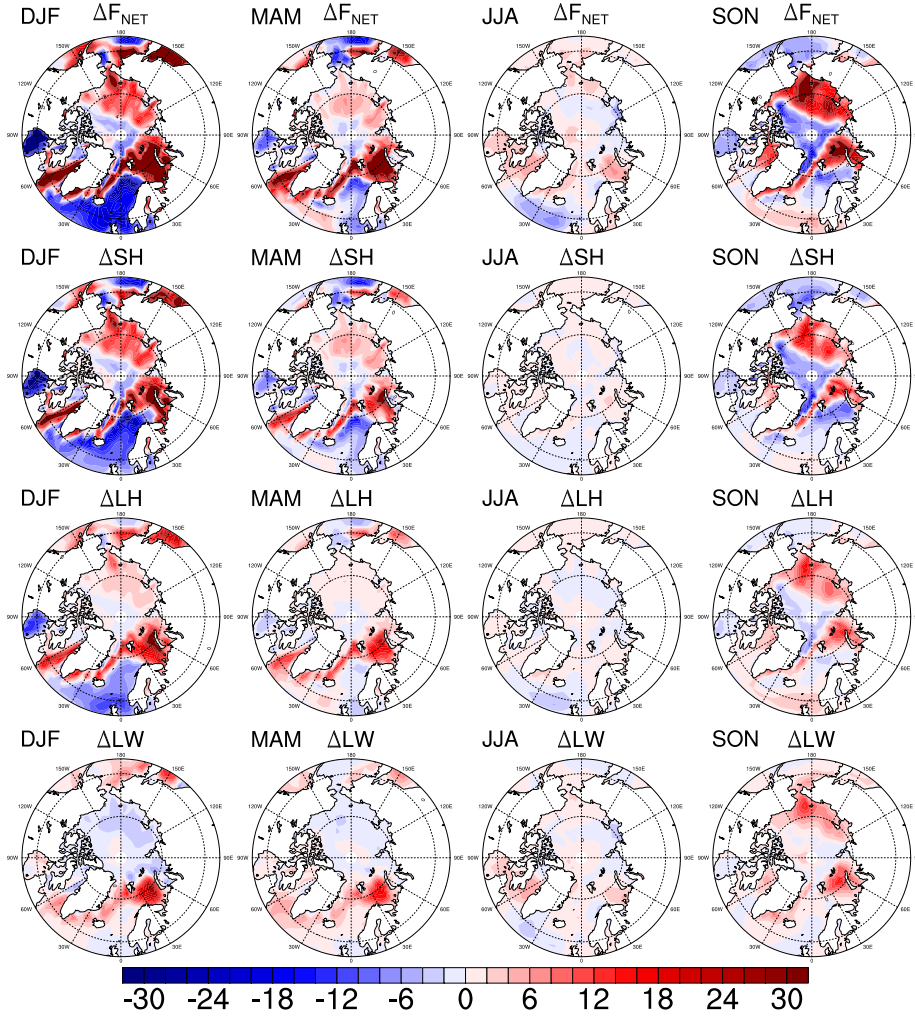
Figure 4.2: Surface fluxes in W/m^2 – difference from CMIP to ERA-Ice. Displaying all four seasons from left to right (DJF, MAM, JJA and SON) for all the surface energy flux types. From the top: Net flux, sensible, latent, and longwave fluxes. Positive changes are fluxes directed upwards from the surface.

layer. The sea ice cover inhibits heat and moisture fluxes between ocean and atmosphere, which (at least in the cold seasons) leaves the air above the ice covered regions very cold and dry – i.e. the sea ice cover changes the climate regime from marine to more continental characteristics. At the ice edge the cold and dry air regains contact to the much warmer open ocean, and the steep gradients in heat and moisture causes a substantial turbulent energy flux from the ocean to the atmosphere. The steep gradients will gradually be smoothed out southward from the ice edge, which will quickly limit the energy flux. As the ice edge is positioned more northerly in ERA-Ice than in the CMIP simulation (Figure 3.3), the region of high turbulent energy flux from the ocean to the atmosphere also shifts northward, which leaves the dipole-signature seen in turbulent flux change in Figure 4.2: A reduction just south of the previous ice edge, and an increase near the new ice edge, over the previously ice covered area.

The analysis of the surface energy fluxes reveals that the turbulent fluxes (especially the sensible heat) are the dominant drivers of the surface based changes, with a limited contribution from the longwave fluxes. It should be noted that while the maximum sea ice changes are found in the autumn (SON), the flux changes are equally big (if not bigger) in winter (DJF). This delay is confirmed by the annual cycle of the net surface flux in Figure 4.3, which shows the monthly variation of the sea ice cover and the Arctic mean fluxes. The net flux, which is driven by the turbulent energy flux changes (note the different scales in Figure 4.3), increases from September until it peaks in February, which is consistent with maximum warming sometime during the winter season. Hence the climatic changes are delayed somewhat compared to seasonal cycle of the sea ice cover – similar patterns are seen by *Parkinson et al.* [2001] and *Deser et al.* [2009].
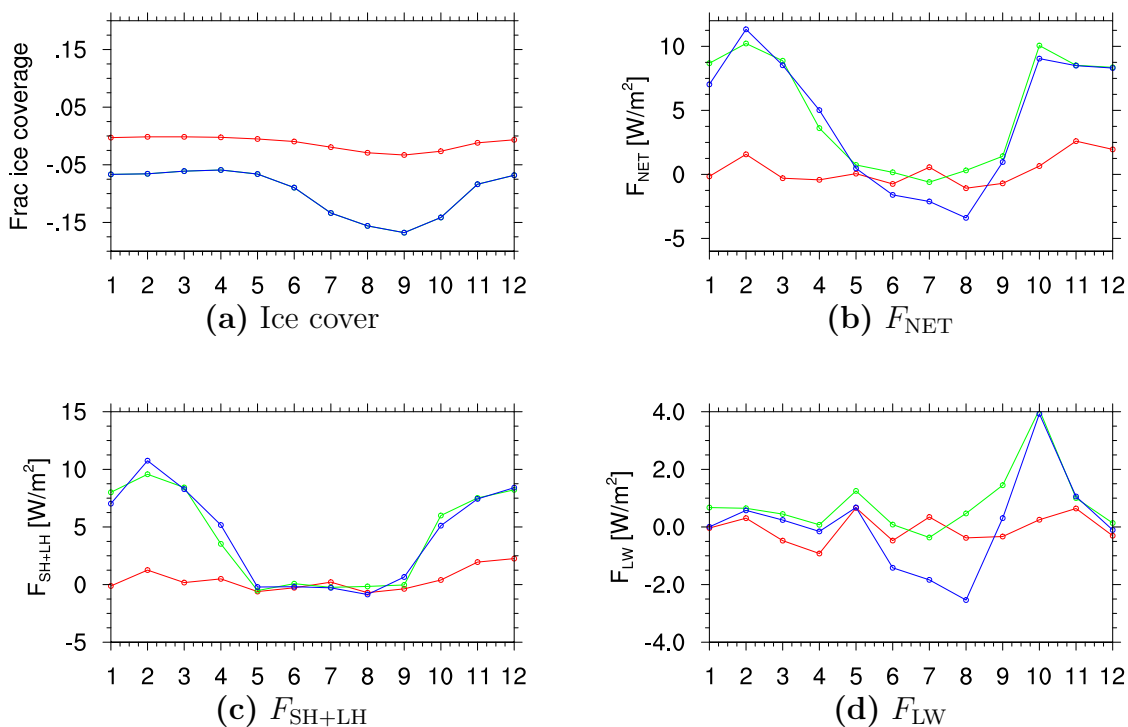
Figure 4.3: Monthly variations of sea ice and surface fluxes in Arctic means for CMIP (**red**), ERA-Ice (**green**), and ERA-All (**blue**). **(a)** Sea ice (note that ERA-Ice and ERA-All are identical), **(b)** Net flux, **(c)** Turbulent, and **(d)** Longwave flux.

Figure 4.4 shows increased surface air temperature in ERA-Ice compared to CMIP (i.e. the result of the 2006-10 mean sea ice cover reduction), which reveals that the spatial pattern of the warming resembles the pattern of the sea ice loss (compare with Figure 3.3), and consequently also the pattern of the surface fluxes. The largest warming is correlated with the areas of immense sea ice loss, and is thus found during SON and DJF in the Barents Sea and the East Siberian Sea (off

the coast of Siberia, extending towards Alaska). This high spatial correlation is in line with similar studies investigating the surface air temperature changes following sea ice reduction in climate models, observations, and reanalysis data (e.g. *Serreze et al.* [2009], *Kumar et al.* [2010] and *Porter et al.* [2011]).
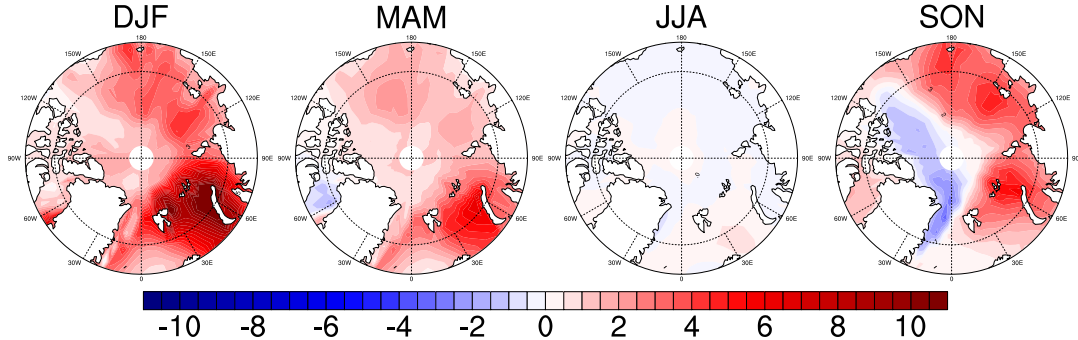
**Figure 4.4:** The seasonal Arctic surface air (2 meter) temperature change [K] in ERA-Ice compared to CMIP. Positive values indicate warming in ERA-Ice.

Especially the SON pattern strongly resembles the sea ice changes. Even the slight increase in the sea ice concentration north of Greenland and the Canadian Archipelago extending towards the North Pole is seen as a clear cooling signal, which is most likely connected to an increased "insulation effect": The increased density of the sea ice cover limits the heat transfer from the relatively warmer ocean to atmosphere.

4.1.3 Vertical structure of warming

The vertical structure of the Arctic warming is calculated by comparing the three scenarios to the same reference climate (CTRL-DOM), resulting in the profiles shown in Figure 4.5 along with the variability in each of the three simulations. The variability at each level is indicated by error bars of two standard deviations of the ensembles of the individual model years – i.e. error bars at level p are defined by $T_{\mathrm{mean}}(p) \pm 2\sigma(p)$. Note that the lowest level of the vertical profile is chosen at 975 hPa, instead of the more obvious choice at 1000 hPa. The 1000 hPa mean value is often not well determined, as some seasons may have several cases where the surface pressure is consistently below 1000 hPa, as a result of deep low pressure systems in the Arctic (*Serreze and Barrett* [2008]). Consequently the 1000 hPa mean would only be based on a subset of the individual model years, while the preferred value at the 975 hPa level is consistently above the mean surface pressure, and thus includes all years in the mean. This choice of the near-surface pressure levels applies to all vertical profiles presented in this thesis.

A comparison of the CMIP and ERA-Ice simulations (red and green respectively, in Figure 4.5) reveal that the reduced sea ice cover has a significant impact on
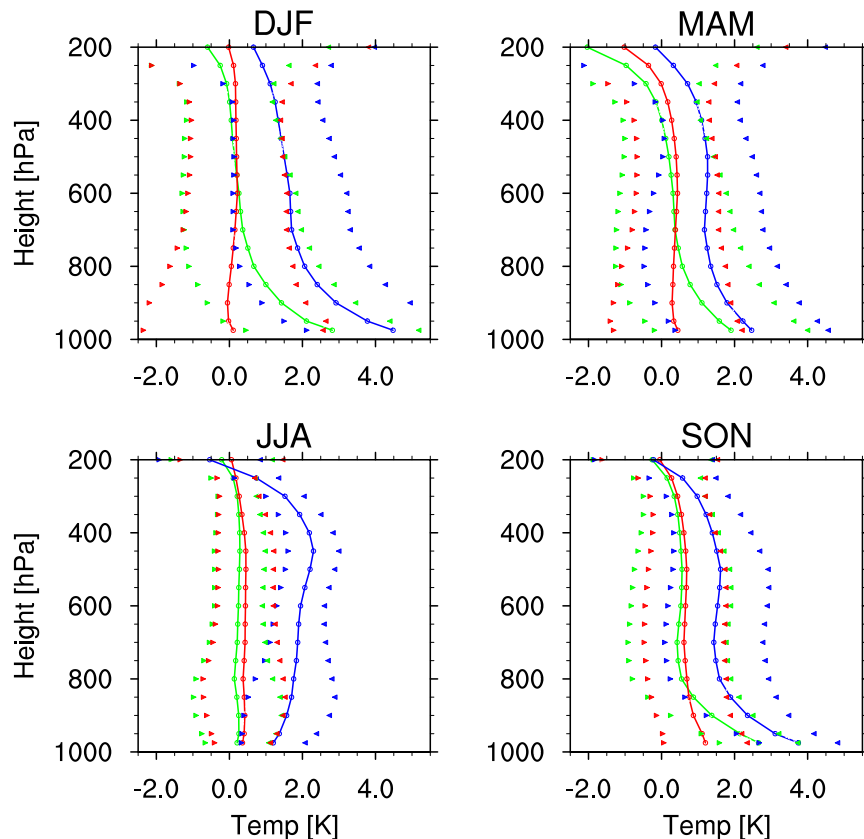
Figure 4.5: The vertical structure of warming in the DOM simulations: CMIP (**red**), ERA-Ice (**green**), and ERA-All (**blue**). Arrows indicate $\pm 2\sigma$ at each level for each of the profiles.

the low level warming, while the upper levels are left unaffected. Winter (DJF) show the most pronounced change with increased near-surface warming above 2 K in ERA-Ice compared to CMIP, while spring (MAM) and autumn (SON) have an increase around 1 K. The summer warming profile is very similar in the two simulations, and almost equal to the reference climate. The increased warming in winter, means that the sea ice reduction results in a model-generated warming structure, which resembles the lower part of the ERA-Interim mean used in the analysis by *Chung and Räisänen* [2011] (compared with Figure 3.1). The near-surface peak (around 950 hPa) in JJA is however still not evident from the model results, even with the reduced sea ice cover accounted for.

The pattern is for a large part consistent with the difference in the surface fluxes (Figure 4.2). Due to the high static stability of the Arctic lower atmosphere, the warming from the turbulent surface fluxes is expected primarily to heat the low-ermost layers, with maximum warming at the surface gradually decreasing in the vertical, at least in the colder seasons. Hence the increased turbulent fluxes can explain the increased near-surface warming in MAM, SON, and especially DJF. The increase outgoing longwave surface flux from the newly ice free areas will likely have a more vertically widespread warming effect, as the radiation is gradually ab-

sorbed by greenhouse gases and water particles (liquid water or ice, especially in clouds), which are distributed throughout the atmospheric column.

The warmer SSTs of ERA-All also change the vertical structure of Arctic warming, although SST changes within the Arctic are limited (Figure 3.4). The winter, spring and autumn profiles show an unchanged structure compared to ERA-Ice, but with an almost uniform warming at all levels – about 2 K in DJF and 1 K in MAM and SON. The summer profile has noticeable warming aloft with a maximum around 500 hPa, while the near-surface warming is limited. The latter is line with the expected, as the near-surface temperature will be kept near freezing as long as sea ice is present – as explained earlier; all additional energy will act to melt ice rather than warm the ambient air. The warming aloft could be a result of an increased atmospheric heat transport from lower latitudes, as found in reanalysis data around 600 hPa by *Graversen et al.* [2008a] and around 500 hPa in the CMIP3 mean and the GCM simulations by *Chung and Räisänen* [2011].

4.2 SOM experiments

4.2.1 Ice cover and surface fluxes

The forced simulations of the albedo-tuned simulations are based on three different scenarios: a 2006-10 analogue ("present day", suffix "PD"), a CO_2 doubling (suffix "2"), and an in-between scenario (1.5 times the reference CO_2 level, suffix "1.5"). The development of the sea ice cover is central to this analysis, and a comparison of the different states in the CO_2 forced and albedo-tuned scenarios provide a broader basis for the interpretation of the warming signal. The total area of sea ice is reduced following both increasing CO_2 concentrations and sea ice albedo reductions, but a closer examination of the sea ice area (absolute area of sea ice cover) and extent (area of grid cells with at least 15% sea ice cover) does not exactly duplicate the look of the idealised sketch in Figure 3.5: The two control climates have differing sea ice covers. The September and annual mean sea ice extent and area (shown in Figure 4.6) reveal that despite the Q-flux tuning, the sea ice covers in the control climates differ. Nevertheless the desired effect of accelerated sea ice loss is obtained through the sea ice albedo reduction, and the combination of the albedo reduction and doubling of CO_2 results in almost completely ice free conditions at the annual minimum.

Despite the differing sea ice covers of the control simulations, Figure 4.6 indicates that the albedo change has worked as planned, as the ALB simulations show a steeper slope (i.e. a more drastic reduction) than the NOALB simulations. The September annual minimum is the final result of the melt period, and thus a good indicator of the effect of the albedo reduction. Therefore it is satisfactory that the September extent clearly show the desired accelerated loss of sea ice. The September area initially exhibits the same trend, while a flattening of the slope is
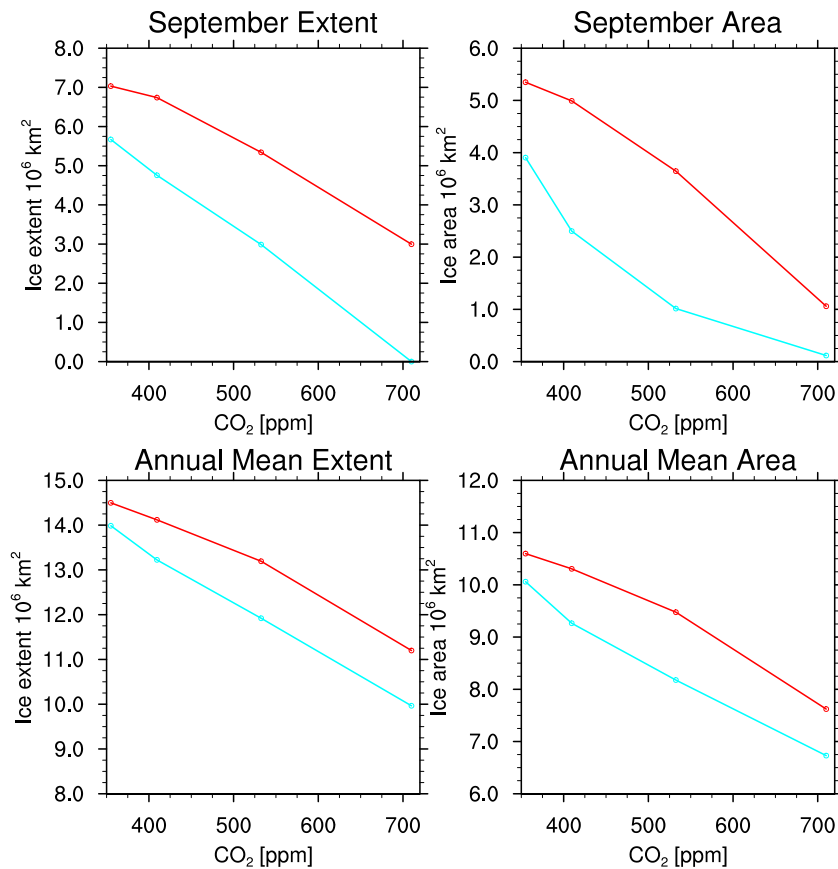
Figure 4.6: September and annual mean sea ice extent and area for the NOALB (**red**) and ALB (**blue**) simulations series shown as a function of the CO_2 concentration.

seen following the ALB-1.5 simulation. This is expected as a result of the very low abundance of sea ice – there is simply no more ice left to melt, and the remaining ice is likely be more "stable" (i.e. less sensitive to warming, resulting from residence at higher latitudes, orographic or other geographical features).

The ALB-PD simulation was designed as an analogue (in terms of sea ice loss) to the ERA-Ice DOM scenario, but has a more limited ice cover reduction. This is primarily owing to the fact that the Q-flux tuning did not bring the ALB-CTRL simulation to the same sea ice extent as NOALB-CTRL. It is, however, still a good basis for comparison, as the vertical structure of warming is in focus rather than the magnitude of the temperature increase. Due to the strictly thermodynamic sea ice model, the sea ice cover and the pattern of reduction will have a different spatial distribution than the reanalysis data used in the DOM simulations – Figure 4.7 shows the sea ice covers of the NOALB- and ALB-PD simulations (compare with the reduction in the DOM simulations in Figure 3.3).

Evidently the model does not duplicate the pattern of sea ice loss seen in the observations (here meaning reanalysis data). The reduction is more general and
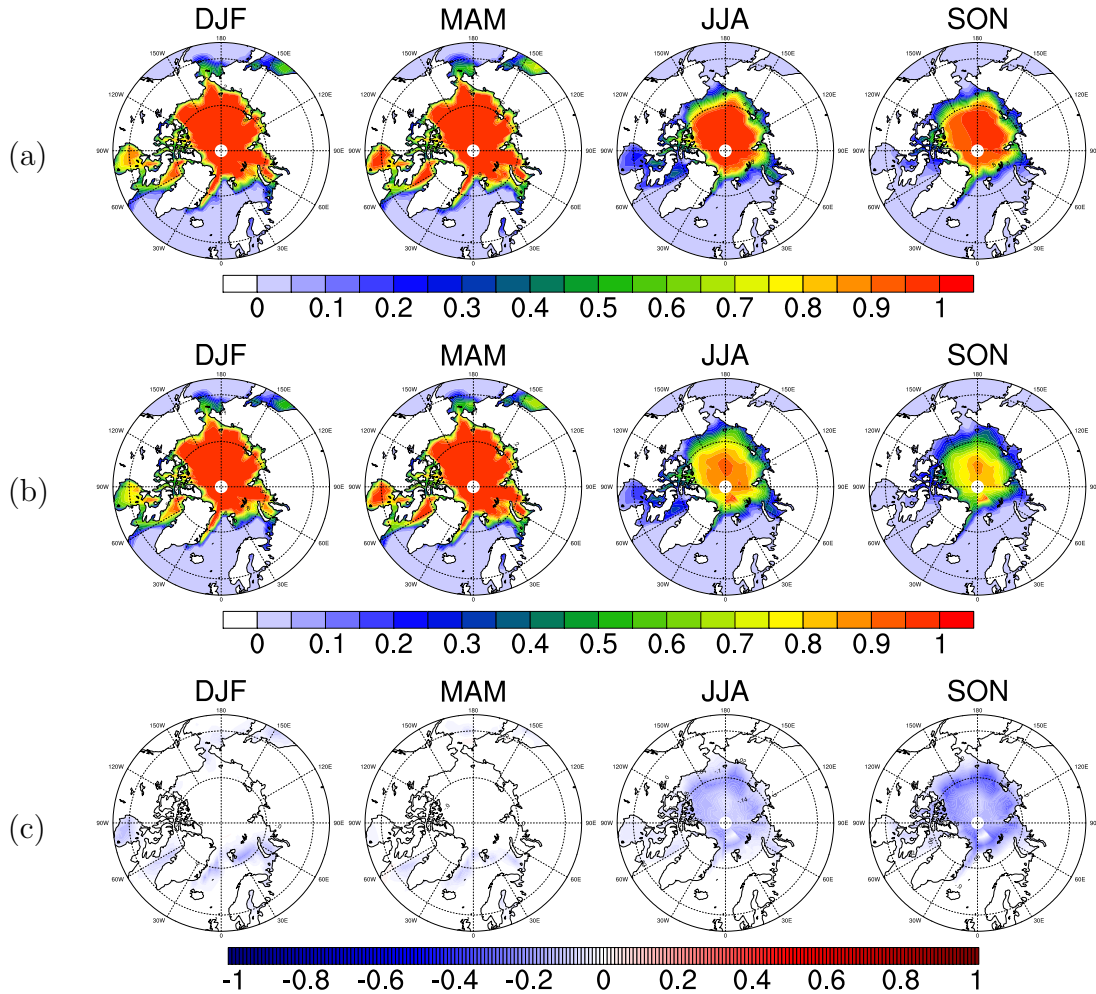
Figure 4.7: Seasonal sea ice cover from the SOM simulations. (a) NOALB-PD, (b) ALB-PD, and (c) Difference ALB-PD - NOALB-PD: **Blue** shading indicates reduction from NOALB to ALB.

spatially uniform than the very regionally dependent observed sea ice loss. These different patterns of reduction indicate that dynamic effects from ocean and wind are crucial in deciding the spatial distribution of sea ice. This is in line with a range of studies, which indicate that oceanic and atmospheric effects are central for the state of the sea ice cover (*Kwok* [2011], *Zhang et al.* [2008a], and *Maslanik et al.* [2007]).

In terms of sea ice extent, the model produces a sea ice reduction completely in line with the expectations based on the study by *Stroeve et al.* [2007]. In Figure 4.8 the original figure from the study has been expanded with points illustrating the sea ice extents of the different SOM simulations. The calculated extents are marked at the year equivalent to the simulated CO_2 level in the SRES A1B scenario (*Nakićenović et al.* [2000]), on which the *Stroeve et al.* [2007] future data is based. The CO_2 level of ALB-PD/NOALB-PD corresponds (by design) approximately to

the present day level, while the 1.5 and $2\times CO_2$ scenarios correspond to 2050 and 2100 respectively.
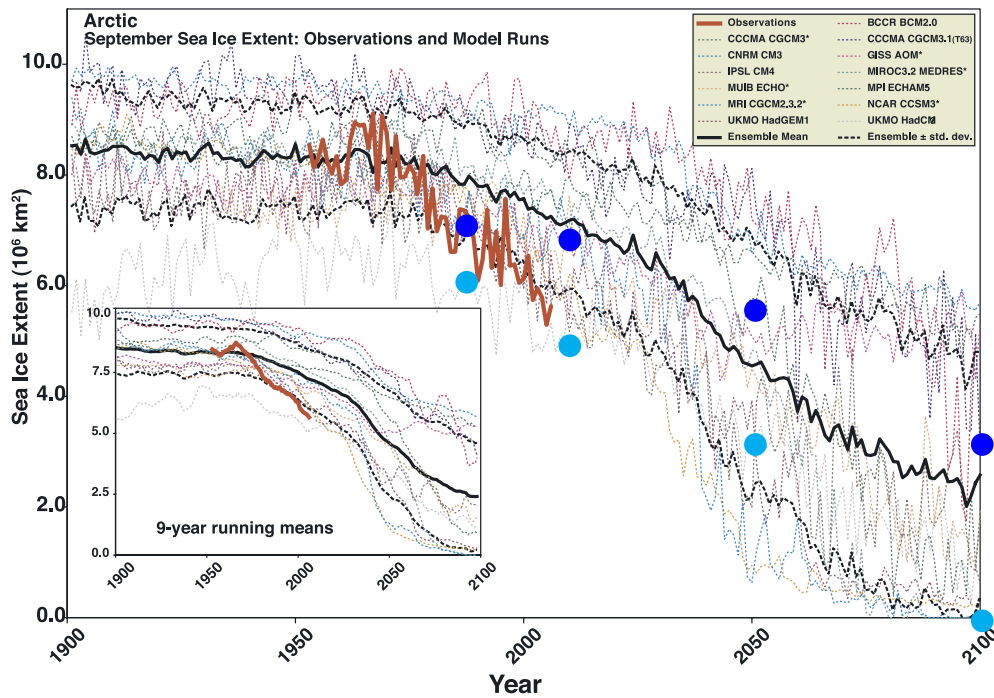
Figure 4.8: Mean September sea ice extent in 10^6 km^2 for the SOM simulations marked on top of the comparison figure from *Stroeve et al.* [2007] (see detailed description in Figure 3.2). The NOALB simulations are marked with **blue**, and the ALB simulations in **light blue**.

A comparison of the series of unchanged (NOALB) and albedo-reduced (ALB) simulations clearly reveals that the gradual sea ice cover decline is more drastic and thus closer to observed trend after the albedo reduction. The albedo reduction is, however, not resulting in a decline, which is far beyond the group of CMIP3 models, but seems to be within the range of the models with fastest reduction.

The surface energy fluxes give an indication of the effect of the changed sea ice cover on the atmospheric energy budget. Figure 4.9 shows the difference in surface fluxes between ALB-PD and NOALB-PD – revealing the effect of the reduced sea ice cover.

Keeping the different configurations of the ice covers in mind, the pattern of the response in the surface fluxes is comparable to the fluxes in the DOM simulations (Figure 4.2, note the different scales). The response is driven by the changes in turbulent fluxes, with a contribution from an increased LW input from ocean to the atmosphere – perhaps the LW constitutes a bigger contribution than in the
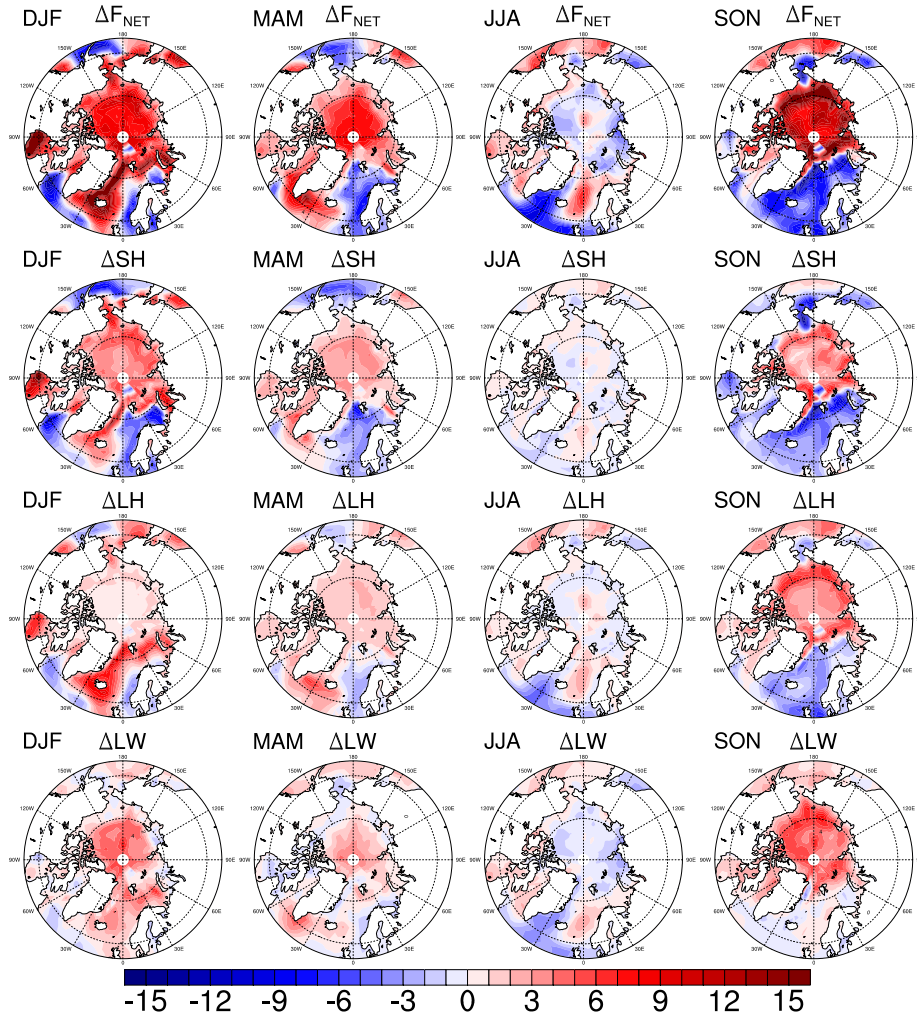
Figure 4.9: Surface fluxes in W/m^2 – difference from NOALB-PD to ALB-PD. Displaying all four seasons from left to right (DJF, MAM, JJA and SON) for all the surface energy flux types. From the top: Net flux, sensible, latent, and longwave fluxes. Positive changes are fluxes directed upwards from the surface.

DOM experiment. This could be connected to the inclusion of the slab ocean, which allows for a more "realistic" response to the sea ice changes. The SW flux still does not contribute to warming of the atmosphere in a direct manner, but in this SOM setup the increased absorption by the ice free ocean surface, results in heat storage in the ocean. The heat storage results in increased upper ocean temperatures, which means increased outgoing LW contributing to atmospheric warming. The warmer ocean also causes increased turbulent fluxes, when the atmospheric temperature drops in the Arctic in the dark period. This ocean heat storage is likely the explanation for the increased influence of the LW flux and the more widespread, southerly extent of positive turbulent fluxes compared to the DOM pattern.

In the warmer scenarios, forced with 1.5 and 2×CO$_2$ the sea ice changes also

reveal the strictly thermodynamic nature of the sea ice model. The sea ice reductions in the warmer scenarios are seen as a widespread, general reduction of the sea ice concentration, rather than the more regional sea ice loss seen in observations (compare with the sea ice cover in the ERA-Ice simulation in Figure 3.3, based on the reanalysis data from 2006-10). The seasonal mean sea ice conditions for the warmer scenarios are shown Figure 4.10. The difference in the summer (JJA) ice cover shows that the primary reduction is in the central, densest part of the ice cover, while the low concentration areas in the margins remain relatively unchanged in all four simulations. This could be the result of the thermodynamic effect referred to as the growth–thickness feedback described by *Bitz and Roe* [2004] – mentioned in Section 2.5.1. The basis of the feedback is that thinner ice re-grows faster, which limits the melt of the thin ice compared to the thicker. This feedback would work to stabilise the marginal ice zones with thinner ice, compared to the central regions with denser and thicker ice. The thickest and densest ice in the model is found in the central Arctic Ocean, due to the purely thermodynamic ice model – as the northernmost grid cells on average will be the coldest, due to the longer absence of sunlight during winter.

The pattern of flux changes, and the sea ice reduction in the warmer scenarios (not shown) is very similar to the simulations presented so far: The net surface flux is dominated by turbulent flux changes, with an increasingly big contribution from the LW. The turbulent fluxes work to warm the atmosphere in the areas of sea ice loss – which, with increasing CO_2, is spread to the entire Arctic Ocean. The increased potential for heat storage, due to absorption of solar SW radiation, causes a slightly delayed increase of LW fluxes peaking in late autumn and early winter. The gradual warming and increasing sea ice loss changes the gradients between the ocean and the atmosphere, and consequently affects the turbulent flux changes. The warming's influence on the relative changes in the two turbulent fluxes (the sensible and latent heat fluxes) is examined in Section 5.3.
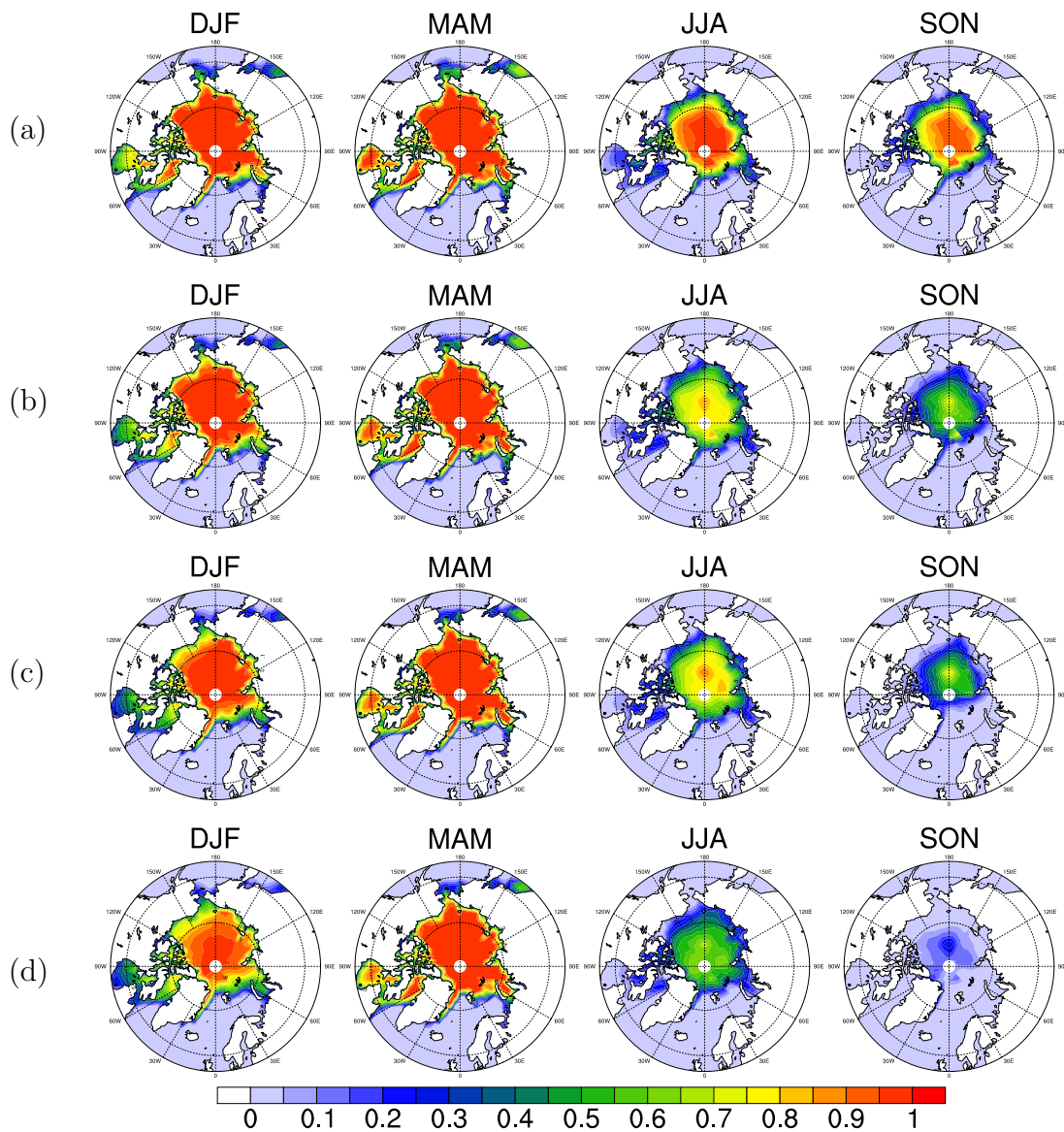
Figure 4.10: Seasonal sea ice cover from the "warmer" SOM simulations. (a) NOALB-1.5, (b) ALB-1.5, (c) NOALB-2 and (d) ALB-2.

4.2.2 ARCTIC AMPLIFICATION

In line with the DOM experiment, all SOM simulations show clear Arctic amplification (Figure 4.11), and both CO_2 increase and sea ice reduction causes increased amplification. A comparison of the respective ALB and NOALB simulations in Figure 4.11 reveals that the albedo-reduction results in additional Arctic amplification, except in the CO_2 doubling scenario. This is explained through the almost complete loss of sea ice in September in the albedo-tuned scenario, which naturally inhibits further reduction. As the reference climate in the NOALB series (NOALB-CTRL) has more sea ice than the ALB reference (ALB-CTRL), the NOALB-2 simulation does not reach near ice-free conditions, and the reduction can thus continue at an almost constant rate – illustrated in Figure 4.6, September area (upper right panel).
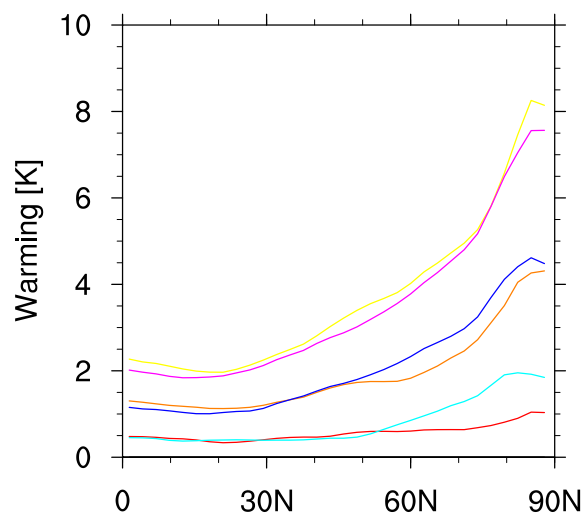
Figure 4.11: Zonal mean warming in the NOALB (NOALB-PD (red), NOALB-1.5 (orange) and NOALB-2 (yellow)) and ALB (ALB-PD (light blue), ALB-1.5 (blue) and ALB-2 (magenta)) simulations compared to the respective reference climates.

The albedo-reduction has no direct influence on the warming outside the Arctic, and hence the Arctic amplification indices are relatively constant – see Table 4.2. In general the NOALB simulations have lower amplification indices than the ALB simulations, which is the expected outcome of the increased reduction of sea ice. The relative values of amplification corresponds to the September sea ice loss (Figure 4.6, upper left panel) – meaning that the biggest difference in the indices is found in the scenarios with most differing sea ice loss compared to the respective reference climates. Hence the indices of the CO_2 doubling experiments are almost equal, while the indices of the present-day (PD) simulations deviate the most. It is noteworthy that the indices of the NOALB simulations increase with the CO_2 level, while it decreases in the ALB simulations. As the sea ice reduction have a significant impact on the magnitude of the amplification index (as indicated by

the DOM experiment), the decreasing factors in the ALB series may be connected
to the gradually flattening slope of sea ice loss (Figure 4.6). The changed indices
could, however, also be connected to changes in the atmospheric heat transport –
investigated in Section 5.4.

| 4.2 SOM: Arctic Amplification ||
Simulation	Amp. index
NOALB-PD	1.56
NOALB-1.5	2.08
NOALB-2	2.10
ALB-PD	2.89
ALB-1.5	2.35
ALB-2	2.19

Table 4.2: Arctic amplification indices for the SOM simulations.

Similar to the DOM experiments, there seems to be a high spatial correlation
between sea ice loss, the flux changes, and the surface air warming in the SOM
simulations. The surface air temperature difference between the three ALB and
NOALB scenarios, shown in Figure 4.12, resembles the pattern of sea ice loss (com-
pare with Figures 4.7 and 4.10). Furthermore the warming seems to be increasing
with increasing sea ice loss, as the relatively similar $2\times CO_2$ climates are associ-
ated with the least pronounced warming, following the limited sea ice differences
(comparing NOALB-2 and ALB-2).

It is noteworthy that the JJA warming is very limited in all three cases – the
albedo decrease causes additional sea ice loss, but does not change the near-surface
temperatures even in the warmest simulations. As long as sea ice is present, the
surface air temperature is confined to the freezing point, as all excess heat acts
to melt additional ice – however in the $2\times CO_2$ climates, the more revealed ocean
surface could allow for some warming. The pattern of reduction in the SOM ice
model however shows that despite the large area of ice loss, most of the Arctic
Ocean still has ice present (albeit in low concentrations), which probably is the
cause of the unchanged near-surface temperature during summer. This indicates
that even low sea ice concentrations effectively inhibit warming in the adjacent
region. An example is the central Arctic sea ice reduction from approximately
80% sea ice cover in NOALB-2 to 50% in ALB-2, which produces no near-surface
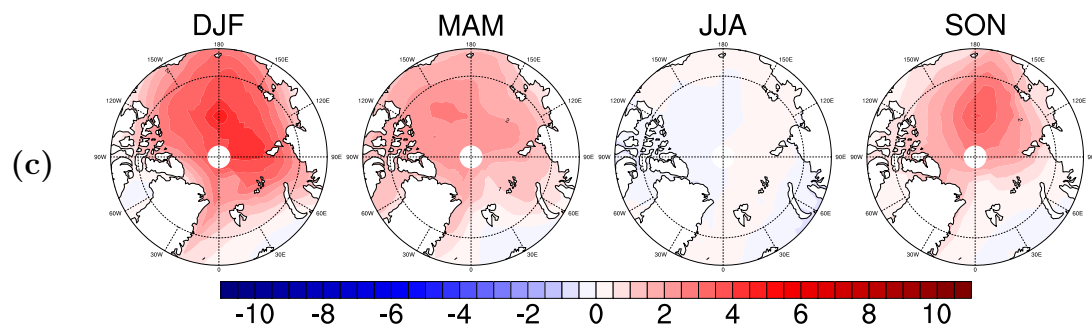warming signal at all (cf. Figure 4.12.c).

ALB-PD - NOALB-PD



(a)

ALB-1.5 - NOALB-1.5

(b)

ALB-2 - NOALB-2

(c)
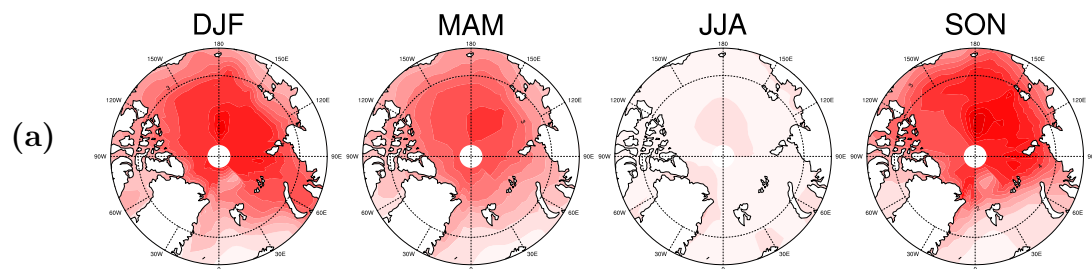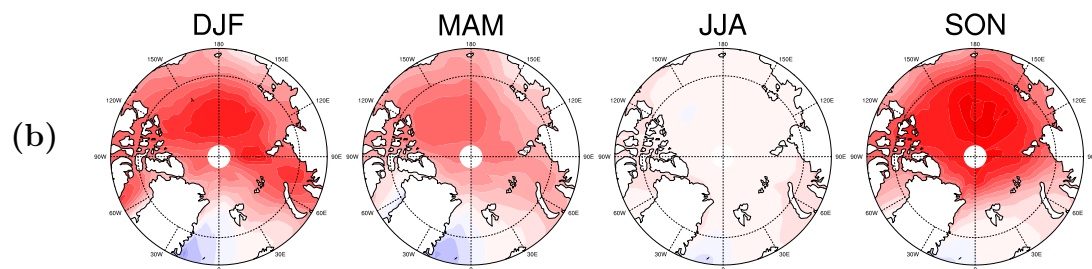
Figure 4.12: The seasonal Arctic near-surface warming [K] resulting from a sea ice reduction. Positive values indicate warming in the ALB compared to the NOALB simulation in (a) the PD, (b) the $1.5\times CO_2$, and (c) the $2\times CO_2$ scenarios.

4.2.3 VERTICAL STRUCTURE OF WARMING

Due to the high static stability most of the year in the lower Arctic atmosphere the pattern of near-surface warming is not necessarily reflected in the temperature changes at more elevated levels. Figure 4.13 shows the vertical warming of the ALB-PD simulation, which is designed to correspond approximately to the ERA Interim 2006-10 mean examined in *Chung and Räisänen* [2011] and the DOM experiments. Note, however, that the changes in temperatures and sea ice cover are more limited, which is likely due to the control climate ALB-CTRL having a too reduced sea ice cover, and consequently being too warm compared to the desired 1979-83 mean reference climate. Hence, the focus here is on the structure of vertical warming profile, and the relative warming at different levels. The general warming pattern in all four seasons in Figure 4.13 is quite similar to the ERA-Ice DOM simulation, but differs in one central part: the low-level JJA warming (compare with Figure 4.5).
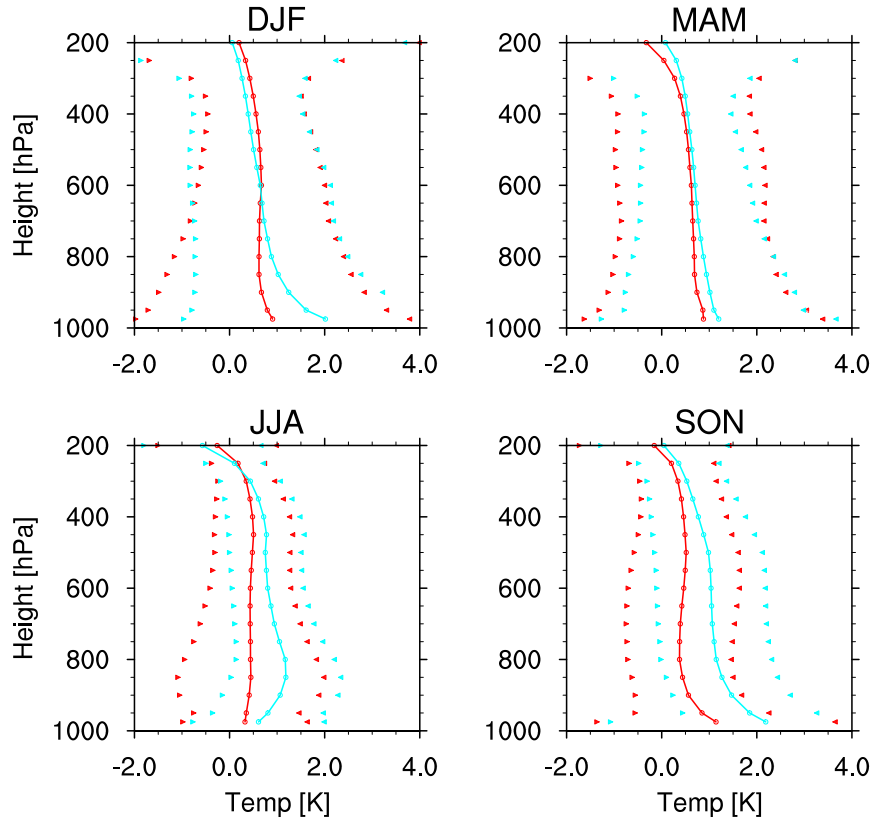
Figure 4.13: The vertical structure warming in the ALB-PD simulation (blue) compared to the NOALB-PD simulation (red) compared to the respective control climates. Error bars marked with arrows are $\pm 2\sigma$ at each level for each of the profiles.

The JJA profile has a distinct low-level peak centred on 850 hPa, and perhaps a hint of a minor peak around 450 hPa. During summer (the melt period) the

surface temperature is confined to near-freezing due to the presence of melting sea ice, but somehow a clear warming signal still appears in the low levels just above the surface, creating a profile slightly more reminiscent of the ERA-Interim profile presented in Figure 3.1. The warming aloft around 500 hPa corresponds to the height in which *Chung and Räisänen* [2011] expects warming from atmospheric meridional heat transport. The accelerated sea ice loss in ALB-PD compared to NOALB-PD apparently creates a JJA warming peaking at a lower level, along with some less pronounced warming with more widespread vertical extent.

While they do not directly explain the appearance of the JJA low-level peak the pattern, the surface fluxes in Figure 4.9 are generally consistent with the pattern of warming. The turbulent fluxes are connected to the increased low level warming, and the increased LW flux might explain part of the minor warming increase at higher levels.

The structure is comparable in the 1.5 and $2\times CO_2$ scenarios, as the same main features appear – cf. Figure 4.14[4]. There is a general tendency of an increased warming with wide vertical extent, which could be connected to increased ocean temperatures, resulting in increased LW fluxes. The LW fluxes could, as explained in the DOM results section, lead to warming spread out over the atmospheric column. The more widespread warming in the vertical could however also be connected to changes in the atmospheric stability, allowing for a larger degree of convection and vertical mixing, which would distribute energy from the surface and upwards. Continuous warming of the surface and the lowest part of the atmosphere will affect the stability, as it will gradually work to weaken, and ultimately destroy, the inversions. As described in the Scientific Introduction (Section 2.3) inversions in the Arctic are dependent on the very low surface temperatures, and will thus weaken with increased surface and near-surface warming.

Focussing again on the JJA profiles, the $1.5\times CO_2$ albedo-tuned simulation also have maximum warming in the lower levels around 850 hPa, while this lower peak is not seen clearly in the NOALB-1.5 simulation. Similar to ALB-PD, the warming in ALB-1.5 is spread out somewhat in the vertical – perhaps again with a hint of a peak aloft around 450 hPa. In the $2\times CO_2$ simulations the warming is substantial in both ALB- and NOALB-2, and the albedo change no longer causes any noteworthy difference in the warming. NOALB-2 has maximum warming aloft around 450 hPa, with noticeable warming below (which is still relatively limited at the surface). The reduction of sea ice in ALB-2 results again in increased warming seen as a low-level peak, while the peak aloft still persists as a clear feature around 450 hPa. The differences between the low-level peak and the warming aloft is greatly reduced in the $2\times CO_2$ simulations compared to the scenarios with more moderate warming.

---

[4]Error bars have been omitted in the plot to ensure a simpler layout.
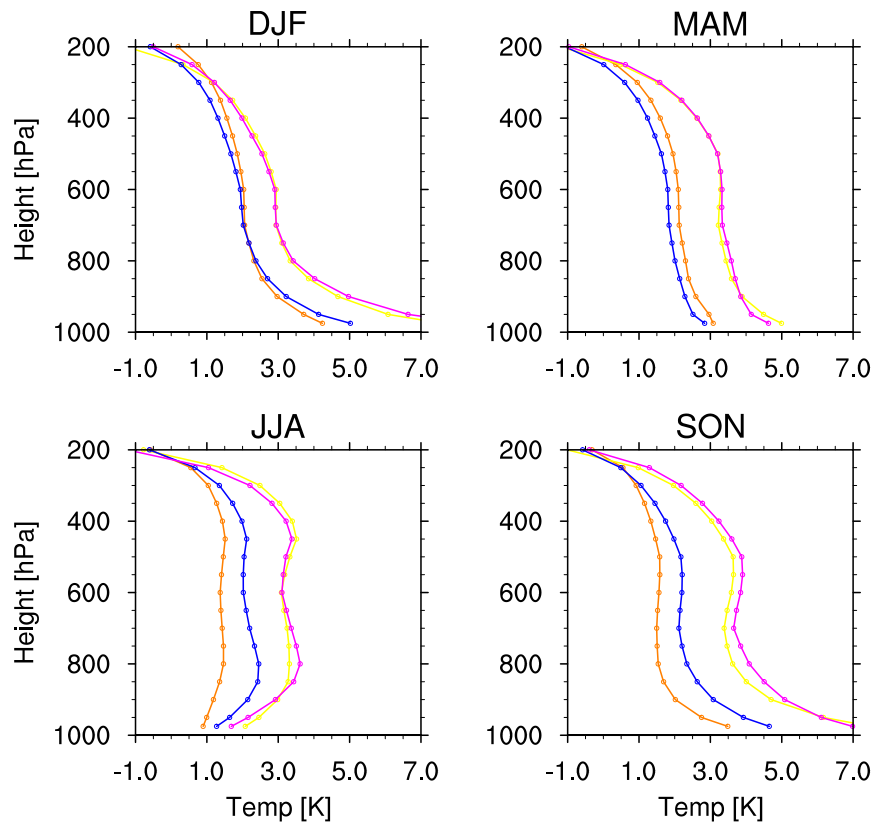
Figure 4.14: The vertical structure warming in the NOALB-1.5 (**orange**) and NOALB-2 (**yellow**) simulations and the ALB-1.5 (**blue**), and ALB-2 scenarios (**magenta**) compared to the respective references.

The very similar magnitude of warming in the two CO_2 doubling scenarios is a result of the immense sea ice loss. Both scenarios have almost ice free conditions at the annual minimum, and thus the albedo change causes very little difference, since the increase SW absorption is diminishing. The small difference in sea ice cover does seem to increase the JJA low-level peak in the ALB-2 simulation compared to NOALB-2 – however, the difference is small compared to the difference in the colder scenarios.

5 ANALYSIS AND DISCUSSION

5.1 STATISTICAL SIGNIFICANCE OF CHANGES

In order to assess, whether the observed changes in the simulations are actual changed properties of the climate system or simply variations within the range of the "natural" climate variability, the results are analysed statistically using the *Student's t-test*. The *t*-test is widely used to estimate the so-called statistical significance of observed changes in a variety of scientific branches. In this context the climate model simulations are assessed, by comparing the changed properties of a climatic response to an induced forcing to the unforced control climate. The *t*-test indicates, how likely it is that the observed values in the forced scenario, are likely to be part of the control climate "population" – i.e. within the variability of the unperturbed climate. By comparing the distributions of a given parameter, the *t*-test can indicate whether the null-hypothesis is likely to be true or false. The null-hypothesis here is that the two distributions are equal, meaning that there is no statistical significant change. The test result is a certain *t*-value, which combined with the degrees of freedom in the assessed system, gives an estimate of the probability of the null-hypothesis to be true. Normally probabilities (p) of 5% or less are taken to mean that the two distributions are significantly different – employing the value of 1-p, the null-hypothesis is said to be rejected at the 95% significance level, if $p \leq 0.05$. The *t*-value is calculated from the means and variances of the distributions, along with the number of samples. The number of samples here, are equivalent to the number of individual model years, as the autocorrelations of all the investigated parameters are below a year. With REF denoting the reference and CHG the changed distribution, the *t*-value is defined as (*von Storch and Zwiers* [1999]):

$$t = \frac{\mu_{\mathrm{CHG}} - \mu_{\mathrm{REF}}}{\sqrt{S^2_{\mathrm{CHG}}/n_{\mathrm{CHG}} + S^2_{\mathrm{REF}}/n_{\mathrm{REF}}}} \tag{5.1}$$

where μ and S^2 are the mean and variance of the distributions respectively, while n is the number of samples. The degrees of freedom (DOF), which links the *t*-value to the probability is calculated as: $\mathrm{DOF} = (n_{\mathrm{REF}} - 1) + (n_{\mathrm{CHG}} - 1) = n_{\mathrm{REF}} + n_{\mathrm{CHG}} - 2$.

The test for significance is primarily employed here as a test of significant features in the vertical structure of warming. The *t*-test should only focus on signifi-

cant warming in this case, and thus the *one-tailed* version of the *t*-test is applied. The one-tailed test focusses on changes in the form of an increase from the reference rather than a general difference (positive or negative). "One-tailed" refer to the bell-shaped normal data distribution, of which only the part with values larger than the mean is considered here – i.e. only one tail of the distribution. In practice this logically changes the probability to half of the two-tailed value $p_{\text{one-tail}} = 0.5\,p_{\text{two-tail}}$.

The *t*-test is used to assess the changed features of the vertical structure of warming in two ways: (1) by comparing the warming at a selected level in two different simulations (e.g. a comparison of changed and control climates), and (2) by comparing the warming at two different levels in the same simulation. Approach (1) could be used to compare the low-level warming in two simulations to decide, if one is significantly bigger than the other, while (2) could be used to assess relative changes in the structure: If the low-level warming is significantly higher than the high-level warming in a simulation, but not in its reference climate, the changed conditions have caused a statistically significant low-level warming.

The different features, at different levels, are compared in terms of the pressure-weighted means of the atmospheric levels, where the changes are observed. A warming feature with a certain vertical range will thus be tested as the distribution of the pressure-weighted mean warming of the vertical levels in the range:

$$x_{\text{wgt,avg}} = \frac{1}{\sum_i w_i} \sum_i w_i x_i \qquad (5.2)$$

where i denotes the vertical levels and the weights w_i are proportional to the atmospheric pressure differences. The pressure-weighting is employed to ensure an energy-consistent comparison, as higher levels are less dense, and thus easier heated.

DOM EXPERIMENTS

In the assessment of the statistical significance of the vertical structure of warming in the DOM simulations, the primary focus will be on the winter and summer seasons (DJF and JJA). Autumn, winter, and spring exhibit the same pattern of changes (cf. Figure 4.5), and DJF is chosen as the changes are most pronounced in winter. JJA is added, as the pattern is different from the remaining seasons. The focus on these two seasons is additionally in line with the analysis by *Chung and Räisänen* [2011]. The reduction of the ice cover in ERA-Ice (compared to CMIP) results in a larger surface based warming during winter, which is confined to the lowest levels. The warming is further increased with the inclusion of the warmer SSTs in ERA-All, but the basic structure is unchanged, as the warming from the increased SSTs is similar at all vertical levels. During summer the CMIP and ERA-Ice simulations are remarkably similar, while the ERA-All simulation exhibit warming with a widespread vertical extent, but a hint of a peak near 500

hPa. These main features are identified, and subjected to a t-test to evaluate the significance of the changes.
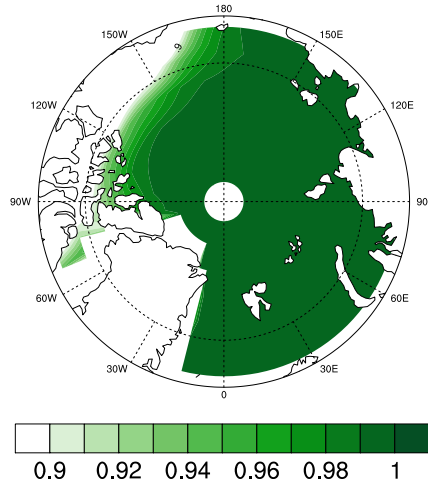
The surface-based warming in DJF is tested in ERA-Ice against the same vertical layers in CMIP to reveal, if the reduction of the sea ice cover results in a statistically significant warming. A pressure-weighted mean of the warming in the layers closest to the surface is calculated, as indicated by the box in Figure 5.1.a. The error bars on the plot illustrates that the warming in ERA-Ice lies within to 2σ interval from the CMIP simulation, and a test of the significance is relevant. The test reveals that the ERA-Ice surface-based warming is statistically significant above the 99.9% confidence level in the Arctic mean.
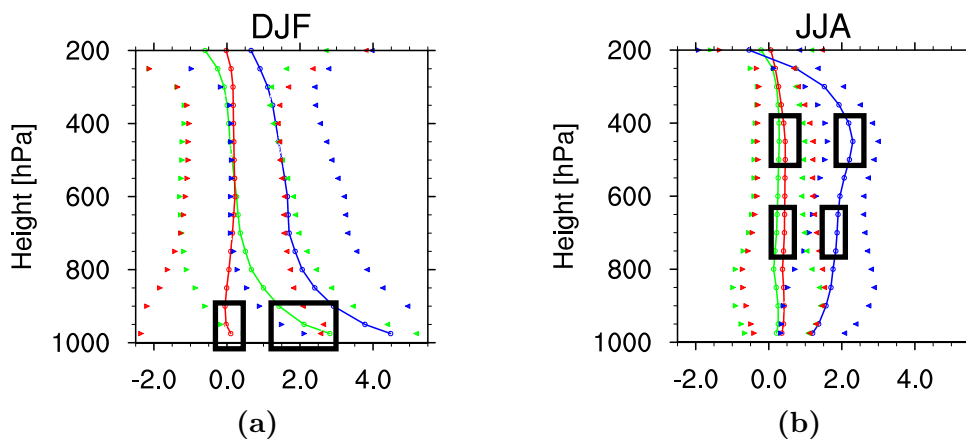
Figure 5.1: Winter **(a)** and summer **(b)** seasons (taken from Figure 4.5) with t-tested main features marked with **black** boxes. CMIP (**red**), ERA-Ice (**green**) and ERA-All (**blue**).

The warming peak has also been tested for significance in a point-wise (grid cell by grid cell) analysis. Although testing point by point is associated with considerably higher variability, the field plot in Figure 5.2 reveals that the DJF surface-based warming is significant in a large area. This test method could give an indirect indication of the factors responsible for the warming: if the significant changes are primarily confined to certain regions, which are spatially correlated with changes in a physical parameter (e.g. the sea ice cover), it could indicate a link. The widespread pattern of significance does, however, not resemble the changes in sea ice cover, cloud cover or the like, but nevertheless it indicates that the warming tendency is unquestionable and widespread over most of the Arctic area.

Similarly the significance is tested of the upper level warming around 450 hPa in JJA. In this case the t-testing is used to assess, whether there is an actual peak in the warming around 450 hPa in each of the simulations. This is done by comparing the ensembles of the pressure weighted means of warming in the upper box to that of the lower box in each simulation (marked in Figure 5.1.b). In the test the effect
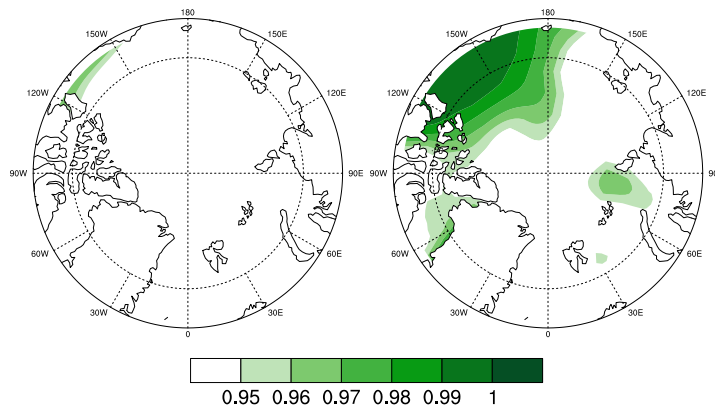
Figure 5.2: Spatial distribution of the statistical significance of the DJF surface-based warming peak in ERA-Ice compared to CMIP. Shading indicates significance level.

of the SST increase is tested, as the ERA-Ice simulation is compared to ERA-All. The expectation is that the ERA-All simulation will have a significant peak in the warming due to increased MHT into the Arctic, following from increased lower latitude SSTs, while the ERA-Ice simulation will not. This is confirmed by the test, which reveals that there is no significant difference between the warming in the upper and lower box in the ERA-Ice simulation, while the difference in warming in the ERA-All simulation is significant at the 99.9% level. The spatial pattern of the point-by-point t-test (Figure 5.3) suggests that the warming in ERA-All is primarily significant in region north of North America and the Pacific Ocean. This could be a hint that the main heat transport increase comes from the Pacific sector, as a result of the increased SSTs. The SST increase (not shown) is however quite similar in the Pacific and Atlantic Oceans – if anything the Atlantic temperatures are warmed the most – and hence there is no indication that the changes in the Pacific should be the primary driver of the increased transport. ERA-Ice, as expected, show no signs of a statistically significant warming aloft, as neither the Arctic mean or the spatial pattern show any signs of significance.

SOM experiments

A similar test of statistical significance is done for the SOM experiments. The relevant peaks that are tested are marked in Figure 5.4. The DJF increased surface based warming is tested in ALB-PD compared to NOALB-PD, yielding a statistically significant change in the Arctic mean at the 99.5% level. In the JJA case the warming in the lower box is compared to that of the higher box, to indicate whether the low-level peak is significantly warmer than the warming aloft. The expectation is that the difference is significant in the ALB case, but not in

Figure 5.3: Spatial distribution of statistical significance of an upper level warming peak in ERA-Ice (**left**) and ERA-All (**right**), comparing the levels around 500 hPa to levels below in both simulations.
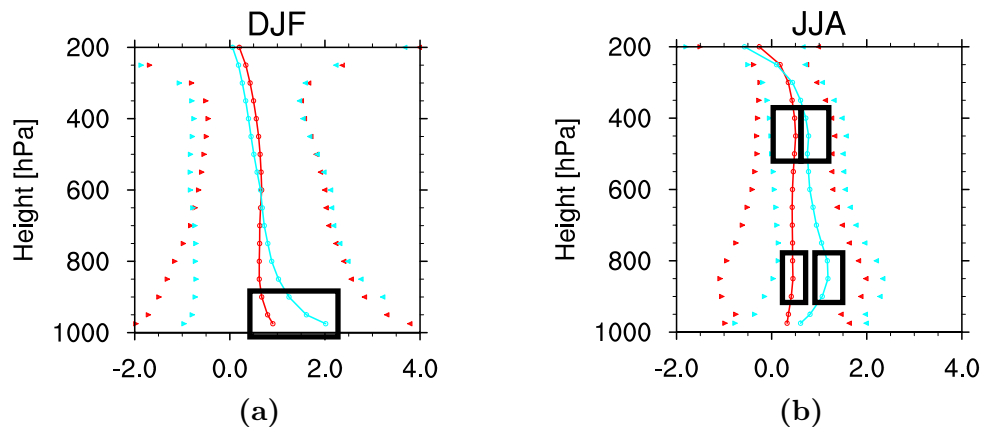
Figure 5.4: Winter **(a)** and summer **(b)** seasons (taken from Figure 4.13) with *t*-tested main features marked with **black** boxes. ALB-PD (**blue**) and NOALB-PD simulation (**red**) compared to the respective references.

the NOALB simulation. This is confirmed by the *t*-test, which shows that the low-level peak is significantly larger than the warming aloft at the 99.9% level in the ALB-PD simulation, while there is no significant difference between low- and high-level warming in NOALB-PD.

Both tests are repeated in a point-wise manner similar to the DOM analysis. The statistical significance of the DJF surface based warming is widespread, but remains insignificant in the region around the Chukchi Sea (near the Bering Strait) between 150°E and 150°W (not shown). Figure 5.5 compares the significance of the low-level JJA warming to the high-level warming in NOALB- and ALB-PD, and clearly reveals that there is no significant warming difference between the two levels anywhere in the NOALB-PD simulation, while the warming is significant in almost the entire area in ALB-PD.
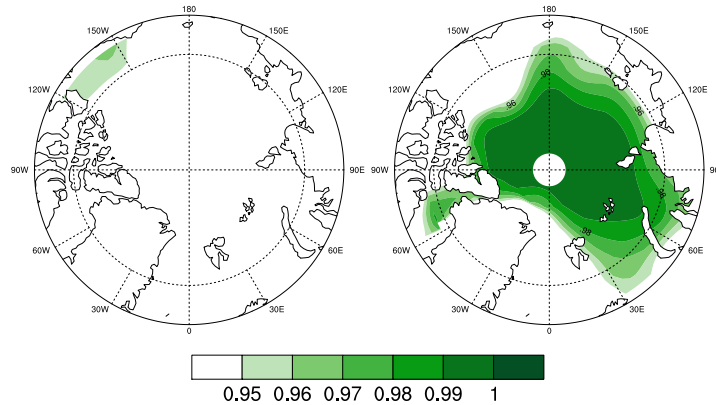
Figure 5.5: Point-by-point t-test of the low-level JJA warming compared to the warming aloft. **Left:** NOALB-PD, **Right:** ALB-PD. Shading indicates statistical significance at the 95% level or higher.

5.2 REGIONAL WARMING DIFFERENCES

Previously (Figures 4.4 and 4.12) the near-surface temperature changes were shown to be spatially correlated with the sea ice loss – a question, however, still remains of whether this correlation also is valid for the more elevated temperature changes. While the spatial t-test of the different warming peaks could hint to the regional differences, it did not reveal any clear patterns. A more direct way of assessing the regional differences in the vertical profile of warming, is to calculate separate warming profiles for regions with different surface properties. Hence, a "masking" analysis has been performed to calculate the average warming in grid cells with certain surface characteristics – e.g. the warming over land, ocean or sea ice covered areas – by masking out all other regions. The aim is to reveal, if the climatic changes are primarily confined to certain regions (e.g. regions of sea ice loss), as this could give an indication of the sources of warming. The different regions are defined in Table 5.1.

The masking makes it possible to calculate a series of vertical profiles of warming in the atmospheric columns over a certain surface-type. Such profiles have been calculated for both the DOM and SOM simulations, to reveal the effects of sea ice loss and SST increases, which could be evident from the different warming patterns in e.g. the Ice, Melt and Ice-free regions.
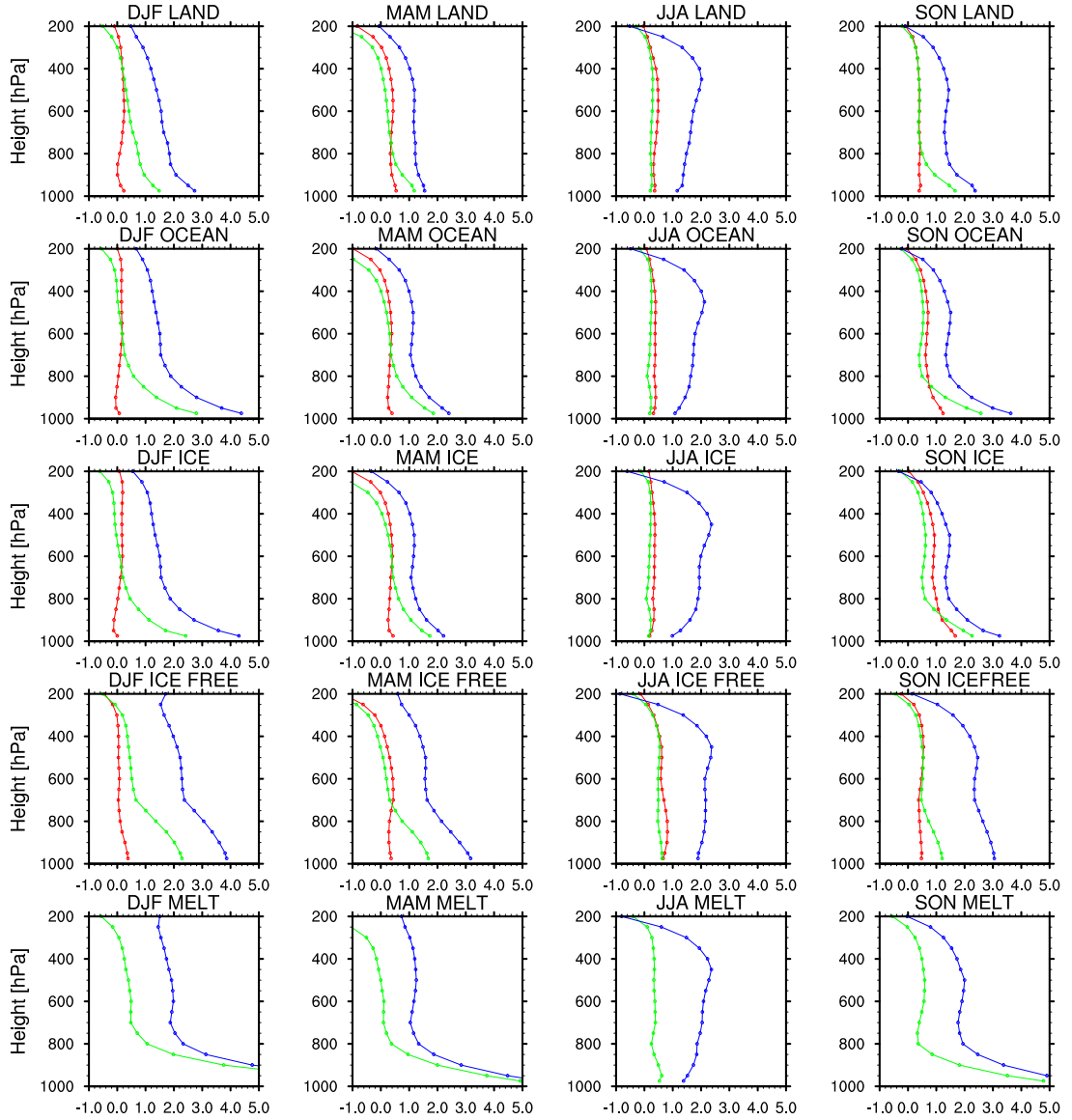
The seasonal vertical warming profiles of the DOM simulations, presented in Figure 5.6, reveal that there is no significant difference between the warming over land, ocean and sea ice covered surfaces. As only the sea ice cover and the SSTs are changed, the very similar warming of the land points indicate that the weather systems effectively even out the warming in the horizontal plane. The near-surface difference between ocean and land point does however indicate that the warming

5.1 Masking Regions	
Region	**Definition**
Land	Land covered region. Fraction of land cover in grid cell exceeds 50%.
Ocean	Ocean covered region. Fraction of ocean cover in grid cell exceeds 50%. Includes both ice-covered and ice-free areas.
Ice	Sea ice covered region. Sea ice concentration above 70% in both compared climates.
Ice-free	Ice-free regions. Sea ice concentration below 20% in both compared climates
Melt	"Newly ice free" regions. Ice covered in reference climate, and ice free in perturbed climate. Sea ice concentration reduced from above 70% to below 20%.

Table 5.1: Names and definitions of masking regions.

is stronger over the ocean – which is consistent with the induced changes. The Ice-free region has little difference to the general Ocean region pattern in CMIP and ERA-Ice, but the warming in ERA-All has changed substantially in some seasons in the Ice-free compared to the Ocean profile. Especially the SON warming is stronger than the general signal, and has a wide extent in the vertical, indicating that the warmer ocean surface is a substantial heat source for the atmospheric column above. In winter and spring the Ice-free regions also show a somewhat increased warming in the lower atmosphere – the limited vertical extent suggests that the warming is confined to the lower layers due to atmospheric stability. The plots of the Melt region does not display profiles from the CMIP simulation. The reason is that no grid points in the CMIP simulation satisfies the criteria of having below 20% sea ice concentration in grid points, which had more than 70% in the control climate. This is unsurprising, as the forcing (i.e. the induced changes in SST and sea ice cover) and the resulting warming signal is relatively limited in the CMIP simulation. The two simulations with the reduced ERA Interim sea ice cover have a number of grid points that satisfy the Melt criteria. In summer these regions exhibit a very similar warming structure to the remaining ocean points, while the SON, DJF and MAM profiles show substantial near-surface warming. Compared to the previous sea ice covered surface, the now open ocean releases a considerable amount of heat in the seasons, where the atmosphere is cold, and the ocean-atmosphere temperature gradient is big. This result corresponds nicely to the flux analysis (Section 4.1.2), which showed large ocean-to-atmosphere energy fluxes in areas of sea ice retreat – especially in the sensible energy (cf. Figure 4.2).

The same analysis has been performed for the two series of SOM simulations and all six profiles of warming from the present-day analogues, the 1.5 and $2\times CO_2$ scenarios are shown in Figure 5.7.

Figure 5.6: Vertical profiles of warming in the selected regions in the DOM simulations: CMIP (**red**), ERA-Ice (**green**), and ERA-All (**blue**). The panels are displaying the seasonal mean warming in the (from the top down) Land, Ocean, Ice, Ice-free, and Melt regions (as defined in Table 5.1).

A comparison of the Land and Ocean regions reveal that the near-surface warming is less pronounced over land in all seasons except summer. A t-test of the difference between surface-based Land and Ocean warming (similar to the testing performed of the near-surface warming in Section 5.1) reveals that the near-surface temperatures over the ocean are significantly warmer in most DJF, MAM, and SON seasons in the 1.5 and $2\times CO_2$ simulations – there is only a few exceptions, where the warming is not statistically significant at the 99% level[5]. In summer there is further a remarkable difference in the low level warming, as the warming around

_____

[5]Changes are *not* statistically significant in NOALB-2 DJF, and ALB-1.5 MAM and SON.
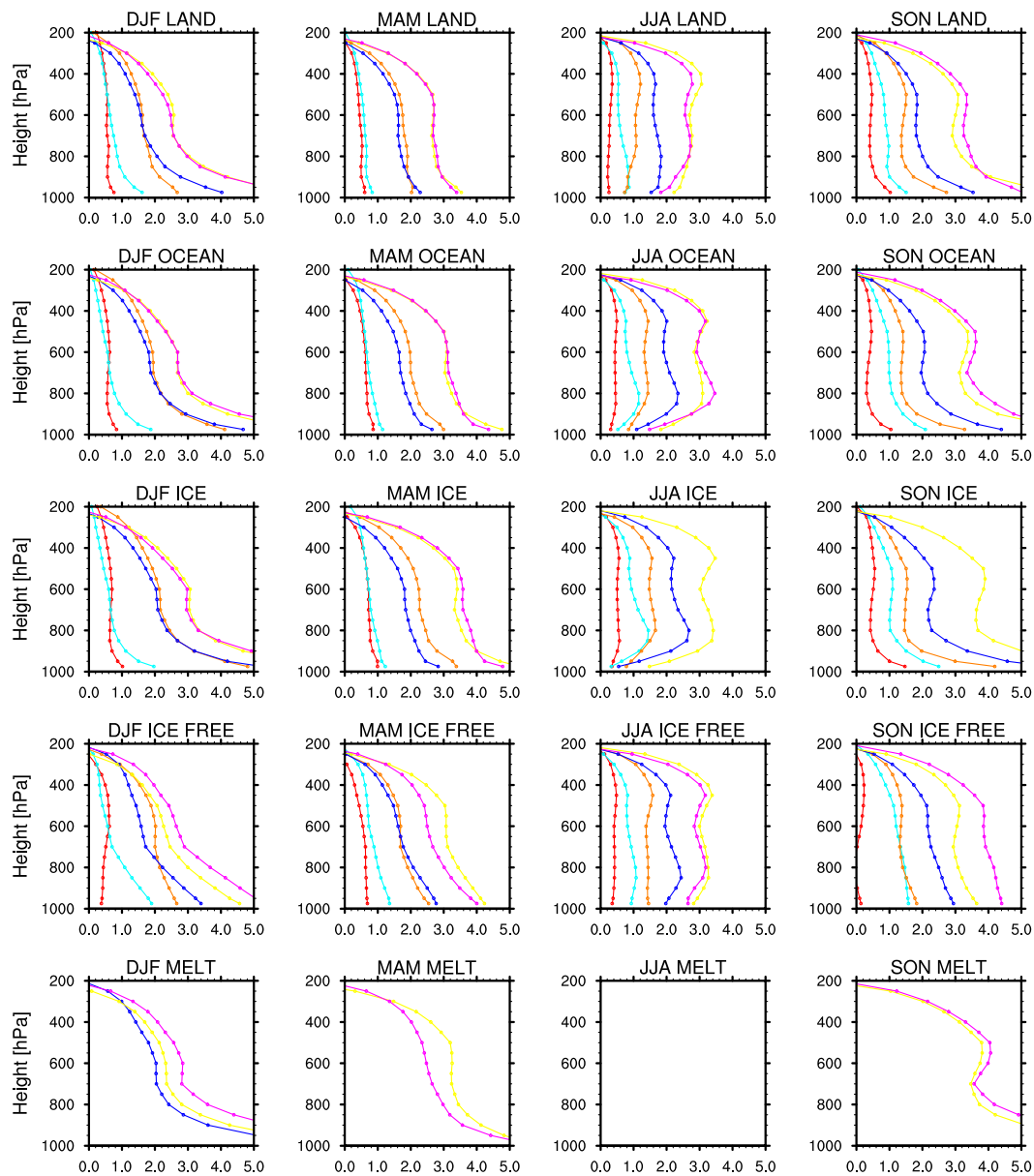
Figure 5.7: Vertical profiles of warming in the selected regions in the SOM simulations: NOALB-PD (**red**), ALB-PD (**light blue**), NOALB-1.5 (**orange**), ALB-1.5 (**blue**), NOALB-2 (**yellow**), and ALB-2 (**magenta**). The panels are displaying the seasonal mean warming in the (from the top down) Land, Ocean, Ice, Ice-free, and Melt regions (as defined in Table 5.1).

the previously identified low-level peak (around 850 hPa) is not as clear a feature over land. The earlier described limitation of near-surface temperature changes in JJA due to the presence of melting sea ice is confirmed by this analysis. The surface warming over ice covered areas is very limited, while a clear warming signal is seen over land covered and ice free regions. The upper peak around 500 hPa, likely associated with increased atmospheric heat transport, is evident over land as well – at least in the warmer scenarios. The Ocean and Ice regions do not differ significantly, except that the ALB-2 profiles are not shown in the Ice profile plots

in JJA and SON. The condition for the Ice region is that the grid points need to have more than 70% sea ice concentration in both simulation and reference, and the nearly ice-free Arctic Ocean in the ALB-2 simulation simply has no areas with concentrations above 70%. Over the Ice-free regions, the SOM simulations exhibit the same warming patterns as the DOM simulations: In the colder seasons SON and DJF there is clear sign of increased warming. In DJF the warming is limited to the lower levels, while it has a wide vertical extent in SON. Very few simulations satisfy the criteria of the Melt regions, but the ones that do show the same tendency of substantially increased near-surface warming as the DOM simulations. These patterns, again, correspond well to the analysis of the flux changes (Section 4.2.1).

5.3 Turbulent fluxes

The main driver of the surface-based changes is the turbulent energy flux, consisting of the sensible and latent heat fluxes (cf. Figures 4.2 and 4.9). These changes are to a high degree spatially related to the sea ice changes, as both flux types increase as a result of the retreating sea ice cover. The sensible flux is expected to increase as the insulating effect of the sea ice is reduced, while latent heat fluxes should increase with warming of the ocean. The ratio of the changes in the surface based sensible and latent heat fluxes is calculated for all scenarios, to find the primary driver of the warming response to the sea ice loss and SST increase. Generally sensible fluxes dominate near the ice edge, due to large temperature gradients between ocean and atmosphere, while latent heat fluxes dominate in the tropics, and other areas of extensive evaporation. Latent heat fluxes are expected to become increasingly dominant in a warming climate due to the non-linearity of the Clausius-Clapeyron equation (as described in Section 2.4), which causes larger latent heat flux increases over the oceans with increasing SSTs (*Wallace and Hobbs* [2006]).

Here, the ratio of the changes in the different turbulent fluxes (R_{TRB}) is calculated as the Arctic mean of:

$$R_{\mathrm{TRB}} = \frac{\Delta F_{\mathrm{SH}}}{\Delta F_{\mathrm{LH}}} \tag{5.3}$$

where ΔF denotes the change in the fluxes resulting from the induced changes. In the DOM experiment the ERA-Ice and ERA-All simulation are compared to CMIP, while ALB and NOALB simulations are compared at respective CO_2 levels in the SOM experiment. Table 5.2 shows the Arctic mean R_{TRB} values in the different simulations, which gives a hint to the relationship between sea ice reduction, ocean warming, and the sensible and latent heat flux changes.

From the DOM simulations it is obvious that the sea ice reduction in itself primarily causes increases in the sensible heat flux: The ratio $R_{\mathrm{TRB}} > 10$ meaning that sensible heat flux changes are ten times larger than the latent heat changes.

5.2 Turbulent Flux Changes	
Simulations	**Arctic $R_{\mathbf{TRB}}$**
ERA-Ice – CMIP	10.77
ERA-All – CMIP	0.96
ALB-PD – NOALB-PD	5.26
ALB-1.5 – NOALB-1.5	4.02
ALB-2 – NOALB-2	1.06

Table 5.2: Arctic mean ratios of changes in sensible and latent heat fluxes resulting from sea ice loss in the different simulations.

Addition of the warmer SSTs in ERA-All leads to a substantial relative increase of the latent heat flux, as the R_{TRB} ratio approaches unity. This clearly supports the expectation that the sea ice loss intensifies the sensible fluxes, while ocean warming works to increase the latent heat flux.

The changes are less clear-cut in the SOM experiments, as sea ice reductions, through increased absorption SW solar radiation, lead to some SST warming. However, there are indications of the same pattern as suggested by the DOM experiments. The warming in the PD simulations is limited, as the sea ice cover is still extensive, and any additional absorbed heat will work towards further sea ice reduction rather than heating of the ocean. Hence the sensible heat changes still dominate. The slightly lower R_{TRB} value compared to the DOM case, is a result of the fact that the sea ice reduction is smaller (leading to smaller sensible flux increase in general), and that the ocean possibly gains some heat through SW absorption, causing an increase in the latent heat flux. The gradually decreasing R_{TRB} values in the 1.5 and $2\times CO_2$ simulations is a result of increasing heat gain by the ocean, resulting in increased latent heat fluxes, while the rate of sea ice loss is gradually weakened as ice-free conditions are approached in the warmest scenarios. This analysis indicates that the reduction of the sea ice cover, initially heats the system due to a diminished insulation-effect letting ocean transfer heat the colder atmosphere (as a sensible flux). Secondly increased SSTs lead to increased latent heat fluxes, which increases with the loss of sea ice and consequent ocean heat gain.

5.4   Atmospheric energy transport

The atmospheric poleward energy transport (or *MHT*, Meridional Heat Transport) is a likely contributor to the Arctic amplification (as described in Section 2.5). The relative importance of MHT as contributor to the amplification is debated, while there is indications that MHT increases in a warmer climate. The MHT increase is seemingly linked to increase of low latitude SSTs (*Alexeev et al.* [2005] and *Screen et al.* [2012]), and is explained through an increased latent heat transport in a warmer (and thereby moister) atmosphere (Section 2.5.1). Hence the latent heat transport, and consequently possibly also the net MHT, into the Arctic is ex-

pected to increase in the simulations with CO_2 forcing or increased SSTs, while it is less clear what to changes to expect from simulations with reduced ice cover only.

The MHT is estimated through a schematic calculation, where the flux balance in zonally averaged, latitude-bounded boxes is used to estimate the implied atmospheric transport between neighbouring boxes. The energy budget is calculated in each box from the long- and shortwave fluxes in combination with latent heat changes, and the imbalance is assumed to correspond to the horizontal energy transport out of the box – corresponding to Equation (2.1). Based on these fluxes the horizontal total and latent heat transport can be estimated, while the dry static energy (DSE) contribution to MHT corresponds to the difference between the two: Following Equation (2.5) the MHT is expressed as $F_{\mathrm{MHT}} = \mathrm{MHT}_{\mathrm{LH}} + \mathrm{MHT}_{\mathrm{DSE}}$. The calculation is done from the South Pole and northwards, to ensure only one unknown flux (horizontal energy transport to the northward neighbouring box) in each of the box budgets. Figure 5.8 show a schematic of the box scheme including the relevant fluxes. The box boundaries are chosen corresponding to the model grid cells.
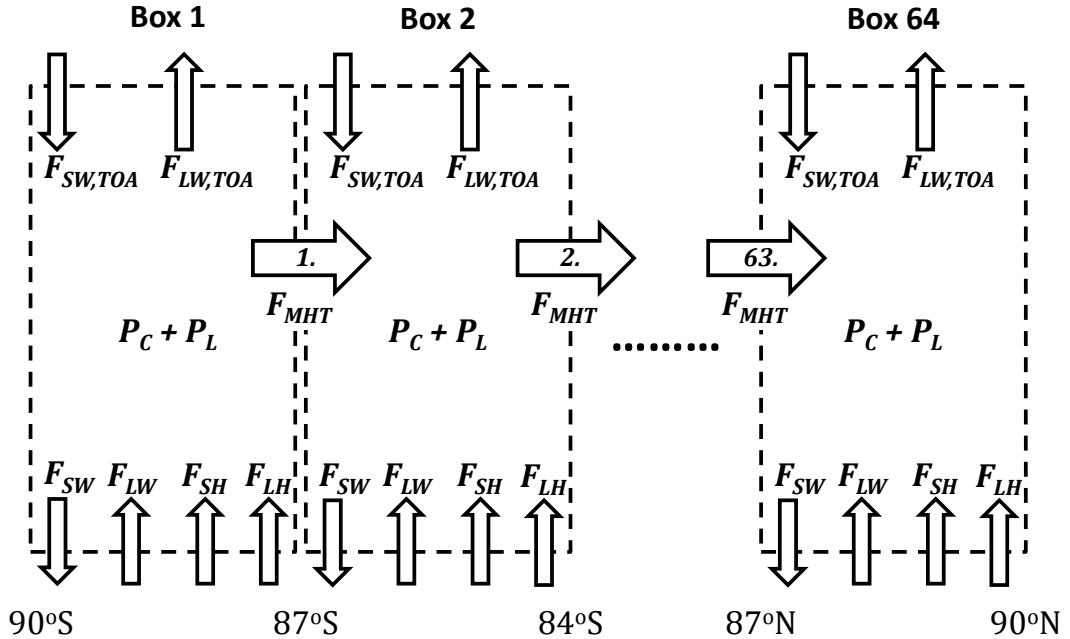
Figure 5.8: Schematic illustration of the estimation of implied MHT. F_{SW} is the net shortwave, F_{LW} the net longwave, F_{SH} the net sensible and F_{LH} the net latent heat flux. P_{C} and P_{L} is the convective and large-scale precipitation respectively.

The total energy budget of a box (equivalent to Equation (2.1)) is rather straightforwardly calculated from the different fluxes at the top of the atmosphere (TOA) and the surface (SFC). The meridional latent heat transport ($\mathrm{MHT}_{\mathrm{LH}}$) corresponds to the box sum of the SFC latent heat flux and the contribution from the net pre-

cipitation. The transport must correspond to the energy imbalance calculated from the total precipitation[6] and the SFC latent heat flux (F_{LH}) as:

$$\mathrm{MHT}_{\mathrm{LH}} = F_{\mathrm{LH}} - (P_L + P_C)\,\rho L_v \tag{5.4}$$

where ρ is the density of water and L_v the specific latent heat of evaporation.

The focus of this analysis is the atmospheric heat convergence in the Arctic area, which corresponds to the net MHT across 70°N, and following *Chung and Räisä-nen* [2011] this analysis will focus on the transport during summer (JJA). The change in total and latent heat transport in JJA in the DOM and SOM simulations compared to the respective reference climates are shown in Table 5.3.

The change in energy transport is difficult to assess directly in relation to the vertical profiles of temperature change. Hence, a crude estimate of the temperature change equivalent to the energy convergence is made, assuming that the convergence is confined to a certain level in the atmosphere, and that the warming is evenly spread horizontally over the Arctic. The transport across 70°N is viewed as a forcing distributed equally across the Arctic area:

$$\Delta F_{70} = \frac{\Delta \mathrm{MHT}_{70}}{A_{70}} \tag{5.5}$$

where ΔF denotes the forcing in [W/m^2], ΔMHT the change in implied atmospheric energy transport estimated with the box schematic, and A the area north of 70°N (assuming a spherical globe with a radius of 6371 km). Assuming that this forcing is balanced by an increase in OLR (outgoing longwave radiation) yields:

$$
\begin{aligned}
\Delta \mathrm{OLR} &= \frac{\partial \mathrm{OLR}}{\partial T}\Delta T = \Delta F_{70} \\
\Rightarrow \quad \Delta T_{est} &= \Delta F_{70}\left(\frac{\partial \mathrm{OLR}}{\partial T}\right)^{-1}
\end{aligned}
\tag{5.6}
$$

which is calculated using the derivative of Stefan-Boltzmann's law: $\frac{\partial \mathrm{OLR}}{\partial T} = 4\sigma T^3$. This calculation assumes that the OLR is emitted from an ideal black body. The calculation has been repeated for a so-called grey body incorporating the emissivity ϵ, such that: $\frac{\partial \mathrm{OLR}}{\partial T} = 4\epsilon\sigma T^3$. The emissivity is however, through *grey-body* calculations, found to be very close to 1, indicating that the black body assumption is fair – especially in the context of this crude estimate. The estimated temperature change at the 500 hPa level is shown along with the corresponding energy transport in Table 5.3.

An initial observation is that the transport is increasing with the increasing atmospheric CO$_2$ concentration in the SOM ALB and NOALB series. This change is

---

[6]the model distinguishes between large-scale (P_L) and convective precipitation (P_C)

5.3 Atmospheric Energy Convergence Anomalies			
Simulation	$\Delta F_{\mathbf{MHT,70}}$ [W]	$\Delta\mathbf{MHT_{LH}}$ [W]	$\Delta T_{\mathbf{est}}$ [K]
CMIP	0.96×10^{13}	1.52×10^{13}	0.17
ERA-Ice	1.09×10^{13}	1.24×10^{13}	0.20
ERA-All	5.20×10^{13}	4.28×10^{13}	0.94
NOALB-PD	0.52×10^{13}	0.25×10^{13}	0.10
NOALB-1.5	3.87×10^{13}	3.72×10^{13}	0.56
NOALB-2	6.70×10^{13}	4.35×10^{13}	1.37
ALB-PD	2.08×10^{13}	1.02×10^{13}	0.39
ALB-1.5	4.69×10^{13}	3.43×10^{13}	0.91
ALB-2	6.95×10^{13}	8.05×10^{13}	1.43

Table 5.3: Arctic energy convergence anomalies and estimated corresponding temperature change in JJA. $\Delta F_{\mathrm{MHT,70}}$ is the change in atmospheric energy transport across 70°N estimated through the box analysis, $\Delta\mathrm{MHT_{LH,70}}$ is the latent contribution, and ΔT_{est} is the estimated corresponding temperature change.

primarily driven by increased latent heat fluxes, which is in line with several studies indicating that the latent MHT is increased in a warmer climate (e.g. *Alexeev et al.* [2005] and *Solomon* [2006]). In the DOM simulations the MHT across 70°N is largest in the ERA-All simulation, which is an equivalent observation to the above, as the increased transport in a warmer climate is likely connected to warming of lower-latitude SSTs (*Alexeev et al.* [2005], *Porter et al.* [2011] and *Screen et al.* [2012]). The transport is decreased somewhat in ERA-Ice compared to CMIP, where only the sea ice cover is different. This could be owing to the fact that the atmospheric transport is affected by the temperature and moisture gradients between the Arctic and the lower latitudes. The reduction causes an Arctic warming (cf. Figure 4.1), and most likely also an increased moistening due to increased evaporation and the additional areas of revealed ocean surface – which could be the reason for the lowered meridional heat transport.

The same effect could be expected in the SOM experiments, when comparing equivalent NOALB and ALB simulations, which only differ in the response of the sea ice cover. However, the effect here seems to be opposite, as the increased sea ice loss leads to increased atmospheric transport. Comparison of the SOM simulations is not as straightforward as in the DOM experiment, as the references of the ALB and NOALB series are not identical. As shown above, e.g. Figure 4.6, the sea ice cover is already reduced in ALB-CTRL compared to NOALB-CTRL, which could affect the transport in the reference, and hence the pattern of changes seen in the two series. Calculations reveal that the increased transport in the ALB simulations is a general result, as ALB-CTRL has an increased MHT across 70°N compared to NOALB-CTRL, and similar results are found in direct comparisons of the PD and 1.5×CO$_2$ simulations. The 2×CO$_2$ simulations are not associated with any significant difference in transport, which is probably due to the more similar climates of the NOALB-2 and ALB-2 simulations (described under Results, Chapter 4).

As previously noted, several studies indicate that the MHT is linked to low-latitude
SSTs – hence, if the sea ice reductions (meaning the difference between equiv-
alent NOALB and ALB simulations) somehow causes an increase in tropical and
subtropical SSTs, this could explain the increased MHT into the Arctic domain.
Figure 5.9 shows the zonal mean temperature differences in each of the ALB sim-
ulations compared to the equivalent NOALB simulation, and reveals that there is
some difference in the temperatures in the albedo-tuned scenarios.
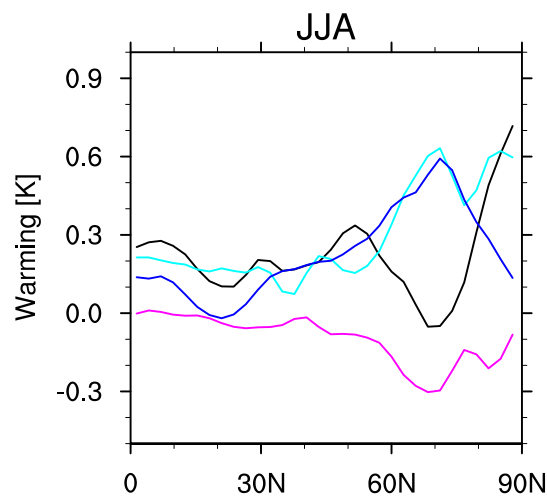
Figure 5.9: JJA zonal mean warming [K] in the ALB simulations compared to the equiv-
alent NOALB simulations: CTRL (**black**), PD (**light blue**), $1.5 \times CO_2$ (**blue**), and $2 \times CO_2$
(**magenta**).

The tropical and subtropical temperatures are increased in the ALB simulations
(except $2 \times CO_2$ case), which has been known to increase the poleward energy
transport. The temperature differences do, however, not indicate a strengthening
of the meridional temperature gradient, but the increased tropical SSTs could still
be a likely cause of the changed transport. The connection between the changed
sea ice albedo and the warming of the tropical SSTs is unclear, but most likely
linked to changes in the large-scale circulations. Similar effects have been found
in multiple GCM studies, which indicate that Arctic climate changes can have
widespread impacts on the climate of the lower latitudes (e.g. recent studies by
Strey et al. [2010] and *Semmler et al.* [2012], and a review of earlier studies by
Budikova [2009]). The transport changes in the DOM simulations are more eas-
ily interpreted, and here the expected effect of the decreased meridional gradients
in temperature and moisture is expressed in a decreased transport following the
reduction of the sea ice cover. This analysis is the first indication that the sea
ice losses in the DOM and SOM simulations have quite different impacts on the
atmospheric circulation.

The estimated MHT related temperature changes, from Equation (5.6), seem –

despite the rough estimate – to correspond well to the observed warming around
500 hPa in the different simulations (more precisely centred on 450 hPa). The
warming of approximately 1 K in the ERA-All simulation is close to, but slightly
bigger than, the magnitude of the peak around 500 hPa (compared to a vertically
uniform warming, cf. Figure 4.5). Assuming that the warming is not entirely
confined to the 500 hPa level, but spread out to the adjacent levels, the slightly
smaller, but wider peak in the vertical profile seems to correspond well to the es-
timate.

Turning to the assessment of the warming estimates for the SOM simulations,
the quite low warming increase in the ALB-PD seems reasonable, although it is
difficult to assess such a small offset in the vertical warming structure (Figure 4.13)
– especially as a result of the expected "smoothing" of the signal to the adjacent
levels described above. The upper-level warming in the 1.5 and 2×CO_2 is more
substantial (cf. Figure 4.14), and the gradual increase in transport corresponds
to the increasingly clear upper-level peak around 500 hPa. The increasing upper
level warming can be interpreted as a combined result of a general warming with
a wide vertical extent, and some process causing a (local) maximum in the warm-
ing around 500 hPa. Consistent with this thought, the difference between the
warming in the different simulations corresponds to the estimated warming from
the transport combined with an extra contribution. These calculations of implied
transports and estimated temperature changes indicate that the elevated warming
peak is likely to be connected to the changes in MHT.

5.5   Circulation changes

As indicated by the MHT changes, the induced changes in sea ice cover and CO_2
concentration may affect the large-scale atmospheric dynamics. The meridional
circulation in the Northern Hemisphere is dominated by three large circulation
cells (the Hadley, Ferrel and Polar Cell), which create substantial up- or downdraft
in their intermediate regions – schematic circulation is shown in Figure 5.10.

Changes in the circulation, and especially in the Polar Cell, could influence the
vertical structure of warming in the Arctic substantially, and is hence analysed
in the following. The Polar Cell downdrafts cold, dry air (a process known as
subsidence) over the central Arctic, and plays a central role in the Arctic climate
system – e.g. in cloud formation. The circulation of the cell is studied through the
zonal mean *stream function* ψ, which gives a clear picture of the meridional circu-
lation pattern in the large scale cells (i.e. the Hadley, Ferrel and Polar Cells). The
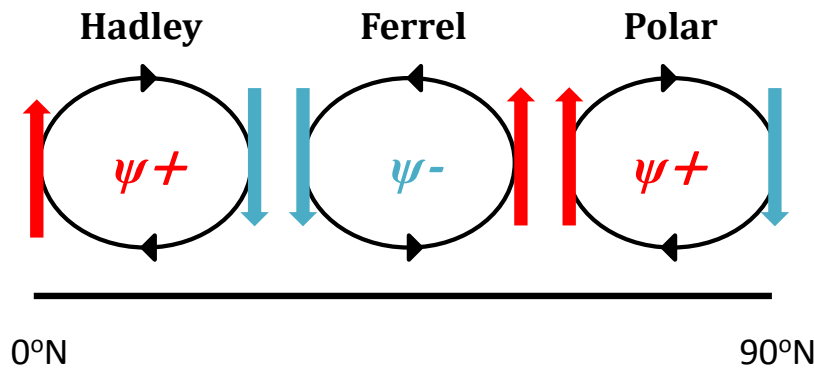
Figure 5.10: Sketch of the large-scale meridional circulation, and the three dominant cells. Each cell is marked with an indicator of the stream function sign, as it would be calculated here (see details below).

stream function is defined such that the vertical (w) and meridional (v) velocities are expressed as (*Kundu and Cohen* [2008]):

$$w \equiv \frac{\partial \psi}{\partial y} \tag{5.7}$$

$$v \equiv -\frac{\partial \psi}{\partial z} \tag{5.8}$$

The flow is often illustrated using the stream function, as constant values ($d\psi = 0$) – so-called streamlines – are parallel to the flow everywhere. Following the continuity equation the flow rate (mass advected per time [Kg/s]) between two streamlines equals $d\psi$, with a direction 90° clockwise from the direction of differentiation (usually along z from the surface up, but here from the top down, as the differentiation follows the model pressure levels in the vertical). The relationship between the sign of the stream function and the direction of circulation is indicated on Figure 5.10. The flow rate in the Arctic Polar Cell is significantly smaller than in the Hadley and Ferrel Cells, and hence the circulation is in the following presented only for the Arctic area – to avoid the Polar Cell "disappearing" due to the larger scale of the mass fluxes in southerly cells. The initial focus will be on the SOM simulations, followed by an overview of the similar analysis of the DOM simulations.

SOM SIMULATIONS

The meridional pattern of the stream function has been evaluated for the ALB- and NOALB-PD simulations. The upper panel in Figure 5.11 presents the seasonal mean stream function in the Arctic domain in the ALB-PD simulation, showing the northernmost part of the Arctic Cell. The positive sign of the stream function indicates subsidence (due to integration following pressure from top to bottom) along the streamlines. The lower panel shows the relative change in the circulation compared to the NOALB-PD simulation – i.e. the changes following from reduction of the sea ice cover.
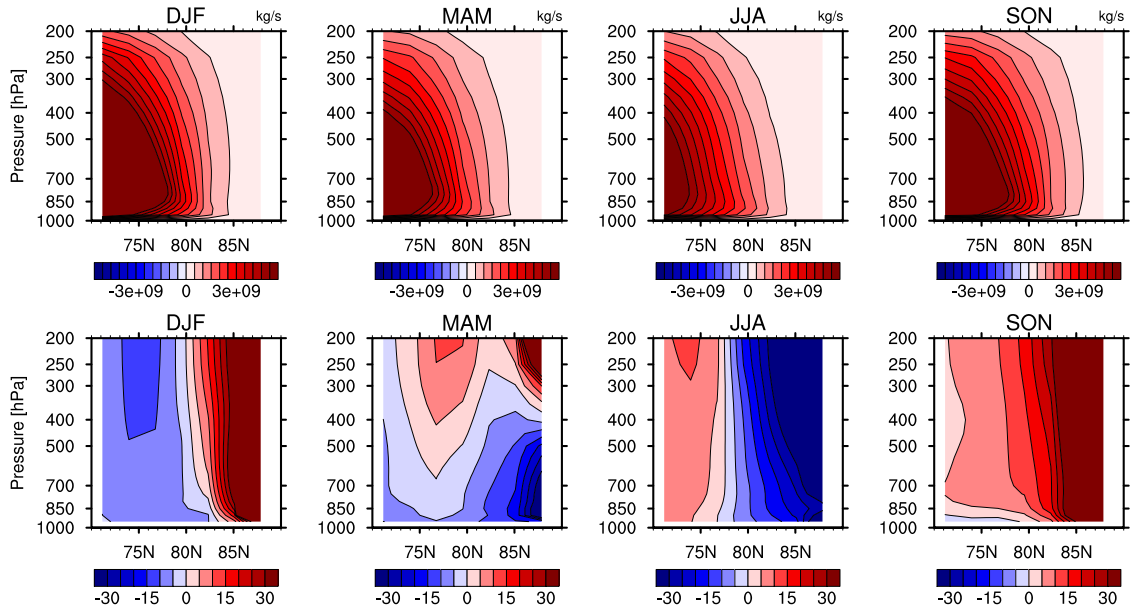
Figure 5.11: Upper panel: The seasonal mean stream function in the Arctic domain, corresponding to the northernmost part of the Arctic Cell. Lower panel: Relative difference of the stream function in [%] in the ALB-PD and NOALB-PD simulations.

The most notable differences in circulation between the ALB-PD and NOALB-PD simulations (cf. Figure 5.11) is the signature of updraft around 80°N (to be interpreted as a decrease in the general downdraft) during winter (DJF) and the increased subsidence in the same area in summer (JJA).

The increased subsidence in JJA could affect the energy budget and change the cloud cover. When the dry, cold subsiding air meets the moister air in the lower atmosphere, condensation and cloud formation is a likely result – why subsidence is often related to formation of low-level stratus clouds (*Wallace and Hobbs* [2006]). Increasing the downwelling flow could however decrease the relative humidity in the layer (assuming moisture sources are constant), which would result in a low cloud decrease. Condensation and hence cloud formation is highly dependent on the relative humidity (especially in the model, cf. *Collins et al.* [2004] and further description in Section 5.6), and subsiding dry air could cause a substantial decrease herein – especially through adiabatic heating, which could cause cloud suppression or evaporation. The correlation between subsidence and cloud formation and dissipation in the Arctic, is studied by *Zuidema et al.* [2005], who finds that increased subsidence is resulting in thinning of the low level clouds (in the late spring).

The decreased DJF subsidence could be the reason for the upper level cooling seen above 600 hPa in ALB-PD compared to NOALB-PD (Figure 4.13). The reduced subsidence would mean less adiabatic heating, which could be the cause of the observed difference.

The vertical circulation patterns are linked to the horizontal circulation as a conse-

quence mass continuity: horizontal divergence demands vertical convergence, and vice versa. Hence, the observed changes in the meridional overturning patterns, may be linked to changes in the horizontal circulation, which would show from an analysis of the surface pressure (PS). In terms of PS, high pressure systems (anticyclones) are – due to air mass divergence – linked to subsidence, while low pressure systems (cyclones) are linked to updraft due to air mass convergence. Figure 5.12 present the surface pressure patterns in the present-day simulations, along with the difference between ALB-PD and NOALB-PD, which illustrates the pressure change following the sea ice reduction.
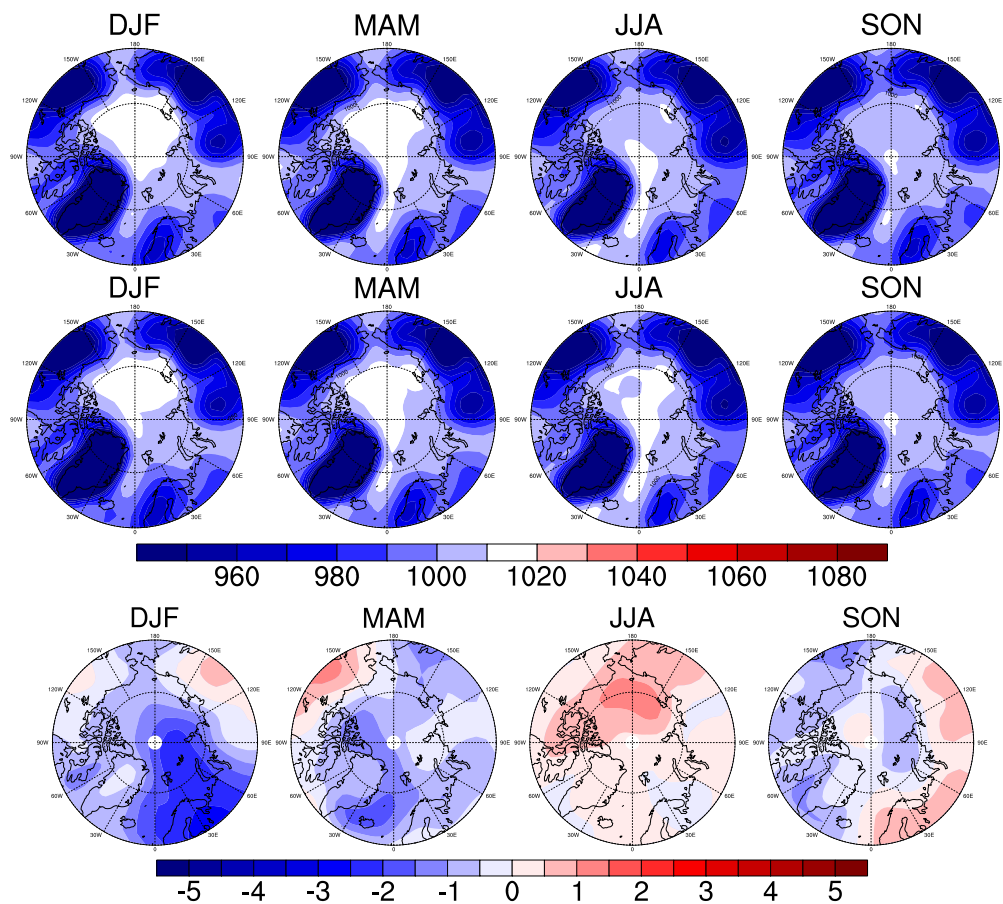
Figure 5.12: Seasonal mean surface pressure [hPa] in NOALB-PD (upper panel) and ALB-PD (second panel), and the pressure difference ALB - NOALB (bottom panel) illustrating the pressure change following the sea ice reduction.

It is evident that the differences in surface pressure in summer and winter are consistent with the observed trends in the vertical circulation. DJF has an Arctic-wide lower pressure, with a substantial change in the Eurasian Arctic, consistent with a limitation of the subsidence. The JJA difference shows a substantial high pressure increase along the Siberian coast, consistent with the increased subsidence. In both instances the latitudes of the maximum pressure difference coincides with

the latitude of the subsidence changes around 80°N (compare with Figure 5.11).

The same tendencies, albeit with some variations, are seen in the 1.5 and $2\times CO_2$ simulations. The difference between NOALB-1.5 and ALB-1.5 has the same change in surface pressure and vertical motion during winter, but a shifted pattern in summer compared to the present-day simulations. The sea ice reduction in JJA still causes an increased high pressure pattern associated with increased subsidence, but the region is shifted southward to around 70°N. The $2\times CO_2$ simulation on the other hand, show changed patterns very similar to the ALB- and NOALB-PD patterns shown here. The magnitude of the pressure differences are gradually bigger following the CO_2 level, suggesting that the sea ice reduction has a bigger impact on the circulation in a warmer climate, or that other factors in a warming climate also affect the circulation.

DOM simulations

The DOM simulation show a less pronounced change in the circulation patterns following the sea ice reduction and SST increase. The sea ice reduction (i.e. the difference between CMIP and ERA-Ice) only results in limited, insignificant pressure changes. The wintertime stream function indicate the same pattern of a reduced Polar Cell, while the summertime has no substantial changes within the Arctic domain, except a small northward shift of the cell (not shown). Neither the SST increase (i.e. the difference between ERA-Ice and ERA-All) nor the combined effect of SST and sea ice changes (the difference between CMIP and ERA-All) show any changes similar to what is observed in the SOM simulations. This could indicate that the spatial pattern of sea ice reduction is important for the circulation changes – as the general reduction of sea ice concentration in SOM is quite different from the induced changes in DOM (which is a combination almost complete loss of sea ice in some regions with sustained high concentrations in other areas). Alternatively the feedbacks of ice and upper ocean play a role – or it could be a combination of the two.

5.6   Relative humidity and clouds

A warming Arctic climate is expected to result in a moistening of the atmosphere – i.e. an increase in the specific humidity q. The source of the moisture is to a large degree increased evaporation from the surface, due to a larger area of ice free ocean surface and higher ocean temperatures. The moisture changes have the potential to cause further climate changes – especially in relation to clouds. The humidity and cloud changes are investigated in the following section, again with initial focus on the SOM experiment followed by an overview of the equivalent results in the DOM simulations.

SOM experiments

Figure 5.13, showing the q changes in NOALB- and ALB-PD relative to the respective references, clearly reveals that the specific humidity is increased following the sea ice reduction. The increased moisture generally has a wide vertical extent, but has comparable structure to the temperature changes, with peaks near the surface in DJF and SON, and limited increase near the surface in JJA. This correlation is expected, as a result of the general coupling of warming and moistening, and the fact that moisture and temperature inversions often coincide.
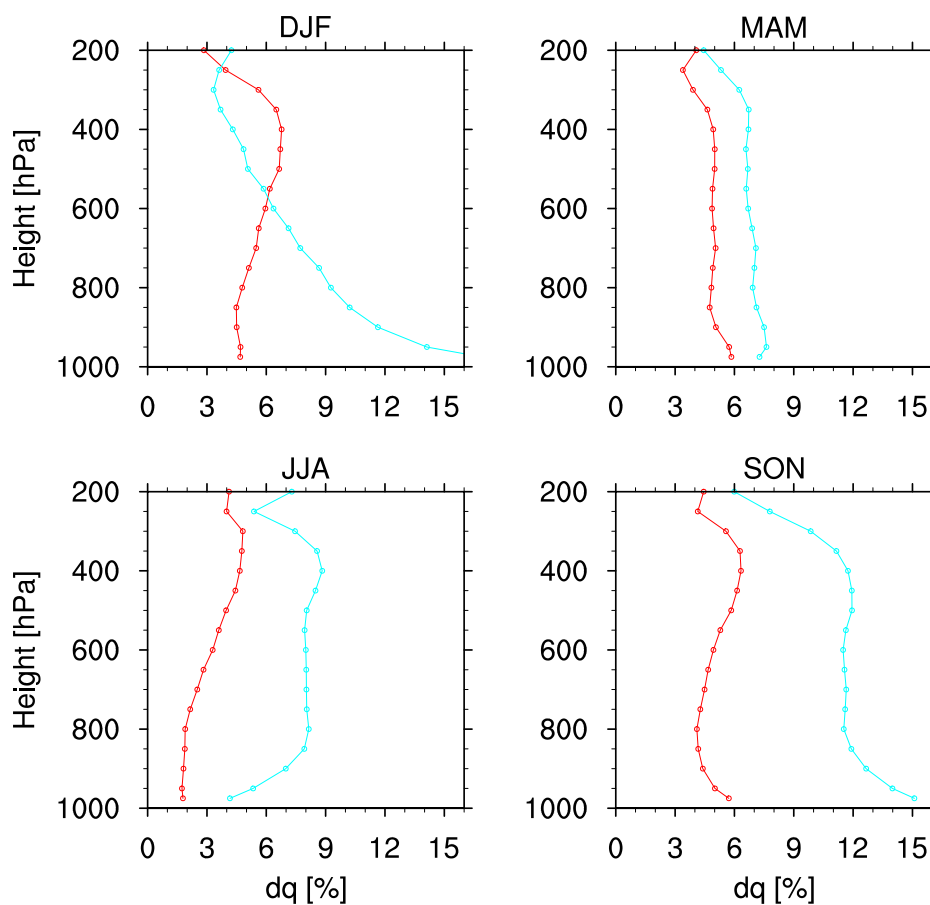
Figure 5.13: Changes in [%] of the specific humidity (q) in NOALB-PD (**red**) and ALB-PD (**blue**) relative to the respective references.

The increase at the higher levels in the atmosphere in JJA and SON is likely contributing to increase the Arctic greenhouse effect. As explained in Section 2.4 water vapour is more efficient as a greenhouse gas, when situated higher in the atmosphere because of the lower emission temperature. Hence – in terms of the LW radiation budget – the more elevated increase likely has a bigger direct effect on the climate, than the occasionally bigger increase near the surface. The indirect effects of the moisture increase can, however, also lead to significant changes.

The pattern of change in the specific humidity does not imply an increase in relative humidity RH, due to the dependence on the temperature (explained in Section 2.4). Condensation, and thereby cloud formation, is highly dependent on RH, which is not necessarily increasing with increased q. Figure 5.14, which show the vertical profiles of the change in RH, reveals that the pattern of change for the two variables is indeed very different.
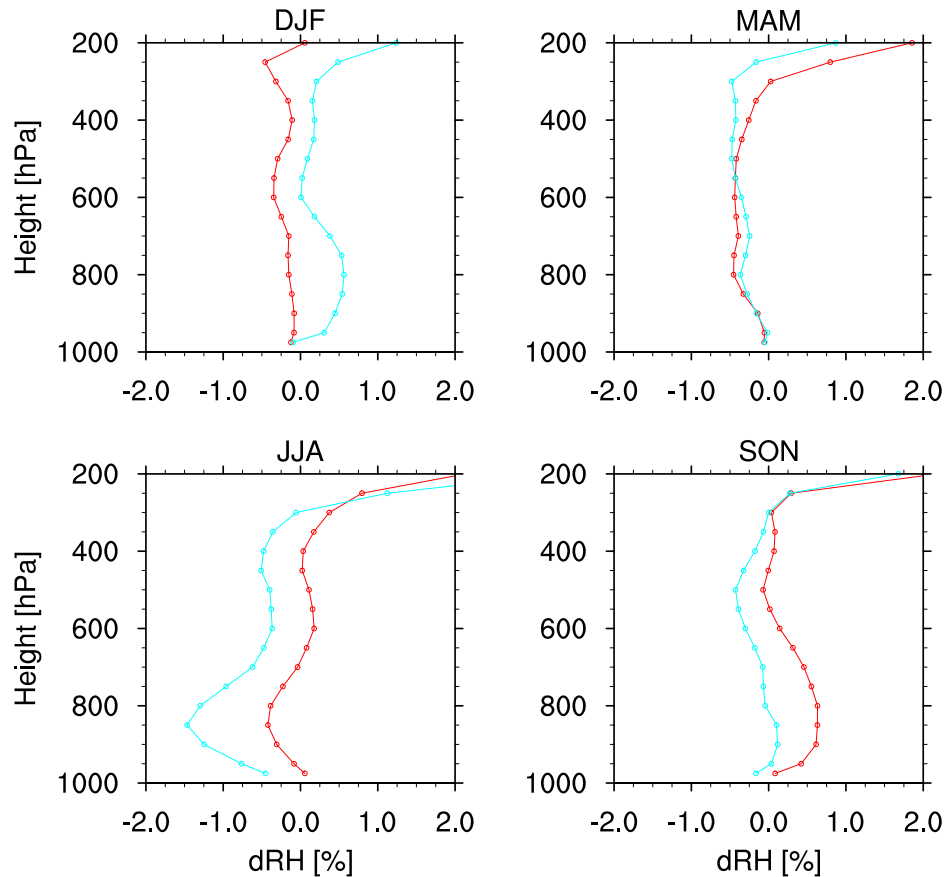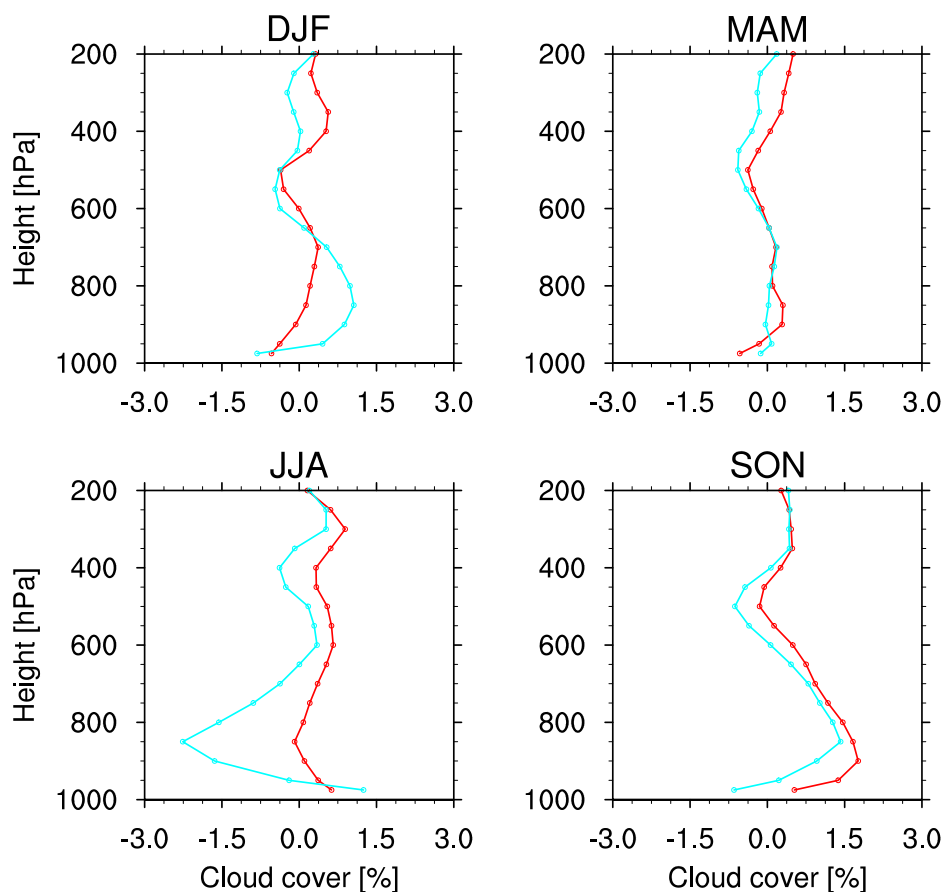

Figure 5.14: Changes in relative humidity (RH) in NOALB-PD (**red**) and ALB-PD (**blue**) relative to the respective references.

The increased sea ice reduction in ALB-PD only cause quite limited changes in RH. Spring (MAM) is completely unchanged, while winter and autumn have small changes of opposite sign, which are biggest at the lower levels slightly above the surface (RH is increased in DJF and reduced in SON). The biggest difference is found in JJA in the low level atmosphere: a RH reduction peaking around 850 hPa. This peak reduction coincides almost perfectly with the peak in warming (Figure 4.13) – intriguing as the warming generally is associated with an increase in moisture. The opposite changes in DJF and JJA are consistent with the observed circulation changes (Figure 5.11). The decreased subsidence in DJF is linked to an

increase in the cloud cover, while the increased subsidence in JJA has the opposite effect.

Cloud formation is highly dependent on the RH, as cloud droplets only will form, when the air is supersaturated with respect to moisture ($e > e_s \Rightarrow \text{RH} > 100\%$) (e.g. *Houze Jr.* [1993]). In the model physics, formation of layered clouds is solely dependent on the RH (*Collins et al.* [2004]), and hence the decrease in RH most likely implies a similar decrease in clouds at the same altitude. The levels around 850 hPa are associated with the – in summer – very widespread Arctic stratus clouds (*Houze Jr.* [1993] and *Serreze and Barry* [2005]), which are likely to be affected (reduced) by the decreased RH. Figure 5.15 shows the vertical distribution of seasonal cloud changes in the NOALB- and ALB-PD simulations, and confirms the decrease in low clouds near the level of increased warming and reduced RH.

Figure 5.15: Vertical distribution of seasonal cloud changes in NOALB-PD (red) and ALB-PD (blue) relative to the respective references.

The increase in low clouds in autumn and winter is an expected result of warming and sea ice reduction, found by *Vavrus et al.* [2009, 2011] and *Liu et al.* [2012], due to increased evaporation from the surface combined with the stable stratification

of the lower atmosphere. The lower-most clouds in JJA are also increased, but at a slightly higher altitude, a clear low-level cloud reduction is evident. As suggested by the steps in this analysis, this reduction could be linked to changed circulation patterns: the sea ice reduction somehow affects the amount of subsiding air, which – through adiabatic warming – reduces the RH and the cloud amount in the extensive Arctic summer low level stratus layer. A reduction of the cloud cover in summer would have a warming effect, as the highly reflective stratus clouds are reduced, which would present itself as a surface based warming. The increased surface based warming could initiate a positive feedback loop, which would increase the cloud reduction, and perhaps contribute to the lower-level JJA warming peak along with the adiabatic heating.

Aside from the low-level JJA reduction, the Arctic cloud cover generally increases as a result of the reduced sea ice cover – and the changes are primarily evident in the low-level cloud cover (i.e. below 700 hPa). The increased evaporation from a warmer ocean, and an increased revealed (ice-free) ocean surface, combined with the stability of the lower atmosphere, means that the moisture increase will primarily affect the low clouds – except in JJA, where low-level stability is less pronounced (see Section 5.7). The spatial pattern of cloud changes (Figure 5.16) clearly shows that the change in cloud cover generally is dominated by changes in low clouds (response in low and total cloud fraction is very similar), while the spatial distribution seems unrelated to the pattern of sea ice loss. The general increase in clouds along the east coast of Greenland is the only clear feature that correlates with sea ice loss (compare with Figure 4.7). Note that the average low cloud change (mean from 1000 hPa to 700 hPa) is positive in JJA, as a result of the substantial cloud increase in the lowest levels.

As argued in the Scientific Introduction (Section 2.4) Arctic clouds have a net warming effect for the entire year except for a brief period in summer. This is especially the case during winter, when sunlight is completely absent in a large part of Arctic. The overall reduction of the cloud cover over the Arctic Ocean in DJF is thus expected to have a cooling effect, and cannot account for the increased near-surface warming – with the caveat that a change in the composition of cloud types could still cause a warming, even with an overall reduction, as some clouds (high clouds, with cold cloud tops) are more efficient in increasing the greenhouse effect, and limiting the LW loss to space.

The warmer scenarios exhibit very similar trends in RH and cloud changes. *Vavrus et al.* [2009] compares CMIP3 model mean data from climate simulations of the late 20th century with simulations of projected climate in the late 21st century, and finds a general increase in Arctic clouds. The increased cloud cover is a combination of an increase in low clouds, peaking between the surface and 850 hPa depending on the season, and an increase in high clouds, peaking around 200-250 hPa. This constitutes a fair basis for comparison with the warmer scenarios,
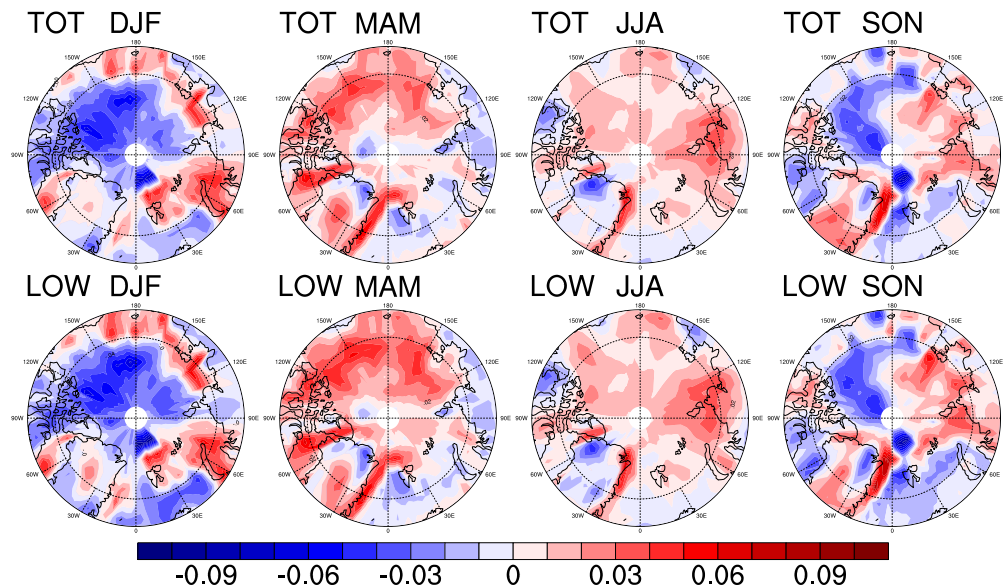
Figure 5.16: Fractional difference in total (upper panel) and low (lower panel) cloud cover in ALB-PD compared to NOALB-PD. Positive values indicate an increase in ALB.

which (using the SRES A1B scenario by *Nakićenović et al.* [2000]) correspond to projections of the climate in approximately 2050 ($1.5 \times CO_2$) and 2100 ($2 \times CO_2$) – where the NOALB simulations can be seen as relatively conservative projections (cf. Figure 4.8).

The general pattern of the cloud changes are in agreement with the findings by *Vavrus et al.* [2009], apart from the – already discussed – low-level reduction in albedo-tuned simulations around 850 hPa in JJA. It is worth noting that the peak is of almost equal size in the ALB-PD, -1.5 and -2 simulations, and that it in all three cases is correlated with a decrease in relative humidity (only shown for ALB-PD in Figure 5.14). Another striking thing is that neither of the warm NOALB simulations have a similar cloud decrease – clouds are almost unchanged at the 850 hPa level in both simulations. Apparently it is not the general state of the sea ice cover that is decisive for the reduction, but rather a ice-ocean-atmosphere feedback that depend on the state of all three elements – as NOALB-2 and ALB-1.5 have very similar ice extents (Figure 4.6), but different cloud and RH responses.
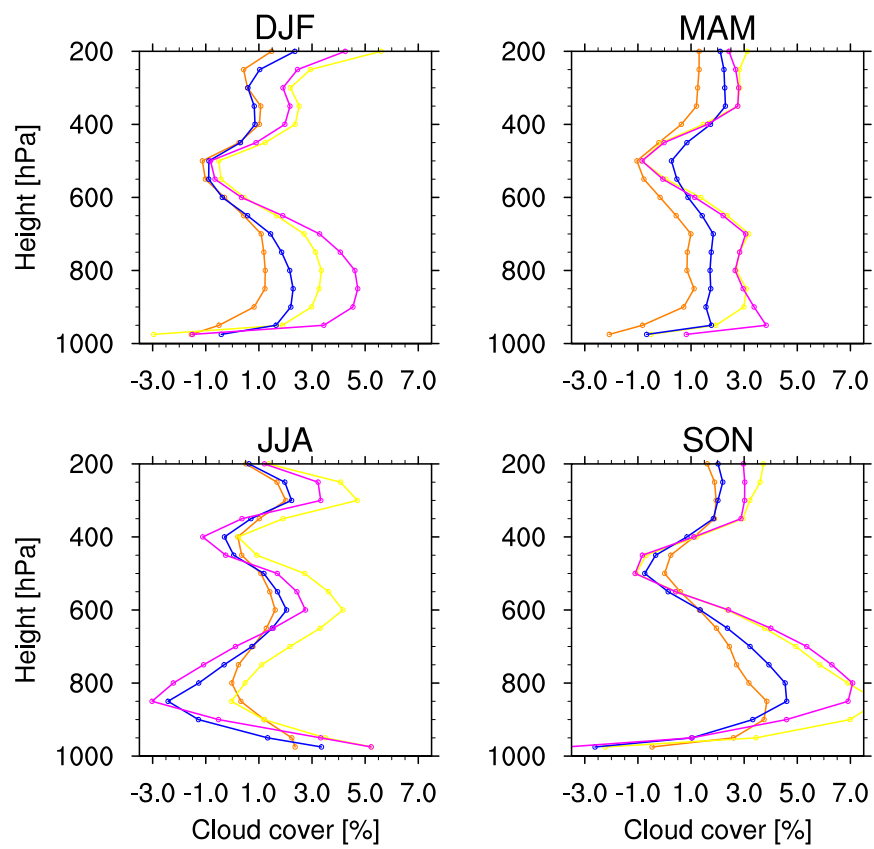
Figure 5.17: Seasonal mean vertical profiles of cloud changes in the "warmer" SOM scenarios: NOALB-1.5 (orange), ALB-1.5 (blue), NOALB-2 (yellow), and ALB-2 (magenta), compared to their respective CTRL climates. Note the shifted axis compared to Figure 5.15.

DOM EXPERIMENTS
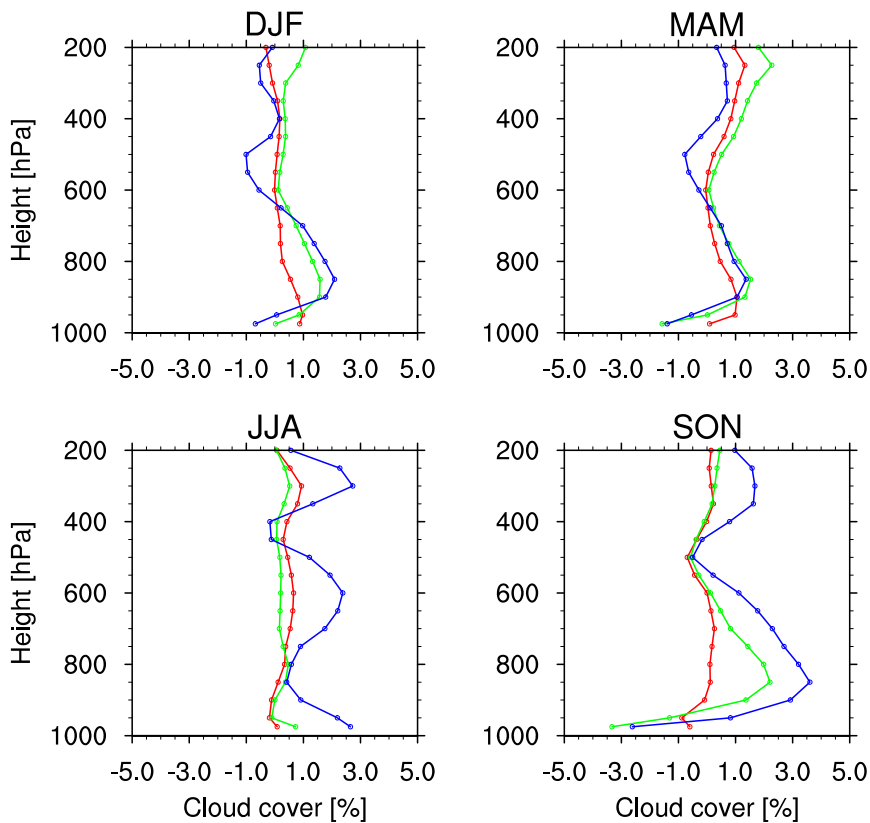
Figure 5.18: Equivalent to Figure 5.17, but for DOM simulations: CMIP (red), ERA-Ice (green), and ERA-All (blue).

The primary cloud change resulting from the ice cover reduction in ERA-Ice compared to CMIP is found in the autumn (SON), where low-level clouds are significantly increased – as shown in Figure 5.18. This is an expected result of the reduced insulation effect of the now diminished sea ice cover, which allows for greater heat and moisture fluxes from the ocean to the atmosphere, when the atmospheric temperature drops in autumn. The low cloud increase persists somewhat into the winter (DJF), but otherwise the cloud changes in ERA-Ice are limited. Increasing the SSTs – the ERA-All simulation – results in more widespread cloud changes that are somewhat reminiscent of the patterns seen in the SOM profiles. The general combined increase of lower and high clouds is evident again, while the low cloud increase exceeds the high cloud increase. The JJA profile show an increase in near-surface and high clouds, along with a mid-level increase, which is also clearly evident in the warmer SOM simulations (Figure 5.17). There is no sign of the low-level JJA cloud reduction in either of the DOM simulations, consistent with the limited changes in the vertical circulation related to the Polar Cell (Section 5.5).

5.7   Atmospheric stability and inversions

As argued earlier, the increased near-surface warming is expected to diminish the surface based inversions, and hence reduce the stability of the lower troposphere, allowing for more vertical mixing. The is expected to result in the wide vertical extent of warming observed in the warmer scenarios. In the following, the inversion strength in the lowermost atmosphere is investigated for all the scenarios, which will reveal how the stability is affected by warming due to increasing CO_2 and reduced ice cover. The inversion strength is here defined by the temperature difference between near-surface level and an adjacent level aloft, here calculated as the difference: $T(850 \text{ hPa})$ - $T(975 \text{ hPa})$.

Figure 5.19 shows the seasonal mean inversion strength in the Arctic for all four NOALB simulations, and reveals the effect of a gradually warming Arctic on the stability of the lower atmosphere. Inversions are widespread in DJF and MAM in all simulations. Although the dominating stable structure persists even in the warmest scenarios, the warming clearly weakens the inversions. The control climate is dominated by inversions in the autumn (SON), but these are quickly destroyed with the rapid increase in near-surface warming. The 1.5 and $2 \times CO_2$ scenarios show no signs of SON inversions anywhere in the Arctic. Opposite to all other seasons JJA seems to have increased inversion occurrence with increased warming. This is likely connected to the limited surface temperature change compared to the more elevated levels (Figure 4.14). The pattern of change in the occurrence of inversions suggests that there is increased potential for vertical mixing in SON, while DJF and MAM still are dominated by surface-based inversions. The JJA warming could lead to an increased stability in the warmest climates simulated here. The low-level peak in JJA warming observed in the ALB scenarios results in an even clearer increased occurrence of inversions, cf. comparison of the ALB and NOALB $2 \times CO_2$ climates in Figure 5.20.

The increased sea ice loss in the ALB-2 simulation leads to a more drastic reduction of the inversion strength in DJF and MAM, as the sea ice loss gives rise to further surface-based warming. The lower level warming peak in JJA seems to cause a slight increase in inversion occurrence in the ALB case, while the almost ice free conditions in SON allows for widespread vertical mixing in both simulations.

The studies by *Bintanja et al.* [2011, 2012] indicate that the existence of wintertime inversions intensifies the Arctic amplification, through dampening of the outgoing longwave radiation (OLR). GCM experiments reveal that the warming below the inversion does not affect the amount of OLR, and hence the LW flux following the warming of the lowest layers must be directed downwards further promoting the near-surface warming. Hence existence of inversions limits the negative Planck feedback. The simulations in this project reveal that a reduction of
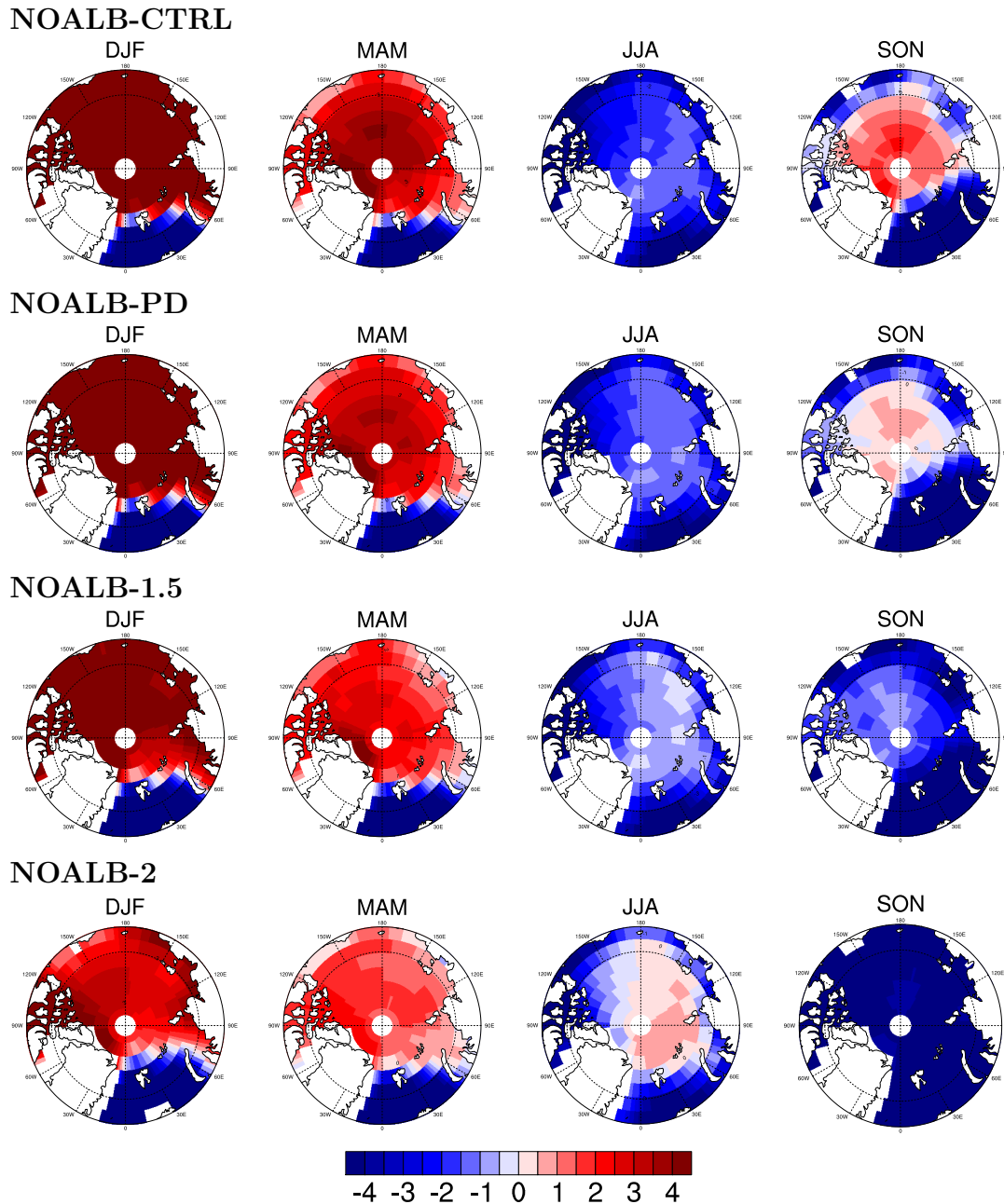
Figure 5.19: Surface-based inversion strength expressed as the temperature difference $T(850$ hPa$)$ - $T(975$ hPa$)$. Hence positive values (red shading) indicate a temperature inversion, while negative values (blue shading) indicate unstable conditions. Each row presents the seasonal means of the inversion strength in each of the four NOALB simulations. From the top down: NOALB-CTRL, -PD, -1.5 and -2.
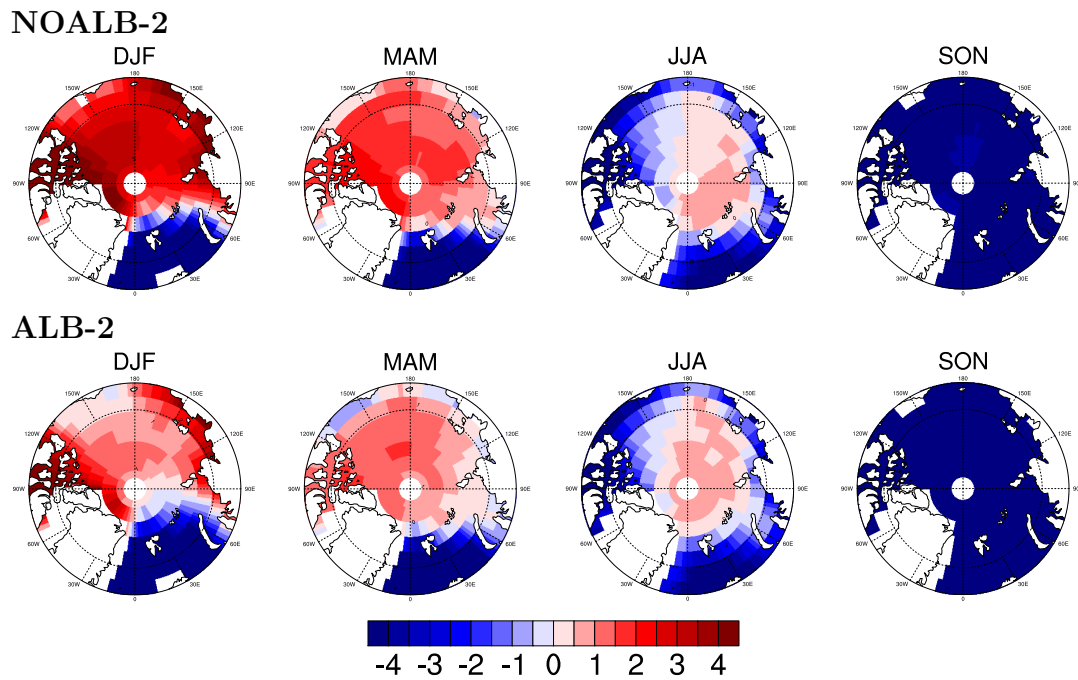
NOALB-2

ALB-2

Figure 5.20: Surface-based inversion strength expressed as the temperature difference $T(850$ hPa$)$ - $T(975$ hPa$)$. Upper (lower) row shows the seasonal means of the NOALB-2 (ALB-2) simulation.

the sea ice cover weakens the inversion strength, which would gradually disable this inversion feedback – as noted by *Bintanja et al.* [2012]. However, the wintertime climate in the $2\times CO_2$ scenarios are still dominated by surface inversions, and thus the system can warm substantially, before the suggested inversion feedback would be completely lost.

6   Discussion summary

The two experiments indicate that the sea ice cover plays a very central role in shaping the Arctic warming. Furthermore this analysis reveals the complexity and high level of interconnection of the climate system, as the Arctic sea ice is affected by, and is itself affecting, the climate change at much more southerly regions. One of the central themes in this thesis is the relative importance of the remote and local factors behind the Arctic amplification of climate change. The results from these experiments stresses that both local and non-local effects work to shape the warming signal. The couplings of the climate system – not least through the Arctic sea ice cover – makes it hard to distinguish the causality patterns, and to decide the origin of the warming tendencies. One clear example of this coupling is that the reduction of the sea ice cover in the SOM simulations introduced through a sea ice albedo reduction, also affects the lower latitude SSTs. The low latitude warming in turn affects the meridional heat transport into the Arctic, which further promotes Arctic climate change. These geographically separated couplings, or *teleconnections*, have received increasing attention in the scientific community, and has revealed that sea ice changes can have implications for the climate far beyond the Arctic area (*Francis et al.* [2009] and *Bader et al.* [2011]).

The focus of this project is on the within-Arctic climate changes, and one clear conclusion from all across the experiments is that the sea ice reduction has a substantial impact on the low-level warming. The warming is primarily driven by changes in the turbulent heat fluxes. The most direct result of the sea ice reduction is an increased sensible flux from the ocean surface to the atmosphere, arising due to the loss of the insulating effect of the sea ice cover. The warming is biggest in late autumn and winter, where the temperature gradient between the ocean and the atmosphere is high, and the regrowth of insulating new ice is still limited. The high static stability of the lower atmosphere (especially during winter) means that the heated air stays confined to the surface layers, and that the warming will be evident as a surface based peak in the vertical profile of warming, which decays quickly in the vertical. The connection between the sea ice loss and low-level warming is especially clear from the DOM experiment, and has been proved by the spatial pattern of the surface energy flux changes (Figure 4.2) and the regional "masking" analysis, which showed the regions of sea ice loss had substantial near-surface warming compared to all other regions and the Arctic (Figure 5.6).

The effect of SST changes is investigated in the DOM experiment directly, but is also evident in the SOM experiment, where SSTs are warming following CO_2 increases and through increased SW absorption (in connection to SAF). Warming of the ocean leads to further increased temperature gradients between atmosphere and ocean, and thus increases the sensible heat flux. The main change following an SST increase is however, as shown in the analysis of the turbulent flux changes (Section 5.3), driven by the latent heat flux increases resulting from increased evaporation from the warmer ocean surface. A reduced sea ice cover has a twofold effect on the latent heat fluxes, as it allows the upper ocean to warm, and allows for increased evaporation from the now greater area of revealed ocean surface.

This surface-based warming effect of a reduced sea ice cover alone means that the conclusions by *Chung and Räisänen* [2011] on the relative high- and low-level warming in GCMs compared to reanalysis data is – as expected prior to this assessment – highly problematic. It seems that the sparse low level warming in the models can simply be explained by the limited sea ice reduction in period from 1970-99 compared to the period 1979-2010, on which the ERA Interim warming estimate is based.

The additional surface-based warming, which is seen in both DOM and SOM simulations, means that the vertical structure of warming in the model simulations resemble the ERA Interim data quite well. One main difference still remains: the low-level warming pattern in summer. The DOM simulations indicate that sea ice reductions leaves JJA temperatures almost unchanged, while the SST increases results in warming with a wide vertical extent, with a peak around 500 hPa connected to atmospheric heat transport from lower latitudes. It is unclear, why the low-level peak in the summer warming profile, which is evident in the ERA Interim mean (Figure 3.1), should be expected. One interpretation is that it is simply the signal from the general surface based warming, which is limited near the surface due to ice melt. "Removing" all heat near the surface from the general warming pattern of the remaining seasons would leave a peak reminiscent of the ERA Interim profile. An alternative explanation is that some effect causes warming at these particular layers in summer. Such a warming could arise from advection of warm air from lower latitudes. *Graversen et al.* [2011] finds that the extreme ice loss of 2007 is connected to an anomalous atmospheric flow of warm, humid air into the regions of accelerating melt. The analysis is based on ERA Interim data, and the transport changes are peaking around 900 hPa, and are thus likely contributing to the low-level warming in peak in the 2006-10 warming mean calculated in this project. However, according to *Graversen et al.* [2011] the transport results in increased humidity and cloudiness, which is inconsistent with the analysis of moisture and cloud changes in the simulations performed here (Section 5.6). The SOM simulations here do reveal a general increase of the specific humidity, but no peak is found around 900 hPa in the profile of relative changes in q (Figure 5.13). Furthermore the cloudiness (following the relative humidity) is

reduced at the levels of maximum warming, which would be an unexpected result of warm, humid air entering the Arctic. Multiple processes could, however, be contributing to the simulated changes, and it is possible that circulation changes causing increased warm air advection into the Arctic contributes to the low-level JJA warming. As the low-level peak is only seen in the SOM simulations, it is clear that the cause of the warming must be connected the spatial distribution of the sea ice cover, or feedbacks involving the ice cover and the upper ocean, which would be disabled in the DOM setup. The gradual stagnation of the relative size of the low-level peak with increasing warming (i.e. comparing ALB-PD, -1.5 and -2 simulations), follows the reduction of the sea ice extent, suggesting a clear link between the warming and the state of the sea ice cover. The analysis of the regional warming differences (Section 5.2) also reveals that the low-level warming peak only is a pronounced feature in ocean covered regions, making the link to the changing sea ice cover increasingly probable. This suggested link, leads me to expect that the low-level peak will not increase substantially with additional forcing (exceeding the level in ALB-2), as seasonally ice free conditions are already reached, and further reduction is naturally limited.

The fact that the JJA low-level warming peak is found to be coinciding with a decrease in relative humidity (RH) and cloud cover at the same altitude, is somewhat surprising. Increased temperature and moisture in the atmosphere following the sea ice loss is expected to increase the cloud cover (e.g. *Liu et al.* [2012]) – a trend which is seen in the lowermost clouds in all simulations (Figures 5.15 and 5.17). The combination of the increased lowermost clouds and the decrease above could indicate a shift in the cloud height. Alternatively the cloud changes are a combined result of a general increase in the lowest clouds, and a specific reduction around 850 hPa caused by some process linked to the sea ice loss. The further analysis of circulation changes in Section 5.5 reveal a possible mechanism behind the cloud reduction: increased subsidence of dry air. The subsiding air becomes relatively warm through adiabatic heating, and the warm dry air could be the cause of the reduction of cloud near the boundary layer, which is dominated by a dense layer of stratus clouds during summer. This process would work to warm the low-levels near the observed warming, and the cloud decrease might further accelerate the surface-based warming through increased SW absorption at the surface. This hints to the existence of a possible positive feedback, increasing the near-surface warming.

The vertical motions are linked to the patterns of the surface pressure, as a consequence of mass continuity: divergence in the horizontal plane, demands vertical convergence, and vice versa. Hence subsidence is connected to high pressure (anticyclonic) systems, and updraft to low pressure (cyclonic) systems. *DeWeaver and Bitz* [2006] compare the Northern Hemisphere circulation in simulations with CAM3 (the atmospheric GCM, which is also employed in this project) to ERA Interim data, and conclude that the summertime circulation patterns are quite different. In the ERA Interim data the traditional three cell pattern (described

here in Section 5.5) is expanded with an additional Ferrel Cell north of the tradi-
tional Arctic Polar Cell. The Ferrell Cell is associated with a low pressure system,
which dominates the central Arctic during summer – in line with observed pat-
terns of a dominating central polar cyclone (*Serreze and Barry* [1988]) bounded
by high pressure areas associated with the subsidence of the Polar Cell. In line
with *DeWeaver and Bitz* [2006] the simulations performed here with CAM3 show
no signs of the summertime polar low and the associated extra Ferrel Cell. The
increased strength of the subsidence of the Polar Cell is found at latitudes between
70 and 80°N indicating consistence between the Polar Cell in the model, observa-
tions (*Serreze and Barry* [1988]), and reanalysis-data (*DeWeaver and Bitz* [2006]).
Although the summertime circulation in the Arctic in CAM3 might be erroneous,
the Polar Cell seem to have the correct properties, and the observed changes is
likely to be more than model artefacts.

How the reduced sea ice cover causes an increased subsidence in the Polar Cell
is not clear. Changes in the surface pressure could be expected from the surface-
based warming, while the increased warming likely would favour cyclonic behaviour
rather than the observed high pressure increase: *Simmonds and Keay* [2009] sug-
gest that sea ice loss would result in enhanced development of already-existing
cyclones. The mean cyclonic pattern of the Arctic is primarily a result of cyclonic
systems originating outside the Arctic migrating into the Arctic area (*Serreze and
Barrett* [2008]), and changed circulation patterns beyond the Arctic thus might
affect the within-Arctic pressure changes.

The sea ice cover's substantial impact on large-scale atmospheric circulation seems
more complex than a straightforward cause-and-effect relationship. The difference
between the results from the DOM and SOM experiments can possibly reveal some
of the driving factors, since the JJA low-level warming and circulation changes are
not seen in the DOM simulations. The crucial factors are apparently only present
in the SOM albedo-tuned simulations. The central factors must thus be connected
to either (1) The spatial distribution of the sea ice cover, (2) Changed storm tracks
affected by sea ice and SST changes, or (3) Some other feedback related to the
inclusion of the upper ocean and active sea ice.

(1) The spatial distribution of the sea ice loss in the SOM simulations, which is
    manifested as a general decrease of the sea ice concentration, means that the
    insulating effect of the sea ice cover is dramatically reduced. The regionally
    dependent sea ice loss observed in recent years (exemplified with the ERA
    Interim 2006-10 mean used in this project) divides the Arctic into ice free
    regions and areas of very dense sea ice concentrations (approaching 100%
    sea ice cover), which results in almost complete insulation of the ocean from
    the atmosphere. These are especially the regions North of Greenland and
    Canada, where the thickest, densest ice is found. The overall reduction in
    the SOM simulations allows for more "communication" between ocean and
    atmosphere over the entire Arctic area, which could influence atmospheric
    circulation, through increased heat and moisture fluxes, changing the atmo-

spheric properties compared to the original colder, dryer air above a dense sea ice cover.

(2) Several studies (e.g. *Magnusdottir et al.* [2004], *Strey et al.* [2010], and review by *Bader et al.* [2011]) have proven that the sea ice cover has a substantial impact on the surface pressure patterns and the storm tracks. The mean surface pressure increase observed in connection to the increased subsidence and low-level warming could be en expression of fewer cyclones entering the Arctic area – which is a possible effect of a storm track shift.

(3) The idea behind including the SOM experiment was that the inclusion of an active sea ice cover and upper ocean could result in a more "true" response, as this setup comes closer to resembling the actual climate system, and allows for more feedbacks than the fixed-surface setup. It is, however, not clear from this analysis, exactly why the SOM experiment apparently comes closer to the trends of the reanalysis. Nevertheless it supports the original suspicion that the additional ice and ocean related feedbacks could be important for the Arctic warming. There may be interconnections and feedbacks that this and other analyses overlooks, as several parts of the climate system are still poorly understood – especially in connection to clouds and teleconnections in the large scale circulation, which are central agents here.

Comparison of the vertical profiles of warming (Figure 3.1) was originally used by *Chung and Räisänen* [2011] to indicate the relative roles of local and remote sources of Arctic warming. The simulations done in this project indicate – in line with observations/reanalysis data – that the low-level warming signal from the sea ice loss exceeds the upper-level warming in all seasons, in the simulated climate states ranging from present-day analogues to CO_2 doubling scenarios. It should be noted that the upper level warming become increasingly dominant with increasing temperatures, as indicated by the future scenarios simulated in the SOM experiment. Comparing the ERA-Interim warming profile in Figure 3.1 to the warming in the ALB-PD simulation (Figure 4.13) does however suggest that the upper level warming is more pronounced in the model. Thus, there may still be reason to debate and investigate the treatment of MHT changes in GCMs – but the basis on which the conclusions in *Chung and Räisänen* [2011] are made, is proven to be invalid.

It is important to stress, that while this analysis reveals that sea ice changes are central in shaping the Arctic warming, it does not necessarily imply that local, within-Arctic processes are the dominant factors behind Arctic amplification. Warming from increased heat transport could very likely be causing sea ice retreat, which would lead to a warming signal, which apparently originates at surface, although it is triggered by remote factors. *Chung and Räisänen* [2011] actually suggest such a mechanism, as a possible cause of Arctic amplification: "*a possibility exists that Arctic warming is remotely induced by the GHG forcing in lower latitudes and is amplified by snow and ice feedbacks.*"

Across the simulations there is a general tendency of a warming peak near 500 hPa. The warming peak indicates a heat convergence, and as neither the cloud, moisture changes or other potential warming factors gives reason to expect an increased convergence, it seems likely that the warming peak is connected to the increasing MHT. This seems increasingly likely considering the estimates of corresponding temperature changes and the pattern of MHT change in the different scenarios.

The test of statistical significance revealed that this upper level warming in the ERA-All scenario was significant in an isolated region in the Pacific sector of the Arctic Ocean (Figure 5.3). Neither the global pattern of SST increase or the regional warming analysis, however, revealed any signs of an increased warming or transport in this particular area. Increased heat transport from the Pacific Ocean could be a potential candidate for increased elevated warming – analogue to the observed pattern in 2007 (*Graversen et al.* [2011] and *L'Heureux et al.* [2009]). As this simulation is done in the DOM setup, there is sadly no response in the sea ice cover to indicate a possible increased melt connected to the transport.

In the warmest scenarios the analysis of the atmospheric stability and temperature inversions (Section 5.7) indicates that the low-level warming peak around 850 hPa combined with the more limited near-surface warming gives rise to an increasingly stable near-surface layer. The seasonal mean inversions are still relatively weak and confined to the central Arctic, and some vertical mixing of the surface-based warming is expected to contribute to the warming of the more elevated layers. This is in agreement with the vertical profiles of warming, which indicate that the warming aloft is bigger than the combined estimated effect of the MHT plus the contribution from LW absorption.

The GCM experiments indicate three central reasons for the elevated warming: (1) Increased meridional heat transport in a warmer climate, (2) Decreased atmospheric stability in winter, spring and autumn, allowing for more vertical mixing and consequent spreading of the surface-based warming, and (3) Increased LW fluxes from the surface, resulting in increased heating from absorption by clouds and greenhouse gases. However, the high-level warming does not reach the magnitude of the low-level warming except in the CO_2 doubling experiments. The simulations achieve an seasonally (almost) ice free Arctic Ocean, and the low-level warming is no longer increased by sea ice related feedbacks.

7   Conclusion

This project has, using two different GCM experiments, investigated the impact of a changing sea ice cover on the Arctic warming. The DOM experiment with prescribed and fixed sea ice conditions revealed that the reduction of the sea ice cover results in substantially increased heat fluxes from the ocean to the atmosphere, which gives rise to a strong near-surface warming signal in all seasons except summer. The lower Arctic atmosphere is in the colder seasons (DJF, MAM, and in part SON) dominated by temperature inversions, which confines the warming to the lowermost layers, and possibly gives rise accelerated near-surface warming by limiting the outgoing longwave radiation through the lapserate feedback. The warming following the sea ice reduction is primarily driven by an increased sensible heat flux from the relatively warm ocean to the atmosphere. The warming pattern and magnitude simulated by the model is quite similar to data from the ERA-Interim reanalysis, and thus proves that the sea ice loss is the main reason for the difference in surface-based warming in the CMIP3 multi-model mean and ERA-Interim data (Figure 3.1). An accompanying increase of the SSTs results in further increase of the heat flux from the ocean to the atmosphere, which is primarily driven by a latent heat flux from increased evaporation. The combined flux change from sea ice and SST changes induced in this simulation leads to approximately equal increases in latent and sensible heat fluxes (Table 5.2).

The fact that the primary warming seems to be surface-based, does not imply that local, within-Arctic factors are the dominant causes of Arctic amplification. The sea ice loss could be triggered by warming from remote sources, which would still result in a surface-based warming signal. Such mechanisms indicate that warming from remote sources can be amplified by local Arctic feedbacks.

The SOM experiment was designed in the hope that the inclusion of an active upper ocean and sea ice cover would result in a more "complete" warming response in the model, which would compare better to the actual climate system. Apparently this setup does improve the warming response (i.e. comes closer to the ERA-Interim warming structure), but the crucial factors behind the improved response are not revealed by this analysis. The warming pattern generally confirm the findings in the DOM simulations, except in the JJA vertical warming structure. Here, the simulations reveal that a sea ice reduction gives rise to a low-level

warming peak, which is reminiscent of a similar feature in the ERA-Interim mean warming profile. The warming seems to be connected to changes in the atmospheric circulation, which leads to increased subsidence in the Arctic following a strengthening of the Polar Cell. The changes in the vertical motion is linked to difference in the surface pressure, which indicates the coupling between vertical and horizontal circulation patterns. Furthermore the increased subsidence, causes a low-level cloud reduction, likely due to warming following adiabatic heating of the sinking air. As the cloud reduction happens in summer, where the clouds primarily have a cooling effect, it results in increased downwelling shortwave radiation, which leads to further surface-based warming.

The circulation changes are only evident in the SOM simulations, indicating that they are somehow linked to the inclusion of the active upper ocean and sea ice cover. The different spatial distributions and patterns of reduction of the sea ice cover are possible candidates for the differences, along with the pattern of upper ocean warming, and feedback effects connecting the sea ice and upper ocean changes to atmospheric large-scale circulation. Several other studies have linked sea ice changes to circulation changes within and far beyond the Arctic, and it is very likely that the spatial distribution of ice is crucial for the pattern of the changes. Furthermore the climate characteristics could be changed dramatically by the general sea ice concentration decrease, which removes the widespread insulation effect of denser sea ice cover. The increased moistening and warming of the Arctic atmosphere could very likely affect weather patterns and storm tracks in a way that would leave its mark on the entire Northern Hemisphere circulation.

The findings here indicate that the conclusion from *Chung and Räisänen* [2011] about climate models' tendency to over-simulate Arctic warming from increased atmospheric heat transport is questionable, and that the basis on which is it found is invalid. The lack of low-level warming in the CMIP3 multi model mean compared to ERA-Interim is caused by the sea ice difference, which can be attributed to the different state of the sea ice cover in the two compared periods, perhaps combined with the models' tendency to underestimate the sea ice loss in a warming climate (*Stroeve et al.* [2007]).

The warming of the lowermost atmosphere exceeds the warming aloft in all of the model simulations, while the upper-level warming around 500 hPa during summer become increasingly dominant in warmer climates. This upper-level warming peak is likely connected to increased atmospheric heat convergence following MHT changes. The ERA-Interim 2006-10 mean JJA warming profile has no similar upper-level peak, which indicates that the model does behave differently with regard to atmospheric transport changes. This does not necessarily imply an overestimated MHT increase, but could be a result differences in the mixing at the elevated level in the Arctic or the circulation patterns.

Sea ice reductions clearly favour Arctic amplification of surface temperatures. Sec-

tion 2.5.3 describes the feedback processes that are assumed to contribute to the amplification, and the simulations have confirmed that the sea ice cover is indeed coupled to all the elements on the list. The sea ice reduction is a central element in the within-Arctic, local contribution to the amplification, through SAF and the diminished insulation effect, allowing for bigger heat fluxes from the ocean to the atmosphere. The SOM simulations reveal that increased absorption of downwelling SW radiation causes additional heat storage in the upper ocean, if sufficiently large ocean areas become ice free, resulting in increased, delayed heat release to the atmosphere in winter. The experiments also reveal that the larger areas of open ocean surface and increased evaporation from the warmer ocean causes a moistening of the atmosphere, and consequently a cloud increase. All of these warming, local feedbacks are unsurprisingly dominating the response, when the sea ice cover is reduced, but the simulations also reveal a coupling between the sea ice cover and the remote contributors to the amplification. Although the sea ice reductions work to decrease meridional temperature and moisture gradients, these results indicate that the poleward heat transport could be strengthened, due to the sea ice covers coupling to the large-scale atmospheric circulation.

The results from this analysis stresses that the sea ice cover plays a very central role in the climate system, and that the expected reductions not only will have a substantial impact on the Arctic climate, but also will affect the climate far beyond the Arctic circle.

Perspectives and future work

The Arctic amplification debate inspires further work within several fields, aiming to improve the understanding of the relative importance of the different contributing factors, which is central in the assessment of future climate changes. The unanswered questions arising from the analyses in this thesis, invite further analysis in two areas: (1) the coupling between the sea ice cover and the large-scale atmospheric circulation, and (2) the change of the meridional heat transport in a warming climate in climate models.

(1) The recent drastic decline of the sea ice cover has already caused increasing focus on the connection between the sea ice cover and the atmospheric circulation. Analysis of the 2007 sea ice extent minimum has revealed dynamic feedback processes, where the sea ice loss gives rise to a changed atmospheric circulation pattern. The changed circulation further affects the sea ice cover, by favouring accelerated sea ice export through the Fram Strait and increased heat transport into the Arctic (*Blüthgen et al.* [2012] and *Zhang et al.* [2008b]). Further studies have, as mentioned Chapter 6, also revealed that these atmospheric circulation changes caused by the retreating ice cover can impact the climate far beyond the Arctic. *Overland and Wang* [2010] expect that this feedback of coupled changes in atmospheric circulation and sea ice loss will continue to modify the circulation pattern with consequences

for the climate both within and beyond the Arctic. Meanwhile the observational data of sea ice loss and circulation changes is still limited to the most recent years, and hence GCM simulation of future scenarios is a central tool in the further investigation of the couplings.

An extension of this study could be aimed at investigating the response of the storm tracks and pressure systems to the reduced sea ice cover. Such an analysis looking further into pressure, precipitation and eddy kinetic energy changes might give additional clues to the link between the sea ice cover and the atmospheric circulation.

As the dynamics of the sea ice cover seems to be adding further strength to the coupling between sea ice and the atmospheric circulation, it would also be interesting to repeat the simulations in this thesis with a more complete sea ice model, which incorporates both thermodynamic and dynamic effects. This might help shed more light on the couplings that are obviously important for the future climate change.

(2) The results presented in this thesis proves that GCM simulations with a realistic sea ice loss, result in maximum warming in the lower-most atmosphere throughout the year. This disproves the comparison, which led *Chung and Räisänen* [2011] to conclude that GCMs had a tendency to over-simulate warming aloft due to increasing poleward atmospheric heat transport in a warming climate. The question of the models' treatment of the meridional heat transport compared to the actual climate however still remains. Comparison of the warming profiles in the ERA-Interim reanalysis data and results from the equivalent model simulations shows that the model data tends to have a warming peak aloft around 500 hPa, which is not evident in the reanalysis data. It should be noted that the variance, and consequently the error bars, of the ERA-Interim warming profile (cf. Figure 3.1) is large, and could be concealing an upper-level warming peak. Assessment of the atmospheric transport in the models will probably have to rely on reanalysis data, as direct observation of atmospheric heat transport is problematic, and the values hence will have to be inferred from the circulation patterns and heat budgets. Nevertheless it is important to assess the behaviour of the simulated atmospheric heat transport in GCMs, as changes herein are very important for future climate change – especially in lieu of the Arctic amplification of surface temperature changes.

BIBLIOGRAPHY

National Snow and Ice Data Center (NSIDC) Press release: Arctic sea ice reaches lowest extent for the year and the satellite record, `http://nsidc.org/news/press/2012_seaiceminimum.html`, Accessed: January 4, 2013, Published: September 19, 2012.

Program for Climate Model Diagnosis and Intercomparison (PCMDI): About the WCRP CMIP3 multi-model dataset, `http://www-pcmdi.llnl.gov/ipcc/about_ipcc.php`, Accessed: January 24, 2013.

Alexeev, V. A., Sensitivity to CO_2 doubling of an atmospheric GCM coupled to an oceanic mixed layer: a linear analysis, *Climate Dynamics*, *20*, 2003.

Alexeev, V. A., P. L. Langen, and J. R. Bates, Polar amplification of surface warming on an aquaplanet in "ghost forcing" experiments without sea ice feedbacks, *Climate Dynamics*, *24*, 2005.

Arrhenius, S., On the influence of Carbonic Acid in the air upon the temperature of the ground, *Philosophical Magazine and Journal of Science*, *41*, 1896.

Arzel, O., T. Fichefet, and H. Goosse, Sea ice evolution over the 20th and 21st centuries as simulated by current AOGCMs, *Ocean Modelling*, *12*, 2006.

Bader, J., M. D. S. Mesquita, K. I. Hodges, N. Keenlyside, S. Østerhus, and M. Miles, A review on Northern Hemisphere sea-ice, storminess and the North Atlantic Oscillation: Observations and projected changes, *Atmospheric Research*, *101*, 2011.

Bekryaev, R. V., I. V. Polyakov, and V. A. Alexeev, Role of Polar Amplification in long-term surface air temperature variations and modern Arctic Warming, *Journal of Climate*, *23*, 2010.

Bintanja, R., R. G. Graversen, and W. Hazeleger, Arctic winter warming amplified by the thermal inversion and consequent low infrared cooling to space, *Nature Geoscience*, *4*, 2011.

Bintanja, R., E. C. van der Linden, and W. Hazeleger, Boundary layer stability and Arctic climate change: A feedback study using EC-Earth, *Climate Dynamics*, *39*, 2012.

Bitz, C. M., and Q. Fu, Arctic warming aloft is data set dependent, *Nature*, *455*, 2008.

Bitz, C. M., and G. H. Roe, A mechanism for the high rate of sea ice thinning in the Arctic Ocean, *Journal of Climate*, *17*, 2004.

Bitz, C. M., K. M. Shell, P. R. Gent, D. A. Bailey, G. Danabasoglu, K. C. Armour, M. M. Holland, and J. T. Kiehl, Climate sensitivity of the Community Climate System Model, version 4, *Journal of Climate*, *25*, 2012.

Blüthgen, J., R. Gerdes, and M. Werner, Atmospheric response to the extreme Arctic sea ice conditions in 2007, *Geophysical Research Letters*, *39*, 2012.

Boé, J., A. Hall, and X. Qu, September sea-ice cover in the Arctic Ocean projected to vanish by 2100, *Nature Geoscience*, *2*, 2009.

Bonan, G. B., K. W. Oleson, M. Vertenstein, S. Levis, X. Zeng, Y. Dai, R. E. Dickinson, and Z.-L. Yang, The land surface climatology of the Community Land Model coupled to the NCAR Community Climate Model, *Journal of Climate*, *15*, 2002.

Bony, S., et al., How well do we understand and evaluate climate change feedback processes? (review article), *Journal of Climate*, *19*, 2006.

Bradley, R. S., F. T. Keimig, and H. F. Diaz, Climatology of Surface-Based inversions in the North American Arctic, *Journal of Geophysical Research*, *97*, 1992.

Budikova, D., Role of Arctic sea ice in global atmospheric circulation: A review, *Global and Planetary Change*, *68*, 2009.

Chapman, W. L., and J. E. Walsh, Simulations of Arctic temperature and pressure by Global Coupled Models, *Journal of Climate*, *20*, 2007.

Chung, C. E., and P. Räisänen, Origin of the Arctic warming in climate models, *Geophysical Research Letters*, *38*, 2011.

Collins, W. D., et al., *Description of the NCAR Community Atmosphere Model (CAM 3.0) – Technical Report*, NCAR/TN-464+STR, National Center for Atmospheric Research, 2004.

Collins, W. D., et al., The formulation and atmospheric simulation of the Community Atmosphere Model version 3 (CAM3), *Journal of Climate*, *19*, 2006.

Colman, R., A comparison of climate feedbacks in general circulation models, *Climate Dynamics*, *20*, 2003.

Comiso, J. C., C. L. Parkinson, R. Gersten, and L. Stock, Accelerated decline in the Arctic sea ice cover, *Geophysical Research Letters*, *35*, 2008.

Curry, J. A., W. B. Rossow, D. Randall, and J. L. Schramm, Overview of Arctic cloud and radiation characteristics, *Journal of Climate*, *9*, 1996.

Dee, D. P., et al., The ERA-Interim reanalysis: configuration and performance of the data assimilation system, *Quarterly Journal of the Royal Meteorological Society*, *137*, 2011.

Deser, C., J. E. Walsh, and M. S. Timlin, Arctic sea ice variability in the context of recent atmospheric circulation trends, *Journal of Climate*, *13*, 2000.

Deser, C., R. Tomas, M. Alexander, and D. Lawrence, The seasonal atmospheric response to projected Arctic sea ice loss in the late twenty-first century, *Journal of Climate*, *23*, 2009.

DeWeaver, E., and C. M. Bitz, Atmospheric circulation and its effect on Arctic sea ice in CCSM3 simulations at medium and high resolution, *Journal of Climate*, *19*, 2006.

Flannery, B. P., Energy balance models incorporating transport of thermal and latent energy, *Journal of the Atmospheric Sciences*, *41*, 1983.

Forster, P., et al., Changes in Atmospheric Constituents and in Radiative Forcing, in *Climate Change 2007: The Physical Science Basis. Contribution of Working Group I to the Fourth Assessment Report of the Intergovernmental Panel on Climate Change*, edited by S. Solomon, D. Qin, M. Manning, Z. Chen, M. Marquis, K. B. Averyt, M. Tignor, and H. L. Miller, Cambridge University Press, 2007.

Francis, J. A., W. Chan, D. J. Leathers, J. R. Miller, and D. E. Veron, Winter Northern Hemisphere weather patterns remember summer Arctic sea-ice extent, *Geophysical Research Letters*, *36*, 2009.

Grant, A. N., S. Brönnimann, and L. Haimberger, Recent Arctic warming vertical structure contested, *Nature*, *455*, 2008.

Graversen, R. G., and M. Wang, Polar amplification in a coupled climate model with locked albedo, *Climate Dynamics*, *33*, 2009.

Graversen, R. G., T. Mauritsen, M. Tjernström, E. Källen, and G. Svensson, Vertical structure of recent Arctic warming, *Nature*, *451*, 2008a.

Graversen, R. G., T. Mauritsen, M. Tjernström, E. Källen, and G. Svensson, Reply to arising debate, *Nature*, *455*, 2008b.

Graversen, R. G., T. Mauritsen, S. Drijfhout, M. Tjernström, and S. Mårtensson, Warm winds from the Pacific caused extensive Arctic sea-ice melt in summer 2007, *Climate Dynamics*, *36*, 2011.

Hansen, J., and L. Nazarenko, Soot climate forcing via snow and ice albedos, *PNAS*, *101*, 2004.

Hansen, J., et al., Efficacy of climate forcings, *Journal of Geophysical Research*, *110*, 2005.

Harvey, L. D. D., *Global Warming – The Hard Science*, Pearson / Prentice Hall, 2000.

Hassol, S. J., *ACIA, Impacts of a warming Arctic: Arctic Climate Impact Assessment*, Cambridge University Press, 2004.

Holland, M. M., and C. M. Bitz, Polar amplification of climate change in coupled models, *Climate Dynamics*, *21*, 2003.

Houze Jr., R. A., *Cloud Dynamics*, Elsevier / Academic Press, 1993.

Hurrell, J. W., J. J. Hack, D. Shea, J. M. Caron, and J. Rosinski, A new sea surface temperature and sea ice boundary dataset for the Community Atmosphere Model, *Journal of Climate*, *21*, 2008.

Intrieri, J. M., C. W. Fairall, M. D. Shupe, P. O. G. Persson, E. L. Andreas, P. S. Guest, and R. E. Moritz, An annual cycle of Arctic surface cloud forcing at SHEBA, *Journal of Geophysical Research*, *107*, 2002.

Kalnay, E., et al., The NCEP/NCAR 40-year Reanalysis Project, *Bulletin of the American Meteorological Society*, *77*, 1996.

Kay, J. E., and A. Gettelman, Cloud influence on and response to seasonal Arctic sea ice loss, *Journal of Geophysical Research*, *114*, 2009.

Kumar, A., et al., Contribution of sea ice loss to Arctic amplification, *Geophysical Research Letters*, *37*, 2010.

Kundu, P. K., and I. M. Cohen, *Fluid Mechanics*, 4th ed., Elsevier / Academic Press, 2008.

Kwok, R., Observational assessment of Arctic Ocean sea ice motion, export, and thickness in CMIP3 climate simulations, *Journal of Geophysical Research*, *116*, 2011.

Kwok, R., and D. A. Rothrock, Decline in Arctic sea ice thickness from submarine and ICESat records: 1958–2008, *Geophysical Research Letters*, *36*, 2009.

Langen, P. L., R. G. Graversen, and T. Mauritsen, Separation of contributions from radiative feedbacks to polar amplification on an aquaplanet, *Journal of Climate*, *25*, 2012.

L'Heureux, M. L., A. Kumar, G. D. Bell, M. S. Halpert, and R. W. Higgins, Role of the Pacific-North American (PNA) pattern in the 2007 Arctic sea ice decline, *Geophysical Research Letters*, *35*, 2009.

Liu, Y., J. R. Key, Z. Liu, X. Wang, and S. J. Vavrus, A cloudier Arctic expected with diminishing sea ice, *Geophysical Research Letters*, *39*, 2012.

Magnusdottir, G., C. Deser, and R. Saravanan, The effects of North Atlantic SST and sea ice anomalies on the winter circulation in CCM3. Part I: Main features and storm track characteristics of the response, *Journal of Climate*, *17*, 2004.

Maslanik, J. A., C. Fowler, J. Stroeve, S. Drobot, J. Zwally, D. Yi, and W. Emery, A younger, thinner Arctic ice cover: Increased potential for rapid, extensive sea-ice loss, *Geophysical Research Letters*, *34*, 2007.

Mauritsen, T., and R. G. Graversen, The recent Arctic amplification debate: Is summer sea-ice melt caused by surface feedbacks or warming from aloft?, *In Prep.*, 2012.

McGuire, A. D., F. S. Chapin III, J. E. Walsh, and C. Wirth, Integrated regional changes in Arctic climate feedbacks: Implications for the global climate system, *Annual Review of Environment and Resources*, *31*, 2006.

Meehl, G. A., C. Covey, T. Delworth, M. Latif, B. McAvaney, J. F. B. Mitchell, R. J. Stouffer, and K. E. Taylor, The WCRP CMIP3 multi-model dataset: A new era in climate change research, *Bulletin of the American Meteorological Society*, *88*, 2007a.

Meehl, G. A., et al., Global Climate Projections, in *Climate Change 2007: The Physical Science Basis. Contribution of Working Group I to the Fourth Assessment Report of the Intergovernmental Panel on Climate Change*, edited by S. Solomon, D. Qin, M. Manning, Z. Chen, M. Marquis, K. B. Averyt, M. Tignor, and H. L. Miller, Cambridge University Press, 2007b.

Nakamura, N., and A. H. Oort, Atmospheric heat budget of the Polar Regions, *Journal of Geophysical Research*, *93*, 1988.

Nakićenović, N., et al., *IPCC Special Report – Emissions Scenarios (SRES)*, Intergovernmental Panel on Climate Change, 2000.

Nghiem, S. V., I. G. Rigor, D. K. Perovich, P. Clemente-Colón, J. W. Weatherly, and G. Neumann, Rapid reduction of Arctic perennial sea ice, *Geophysical Research Letters*, *34*, 2007.

Notz, D., and J. Marotzke, Observations reveal external driver for Arctic sea-ice retreat, *Geophysical Research Letters*, *39*, 2012.

Onogi, K., et al., The JRA-25 Reanalysis, *Journal of the Meteorological Society of Japan*, *85*, 2007.

Overland, J. E., and P. S. Guest, The Arctic snow and air temperature budget over sea ice during winter, *Journal of Geophysical Research*, *96*, 1991.

Overland, J. E., and M. Wang, Large-scale atmospheric circulation changes are associated with the recent loss of Arctic sea ice, *Tellus*, *62A*, 2010.

Parkinson, C. L., D. Rind, R. J. Healy, and D. G. Martinson, The impact of sea ice concentration accuracies on climate model simulations with the GISS GCM, *Journal of Climate*, *14*, 2001.

Polyakov, I. V., et al., Observationally based assessment of polar amplification of global warming, *Geophysical Research Letters*, *29*, 2002.

Porter, D. F., J. J. Cassano, and M. C. Serreze, Analysis of the Arctic atmospheric energy budget in WRF: A comparison with reanalyses and satellite observations, *Journal of Geophysical Research*, *116*, 2011.

Randall, D. A., et al., Climate models and their evaluation, in *Climate Change 2007: The Physical Science Basis. Contribution of Working Group I to the Fourth Assessment Report of the Intergovernmental Panel on Climate Change*, edited by S. Solomon, D. Qin, M. Manning, Z. Chen, M. Marquis, K. B. Averyt, M. Tignor, and H. L. Miller, Cambridge University Press, 2007.

Schweiger, A., R. Lindsay, J. Zhang, M. Steele, H. Stern, and R. Kwok, Uncertainty in modeled Arctic sea ice volume, *Journal of Geophysical Research*, *116*, 2011.

Screen, J. A., and I. Simmonds, Erroneous Arctic temperature trends in the ERA-40 reanalysis: A closer look, *Journal of Climate*, *24*, 2010a.

Screen, J. A., and I. Simmonds, The central role of diminishing sea ice in recent Arctic temperature amplification, *Nature*, *464*, 2010b.

Screen, J. A., C. Deser, and I. Simmonds, Local and remote controls on observed Arctic warming, *Geophysical Research Letters*, *39*, 2012.

Sedláček, J., R. Knutti, O. Martius, and U. Beyerle, Impact of a reduced Arctic sea ice cover on ocean and atmospheric properties, *Journal of Climate*, *25*, 2012.

Semmler, T., R. McGrath, and S. Wang, The impact of Arctic sea ice on the Arctic energy budget and on the climate of the Northern mid-latitudes, *Climate Dynamics*, *39*, 2012.

Serreze, M. C., and A. P. Barrett, The summer cyclone maximum over the central Arctic Ocean, *Journal of Climate*, *21*, 2008.

Serreze, M. C., and R. G. Barry, Synoptic activity in the Arctic Basin 1979-85, *Journal of Climate*, *1*, 1988.

Serreze, M. C., and R. G. Barry, *The Arctic Climate System*, Cambridge University Press, 2005.

Serreze, M. C., and R. G. Barry, Processes and impacts of Arctic amplification: A research synthesis, *Global and Planetary Change*, *77*, 2011.

Serreze, M. C., and J. A. Francis, The Arctic amplification debate, *Climate Change*, *76*, 2006.

Serreze, M. C., J. D. Kahl, and R. C. Schnell, Low-level temperature inversions of the Eurasian Arctic and comparisons with Soviet drifting station data, *Journal of Climate*, *5*, 1992.

Serreze, M. C., A. P. Barrett, A. G. Slater, M. Steele, J. Zhang, and K. E. Trenberth, The large-scale energy budget of the Arctic, *Journal of Climate*, *112*, 2007.

Serreze, M. C., A. P. Barrett, J. C. Stroeve, D. N. Kindig, and M. M. Holland, The emergence of surface-based Arctic amplification, *The Cryosphere*, *3*, 2009.

Shindell, D., and G. Faluvegi, Climate response to regional radiative forcing during the twentieth century, *Nature Geoscience*, *2*, 2009.

Simmonds, I., and K. Keay, Extraordinary September Arctic sea ice reductions and their relationships with storm behavior over 1979–2008, *Geophysical Research Letters*, *36*, 2009.

Soden, B. J., and I. M. Held, An assessment of climate feedbacks in coupled ocean-atmosphere models, *Journal of Climate*, *19*, 2006.

Solomon, A., Impact of latent heat release on polar climate, *Geophysical Research Letters*, *33*, 2006.

Strey, S. T., W. L. Chapman, and J. E. Walsh, The 2007 sea ice minimum: Impacts on the Northern Hemisphere atmosphere in late autumn and early winter, *Journal of Geophysical Research*, *115*, 2010.

Stroeve, J., M. M. Holland, W. Meier, T. Scambos, and M. C. Serreze, Arctic sea ice decline: Faster than forecast, *Geophysical Research Letters*, *34*, 2007.

Thorne, P. W., Arctic tropospheric warming amplification?, *Nature*, *455*, 2008.

Uppala, S. M., et al., The ERA-40 re-analysis, *Quarterly Journal Of The Royal Meteorological Society*, *131*, 2005.

Vavrus, S., D. Waliser, A. Schweiger, and J. Francis, Simulations of 20th and 21st century Arctic cloud amount in the global climate models assessed in the IPCC AR4, *Climate Dynamics*, *33*, 2009.

Vavrus, S., M. M. Holland, and D. A. Bailey, Changes in Arctic clouds during intervals of rapid sea ice loss, *Climate Dynamics*, *36*, 2011.

von Storch, H., and F. W. Zwiers, *Statistical Analysis in Climate Research*, Cambridge University Press, 1999.

Wallace, J. M., and P. V. Hobbs, *Atmospheric Science*, Elsevier / Academic Press, 2006.

Winton, M., Amplified Arctic climate change: What does surface albedo feedback have to do with it?, *Geophysical Research Letters*, *33*, 2006.

Zhang, J., R. Lindsay, M. Steele, and A. Schweiger, What drove the dramatic retreat of Arctic sea ice during summer 2007?, *Geophysical Research Letters*, *35*, 2008a.

Zhang, X., A. Sorteberg, J. Zhang, R. Gerdes, and J. C. Comiso, Recent radical shifts of atmospheric circulations and rapid changes in Arctic climate system, *Geophysical Research Letters*, *35*, 2008b.

Zhang, Y., D. J. Seidel, J.-C. Golaz, C. Deser, and R. A. Tomas, Climatological characteristics of Arctic and Antarctic surface-based inversions, *Journal of Climate*, *24*, 2011.

Zuidema, P., et al., An Arctic springtime mixed-phase cloudy boundary layer observed during SHEBA, *Journal of Atmospheric Sciences*, *62*, 2005.

LIST OF FIGURES

List of Tables